



National Library
of Canada

Acquisitions and
Bibliographic Services Branch

395 Wellington Street
Ottawa, Ontario
K1A 0N4

Bibliothèque nationale
du Canada

Direction des acquisitions et
des services bibliographiques

395, rue Wellington
Ottawa (Ontario)
K1A 0N4

Your file - Votre référence

Our file - Notre référence

NOTICE

The quality of this microform is heavily dependent upon the quality of the original thesis submitted for microfilming. Every effort has been made to ensure the highest quality of reproduction possible.

If pages are missing, contact the university which granted the degree.

Some pages may have indistinct print especially if the original pages were typed with a poor typewriter ribbon or if the university sent us an inferior photocopy.

Reproduction in full or in part of this microform is governed by the Canadian Copyright Act, R.S.C. 1970, c. C-30, and subsequent amendments.

AVIS

La qualité de cette microforme dépend grandement de la qualité de la thèse soumise au microfilmage. Nous avons tout fait pour assurer une qualité supérieure de reproduction.

S'il manque des pages, veuillez communiquer avec l'université qui a conféré le grade.

La qualité d'impression de certaines pages peut laisser à désirer, surtout si les pages originales ont été dactylographiées à l'aide d'un ruban usé ou si l'université nous a fait parvenir une photocopie de qualité inférieure.

La reproduction, même partielle, de cette microforme est soumise à la Loi canadienne sur le droit d'auteur, SRC 1970, c. C-30, et ses amendements subséquents.

UNIVERSITY OF ALBERTA

**COUNTING FLUORESCENT MOLECULES AND HIGH SPEED
DNA SEQUENCING IN CAPILLARY ELECTROPHORESIS**

BY



DAVID DA YONG CHEN

A THESIS SUBMITTED TO THE FACULTY OF GRADUATE STUDIES AND RESEARCH IN
PARTIAL FULFILLMENT OF THE REQUIREMENTS FOR THE DEGREE OF

DOCTOR OF PHILOSOPHY

DEPARTMENT OF CHEMISTRY

EDMONTON, ALBERTA

Spring 1993



National Library
of Canada

Acquisitions and
Bibliographic Services Branch

395 Wellington Street
Ottawa, Ontario
K1A 0N4

Bibliothèque nationale
du Canada

Direction des acquisitions et
des services bibliographiques

335, rue Wellington
Ottawa (Ontario)
K1A 0N4

Your file - Votre référence

Our file - Notre référence

The author has granted an irrevocable non-exclusive licence allowing the National Library of Canada to reproduce, loan, distribute or sell copies of his/her thesis by any means and in any form or format, making this thesis available to interested persons.

L'auteur a accordé une licence irrévocable et non exclusive permettant à la Bibliothèque nationale du Canada de reproduire, prêter, distribuer ou vendre des copies de sa thèse de quelque manière et sous quelque forme que ce soit pour mettre des exemplaires de cette thèse à la disposition des personnes intéressées.

The author retains ownership of the copyright in his/her thesis. Neither the thesis nor substantial extracts from it may be printed or otherwise reproduced without his/her permission.

L'auteur conserve la propriété du droit d'auteur qui protège sa thèse. Ni la thèse ni des extraits substantiels de celle-ci ne doivent être imprimés ou autrement reproduits sans son autorisation.

ISBN 0-315-81973-1

Canada

UNIVERSITY OF ALBERTA

RELEASE FORM

NAME OF AUTHOR: **DAVID DA YONG CHEN**

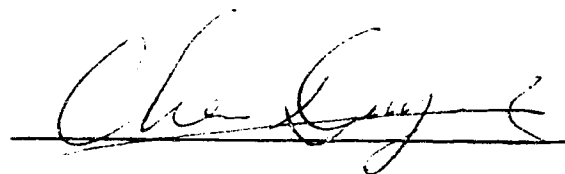
TITLE OF THESIS: **COUNTING FLUORESCENT MOLECULES AND HIGH
SPEED DNA SEQUENCING IN CAPILLARY
ELECTROPHORESIS**

DEGREE: **DOCTOR OF PHILOSOPHY**

YEAR THIS DEGREE GRANTED: **1993**

PERMISSION IS HEREBY GRANTED TO THE UNIVERSITY OF ALBERTA LIBRARY TO REPRODUCE SINGLE COPIES OF THIS THESIS AND TO LEND OR SELL SUCH COPIES FOR PRIVATE, SCHOLARLY OR SCIENTIFIC RESEARCH PURPOSES ONLY.

THE AUTHOR RESERVES ALL OTHER PUBLICATION AND OTHER RIGHTS IN ASSOCIATION WITH THE COPYRIGHT IN THE THESIS, AND EXCEPT AS HEREINBEFORE PROVIDED NEITHER THE THESIS NOR ANY SUBSTANTIAL PORTION THEREOF MAY BE PRINTED OR OTHERWISE REPRODUCED IN ANY MATERIAL FORM WHATEVER WITHOUT THE AUTHOR'S PRIOR WRITTEN PERMISSION.

A handwritten signature in black ink, appearing to read "David Da Yong Chen", written over a horizontal line.

December 21, 1992

*When I consider your heavens,
the work of your fingers,
the moon and the stars
which you have set in place.*

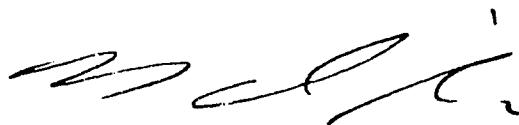
*What is man that you are mindful of him
the son of man that you care for him?
You made him a little lower than the heavenly beings
and crowned him with glory and honor.*

Psalm 8:3-5

UNIVERSITY OF ALBERTA

FACULTY OF GRADUATE STUDIES AND RESEARCH

The undersigned certify that they have read, and recommend to the Faculty of graduate studies and research for acceptance, a thesis entitled **COUNTING FLUORESCENT MOLECULES AND HIGH SPEED DNA SEQUENCING IN CAPILLARY ELECTROPHORESIS** submitted by **DAVID DA YONG CHEN** in partial fulfillment of the requirements for the degree of **DOCTOR OF PHILOSOPHY**.



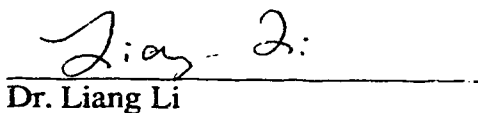
Dr. Norman J. Dovichi



Dr. Byron G. Kratochvil



Dr. Monica Palcic



Dr. Liang Li



Dr. Linda J. Reha-Krantz



Dr. Raymond F. Gesteland

December 16, 1992

To my parents

and my wife

Abstract

Capillary electrophoresis (CE) has attracted much attention in separation and microchemical analysis. Laser induced post column fluorescence detection in a sheath flow cuvette is the most sensitive method of detection for CE. Counting analyte molecules in a high efficiency separation system, one of the ultimate goals in analytical chemistry, becomes a reality with an inexpensive 8 mW He-Ne laser and appropriate optical design for collection and detection of fluorescent signals. After the average signal level from one molecule is determined and appropriate threshold is set, the number of fluorescent molecules flowing through the capillary can be determined by counting the signal peaks above the threshold.

Using a 1 mW He-Ne laser operating at 543.5 nm as the excitation source, a photon counter with cooled PMT as the fluorescence detector, and appropriate digital signal processing, a detection limit of 50 yoctomole (30 molecules, 1 yoctomole = 1×10^{-24} mole) of rhodamine 6G is obtained. This was the state of the art detection limit in CE in 1991. Zeptomole (10^{-21} mole) detection limits are obtained with a simple PMT operating at room temperature. An Ar⁺ laser gives similar detection limits for fluorescein in the same CE system. The very high sensitivity makes this a suitable detector for high speed DNA sequencing by capillary gel electrophoresis. Combining the color encoded base recognition introduced by Smith *et al.*, and the peak height encoded base recognition by Richardson and Tabor, a color and peak height encoded DNA sequencing technique is developed. Sequencing is achieved by using two lasers focused on two separate spots at the end of the capillary; each laser excites a different group of fluorescent dye labeled, peak height encoded DNA segments. Fluorescence is collected in two spectral channels, and the bases are determined by the color and height of the peaks. Less dependence on resolution, simpler data processing and more accurate base recognition are achieved.

Acknowledgment

In the spring of 1988, after half of a year wandering in the department, I made up my mind and joined Norm Dovichi's group. It turned out to be the most important decision I made in the past 5 years and will be the most important decision in my career. His knowledge about chemistry and a rigorous scientific approach make him a great scientist and an excellent supervisor. But what influenced me more is his personality and the way he treats other people, with respect and care. I want to express my sincere gratitude to him for his guidance in research, and for his kindness and patience with me.

Being a member of, what we like to call the Northern Lights Laser Lab, I have been blessed with great coworkers. I want to express my heartfelt thanks to every one of them, for their help, encouragement and care; their friendship will always be treasured. Especially, to Heather Starke, who proofread the whole thesis and made important suggestions.

The machine shop, electronic shop, glass shop, purchasing and all the support staff in this department are simply the best. Without their help, lots of work written in this thesis would not have been finished.

Thanks would not be enough to express my feelings to my parents, who spent all their savings on my air ticket to Canada, and loved me selflessly always. And to my brother, who gave all he had to help me start my study here. And to my parents-in-law. It was with their inspiration I decided to pursue my graduate study.

And finally, to my wife Nancy. She shared every moment of my life in this five and half years. Content or worry, success or failure, she is always there to support me. It is her understanding, love and care that makes our lives full of meaning and joy, and with her support I have done what is written in this thesis.

Table of Contents

| | |
|---|----|
| Part I Laser Induced Fluorescence Detection in Capillary Electrophoresis | 1 |
| Chapter 1 Introduction to Open Tubular Electrophoresis | 2 |
| 1.1 The advantages of capillary electrophoresis compared with conventional electrophoresis methods | 4 |
| 1.2 Open tubular capillary zone electrophoresis | 5 |
| 1.2.1 Zeta (ζ) potential..... | 5 |
| 1.2.2 Electroosmosis..... | 6 |
| 1.2.3 The flow profile | 8 |
| 1.2.4 Electrophoretic migration..... | 9 |
| 1.2.5 The flow rate in CZE..... | 9 |
| 1.2.6 Separation efficiency..... | 10 |
| 1.2.7 Resolution..... | 10 |
| 1.2.8 Discussion..... | 11 |
| 1.3 Micellar electrokinetic capillary chromatography..... | 12 |
| 1.3.1 The principle of MECC..... | 12 |
| 1.3.2 Parameters affecting efficiency in MECC | 14 |
| 1.3.3 Discussion..... | 15 |
| References:..... | 17 |
| Chapter 2. High Sensitivity Fluorescence Detectors | 19 |
| 2.1 Low cost, high sensitivity laser induced fluorescence detection | 19 |
| 2.1.1 The Detector..... | 23 |
| Optical design..... | 23 |
| The Laser..... | 23 |
| The sheath flow cuvette..... | 25 |
| Collection optics..... | 28 |

| | |
|--|-----------|
| Spectral Filter | 29 |
| Photodetector | 31 |
| 2.1.2 Experimental section | 31 |
| Electrophoresis | 31 |
| Optics | 34 |
| Alignment of the fluorescence detector | 34 |
| Reagents..... | 36 |
| 2.1.3 Results and Discussion | 36 |
| 2.2 Improving detection limits by using a cooled PMT..... | 37 |
| 2.2.1 Experimental Section..... | 39 |
| 2.2.2 Detector..... | 39 |
| 2.2.3 Results and Discussion | 39 |
| 2.3 Improving the detection limits by redesigning the sheath flow cuvette and fluorescence collection system..... | 43 |
| The detection system..... | 45 |
| Experimental Section..... | 45 |
| Results and Discussion: | 46 |
| 2.4 Detection of single fluorescent molecules in capillary electrophoresis..... | 56 |
| Instrumentation | 57 |
| Experiment | 59 |
| Results and discussion..... | 59 |
| References:..... | 86 |
| Part II DNA Sequencing with Capillary Gel Electrophoresis | 88 |
| Chapter 3 Single-Color Laser-Induced Fluorescence Detection and Capillary Gel Electrophoresis for DNA Sequencing..... | 89 |
| 3.1 Introduction..... | 89 |
| 3.2 Experimental Section | 92 |

| | | |
|---|--|-----|
| 3.3 | Results and Discussion..... | 93 |
| 3.3.1 | Peak height encoded one color DNA sequencing..... | 93 |
| 3.3.2 | The effect of adding formamide into acrylamide gel on separation..... | 99 |
| | Separation | 99 |
| | Conclusion | 102 |
| | References:..... | 105 |
| Chapter 4 Two-Label Peak-Height Encoded DNA Sequencing By Capillary Gel | | |
| | Electrophoresis | 107 |
| 4.1 | Introduction..... | 107 |
| 4.2 | Experimental procedure | 109 |
| | Instrumental design--Electrophoresis | 109 |
| | Detectors..... | 109 |
| | Sample Preparation..... | 111 |
| | Sequence Determination | 113 |
| 4.3 | Results and Discussion..... | 114 |
| | Two laser-Two collection optic system..... | 114 |
| | One laser-Two collection optic system..... | 118 |
| 4.4 | Conclusions | 124 |
| | References:..... | 126 |
| Part III Hydrodynamic Sample Introduction in CE with a Sheath Flow Cuvette | | |
| Chapter 5. Hydrodynamic Sample Introduction Using a Three Way Valve in | | |
| Capillary Electrophoresis..... | | |
| 5.1 | Sample introduction in capillary electrophoresis | 128 |
| 5.1.1 | Electrokinetic injection..... | 128 |
| | The injection volume..... | 129 |
| | Automation of the electrokinetic sampler | 130 |

| | |
|---|-----|
| Discussion..... | 131 |
| 5.1.2 Hydrodynamic Injection..... | 132 |
| The volume of hydrodynamic injection..... | 132 |
| Automation of hydrodynamic sampling | 133 |
| Discussion..... | 134 |
| 5.1.3 Other injection methods..... | 135 |
| Rotary type injector | 136 |
| Microinjectors..... | 136 |
| Electric sample splitter | 137 |
| Conclusion | 138 |
| 5.2 Hydrodynamic sample introduction using a three way valve..... | 138 |
| 5.2.1 Theory | 139 |
| 5.2.2 Experimental Section..... | 139 |
| Separation and detection..... | 139 |
| Chemicals | 140 |
| The injector..... | 140 |
| 5.2.3 Results and discussion..... | 145 |
| Injection volume..... | 145 |
| Precision test..... | 146 |
| Volume of Injection as a Function of Δh | 148 |
| Peak shape comparison..... | 148 |
| Comparison of two methods of injection..... | 151 |
| Discussion..... | 151 |
| References:..... | 153 |

List of Tables

| | |
|--|----|
| Table 2.1 Properties of 0.75 mW He-Ne laser used in the experiment | 25 |
| Table 2.2 General properties of R1477 photomultiplier tube..... | 33 |
| Table 2.3 Collection efficiencies of lenses with different numerical apertures[14] | 43 |
| Table 2.4 Some values of the constant KLOD at different N^* values..... | 48 |
| Table 2.5 The experiments for single molecule detection..... | 69 |
| Table 2.6 The results of counting molecules at different flow rates..... | 84 |

List of Figures

| | |
|--|----|
| Fig.1.1 Number of papers related to capillary electrophoresis published and collected in Chemical Abstracts in each year since 1966..... | 3 |
| Fig. 1.2 Block diagram of a capillary electrophoresis system..... | 5 |
| Fig. 1.3 Solid-liquid interface at the wall of capillary in CZE and zeta potential..... | 7 |
| Fig. 1.4 Flat flow profile in CE..... | 8 |
| Fig. 2.1 The absorption spectrum of TRITC..... | 21 |
| Fig. 2.2 The fluorescence spectrum of TRITC | 22 |
| Fig. 2.3 Block diagram of the laser induced fluorescence detector..... | 24 |
| Fig. 2.4 The capillary and sheath flow cuvette in laser induced fluorescence detection..... | 27 |
| Fig. 2.5 Spectrum of the interference filter 590DF40..... | 30 |
| Fig. 2.6 Typical spectral response for R1477 photomultiplier tube --From data sheet..... | 32 |
| Fig. 2.7 Arrangement of the optical elements | 35 |
| Fig. 2.8 The effect of cooling a PMT on PMT dark current. Both the background and the noise on the background are reduced. | 38 |
| Fig. 2.9 Capillary free zone electropherogram of 4 zmol (2300 molecules) of tetramethylrhodamine isothiocyanate..... | 42 |
| Fig. 2.10 The difference between the working distances of an microscope objective when the object is located in different media. (a) Both the objective and the object are in the air. (b) The objective is in the air, but the object is in another media which has a greater refractive index than air | 44 |
| Fig. 2.11 Electropherograms of repeated injections of 300 molecules of rhodamine 6G into a capillary..... | 47 |

| | |
|---|----|
| Fig. 2.12 (a) one of the electropherograms in Fig. 11, (b) the results of 3 times binomial smoothing, and (c) the results of 5 times binomial smoothing..... | 49 |
| Fig. 2.13 The real part of a Fast Fourier transform of the same electropherogram as Fig. 2.12 (a). | 50 |
| Fig. 2.14 An illustration of a low pass frequency domain digital filter, F_s is the sampling frequency and F_c is the cut off frequency of the filter..... | 51 |
| Fig. 2.15 The effect of Fourier transform low pass filtering. (a) raw data, (b) filtered data..... | 53 |
| Fig. 2.16 (a) a normalized peak from an electropherogram | 54 |
| Fig. 2.17 Comparison of the original electropherogram and the resultant electropherogram after a Gaussian shaped time domain filter. (a) is the raw data, the detection limit is 53 molecules..... | 55 |
| Fig. 2.18 The optical arrangement of the two channel fluorescence detector..... | 58 |
| Fig. 2.19 The absorption spectrum of sulforhodamine 101..... | 60 |
| Fig. 2.20 The fluorescence spectrum of Sulforhodamine 101 | 61 |
| Fig. 2.21 Electropherogram of an injection of 275 molecules into the capillary..... | 62 |
| Fig. 2.22 Electropherograms of 28 molecules injected into the capillary..... | 63 |
| Fig. 2.23 Electropherograms of injection of 19 molecules into the capillary, raw data..... | 65 |
| Fig. 2.24 Smoothed electropherograms of injection of 19 molecules..... | 66 |
| Fig. 2.25 The reflected light from 0.5 μm polystyrene beads..... | 67 |
| Fig. 2.26 Data for a flow rate of 6 molecules per second in the first 30 seconds. The polarity of the electrophoresis driven voltage is reversed after 30 seconds. The data is binomial smoothed 5 times..... | 71 |
| Fig. 2.27 Autocorrelation of a section of 2000 points from the background in Fig. 2.26..... | 72 |
| Fig. 2.28 Autocorrelation of a section of 2000 points from the signal in Fig. 2.26..... | 73 |

| | |
|--|-----|
| Fig. 2.29 The histogram of the data from Fig. 2.26. The signal part of the histogram is derived from the first 30 seconds with the sample flowing, and the background histogram is derived from the last 30 second (from 40 to 70 seconds) without the sample flowing. There is a significant shift of the maximum for the signal histogram..... | 74 |
| Fig. 2.30 Comparison of the histograms from three sets of data: (a) is from data conditioned by a 1000 Hz low pass filter, (b) 100 Hz filtered, and (c) 31.5 Hz filtered. | 75 |
| Fig. 2.31 The histograms of the data collected at different sample flow rate..... | 77 |
| Fig. 2.32 A segment of data which was collected when the sample flow rate was 6 molecules per second. | 80 |
| Fig. 2.33 A segment of data which is collected when there should be only buffer in the probed volume..... | 81 |
| Fig. 2.34 Counting molecules based on the adjusted threshold, 6 molecules per second is expected..... | 82 |
| Fig. 2.35 Counting molecules based on the adjusted threshold, buffer only..... | 83 |
| Fig. 2.36 The comparison of expected, actual and background counts of molecules flowing out of the capillary..... | 85 |
| Fig. 3.1 Laser-induced fluorescence detector for one-spectral channel sequencing..... | 95 |
| Fig. 3.2 An example of peak height encoded single color DNA sequencing data | 98 |
| Fig. 3.3 Capillary gel electropherogram of M13mp18 reaction fragments: 6%T, 5% C-7M urea acrylamide gel..... | 100 |
| Fig. 3.4 Capillary gel electropherogram of M13mp18 reaction fragments: 6% T, 5% C, 6 M urea, 30% formamide acrylamide gel | 101 |
| Fig. 3.5a A sequencing run of M13mp18 with 30% by volume formamide was incorporated in the 6%T, 5%C, 7M urea acrylamide gel for separation | 103 |

| | |
|--|-----|
| Fig. 3.5b An expanded region corresponding to nucleotides 60-100. Note that the compression around GGGTACCG disappeared. | 104 |
| Fig. 4.1. Two laser-two collection optic fluorescence detector. | 110 |
| Fig. 4.2. One laser-two collection optic fluorescence detector..... | 112 |
| Fig. 4.3a..... | 115 |
| Fig. 4.3b | 116 |
| Fig. 4.3. Sequencing data for M13mp18 generated with the two-laser two-collection optic peak height encoded sequencing method..... | 117 |
| Fig. 4.4a..... | 120 |
| Fig. 4.4b | 121 |
| Fig. 4.4c..... | 122 |
| Fig. 4.4 Sequencing data for M13mp18 generated with the one-laser two-collection optic peak height encoded sequencing method..... | 123 |
| Fig. 5.1a The siphoning injector with a three way valve before and after injection, in a electrophoresis system and a sheath flow cuvette detector. | 142 |
| Fig. 5.1b The siphoning injector with a three way valve at the time of injection, in a electrophoresis system and a sheath flow cuvette detector. | 143 |
| Fig. 5.2 Controlling circuit for the three way valve | 144 |
| Fig. 5.3 Electropherograms for precision test of the hydrodynamic injector..... | 147 |
| Fig. 5.4 Peak height vs. water level difference Δh | 149 |
| Fig. 5.5 Electropherograms for peak shape comparison: (a) electrokinetic injection..... | 150 |
| Fig. 5.6 Comparison of two methods of injection: (a) electrokinetic injection | 152 |

List of Abbreviation

CE: capillary electrophoresis

CZE: capillary zone electrophoresis

IHP: inner Helmholtz plane

OHP: outer Helmholtz plane

MECC: micellar electrokinetic capillary chromatography

cmc: critical micelle concentration

SDS: sodium dodecyl sulfate

HPLC: high performance liquid chromatography

LC: liquid chromatography

SEC: size exclusion chromatography

UV: ultraviolet

DNA: deoxyribonucleic acid

FITC: fluorescein isothiocyanate

TRITC: tetramethylrhodamine isothiocyanate

He-Ne: helium-neon

N.A.: numerical aperture

PMT: photomultiplier tube

GreNe: green helium-neon

I.D.: inner diameter

O.D.: outer diameter

TBE: tris-borate-EDTA buffer

dNTP: deoxynucleoside triphosphate

ddNTP: dideoxynucleoside triphosphate

RSD: relative standard deviation

Part I

Laser induced fluorescence detection in capillary electrophoresis

Chapter 1 Introduction to Open Tubular Electrophoresis

Electrophoresis is the movement of suspended particles or molecules through a fluid or gel under the electric field applied to electrodes in contact with the suspension. If a mixture of dissolved substances is to be separated by electrophoresis, the ideal situation after the separation would be a procession of adjoining zones[1], each zone representing a pure component. Any attempt to achieve zone separation by this electrophoresis technique will be confounded by the onset of convection. According to Poiseuille's law, the pressure required to force a liquid through a capillary tube at a given velocity increases greatly as the radius of the tube decreases. Therefore convection can be suppressed by using a small bore capillary or using stabilizing media like cellulose or gels, and zone electrophoresis can be achieved.

Electrophoresis on slab gels is the most successful and most widely used separation method in protein and polynucleotide analysis. In conventional slab gel electrophoresis, proteins and polynucleotides are separated on gel coated sheets of glass. Although high quality separations are performed by gel electrophoresis, the separation is limited by the relatively poor cooling properties of the glass plate. Open tubular electrophoresis was first described in 1967[2] by Hjerten; the experiment was performed in a quartz tube of 3×7.8×360 mm. Open tubular capillary electrophoresis for zone separation of substances was described by Everaerts in 1970[3] and the power of this technique has been extensively demonstrated since the late 1970s and the early 1980s[4-8].

The number of research articles, with "capillary" AND* "electrophoresis" in their titles and abstracts, collected by Chemical Abstracts each year since 1966 is shown in Fig.1.1. Although not all of the papers on capillary electrophoresis can be found in this search strategy, the graph does show the trend of the development in this field. Before

* AND is a logic operator.

1970, the term capillaries usually refers to the microbores in the anticonvection media, and the papers dealing with real open tubular CE start to appear in 1970. By now in 1992, the power of this technique has attracted much attention in separation and microchemical analysis with its superior separation efficiency and small amount of sample required for analysis.

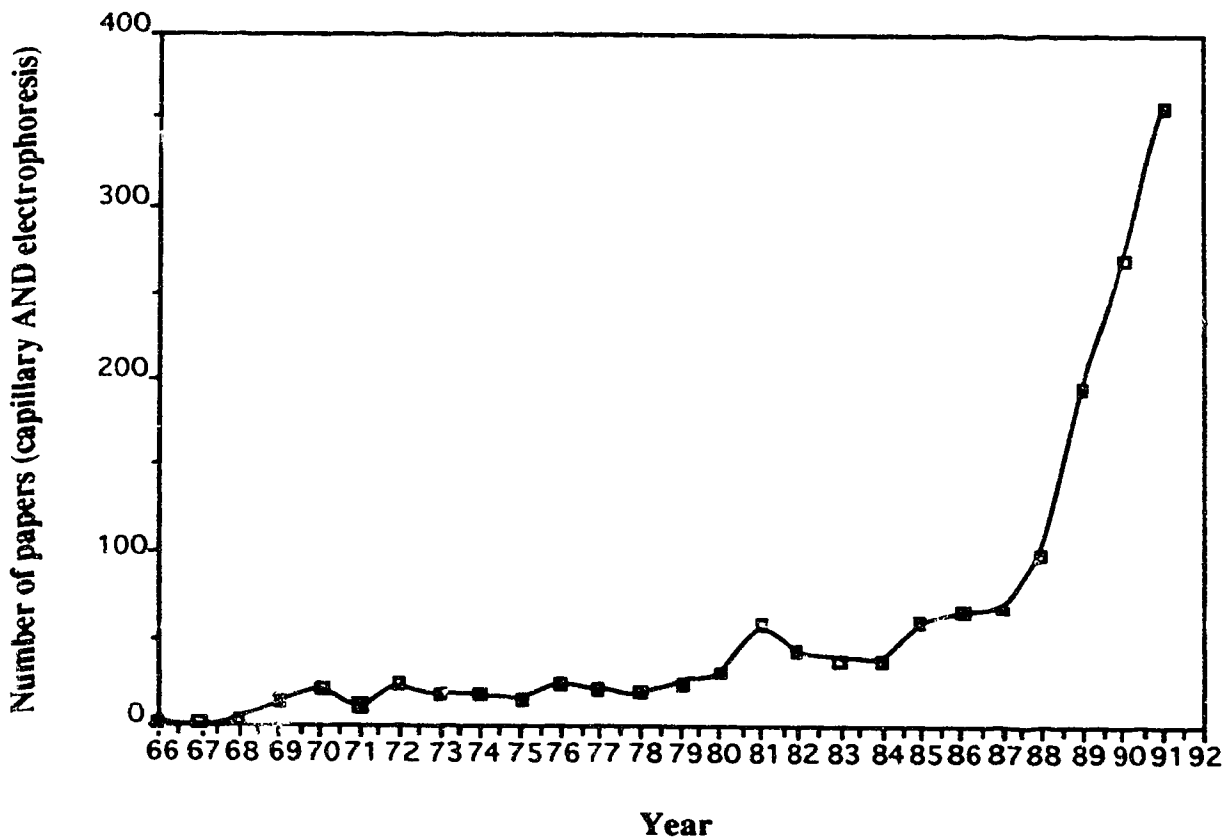


Fig. 1.1 Number of papers related to capillary electrophoresis published and collected in Chemical Abstracts in each year since 1966.

Open tubular capillary electrophoresis includes two kinds of methods: open tubular capillary electrophoresis[4, 5, 9] and micellar electrokinetic capillary chromatography[4, 5, 9]. Micellar electrokinetic capillary chromatography can be viewed as a modified method

of capillary free zone electrophoresis. They are similar in terms of instrumentations used, yet quite different in mechanism. These two methods will be discussed in detail later in this chapter.

1.1 The advantages of capillary electrophoresis compared with conventional electrophoresis methods

The major limitation in conventional electrophoresis is the temperature rise induced by the heat generated by passing of ionic current between two electrodes. Joule heating results in temperature gradients. The subsequent density gradients and convection increase zone broadening, affect electrophoretic mobilities and can even lead to evaporation or boiling of solvent. An advantage of capillary tubes is the enhanced heat dissipation relative to the volume of solution in the tube. The only route for heat dissipation is via the capillary wall. Small bore capillaries have large surface area-to-volume ratio and provide more efficient heat dissipation relative to large scale systems. This enhanced heat dissipation permits the use of very high electric fields, producing fast, efficient separations.

In addition to the enhanced heat dissipation, there are several other advantages to the use of capillaries for electrophoresis. First, convection is minimized in narrow tubes. Convection, of course, leads to mixing of samples and excess band broadening. Second, the ultrasmall volume flow rate obtainable in capillary electrophoresis permits sampling from microenvironments like a single cell[10-12], and the high sensitivity detectors developed for this method often have a mass detection limit much lower than any other method. Third, in capillary electrophoresis, electroosmosis is also important. Electroosmosis is the flow of solvent in a capillary when a tangential field is applied[13]. It is often strong enough to cause anions, neutral species, and cations to elute at the same end of the capillary. This property makes it possible to adapt the detectors that are well developed from column liquid chromatography.

1.2 Open tubular capillary zone electrophoresis

A schematic diagram of a simple system used for capillary zone electrophoresis (CZE) is shown in Figure 1.1. The main components of this system include two electrodes, a fused silica capillary, a high voltage power supply and a detector. The injection end of the system is confined in a Plexiglas box equipped with a safety interlock. The detector can be on column or post column at the end of the capillary. To understand this CZE system, the following concepts have to be understood first.

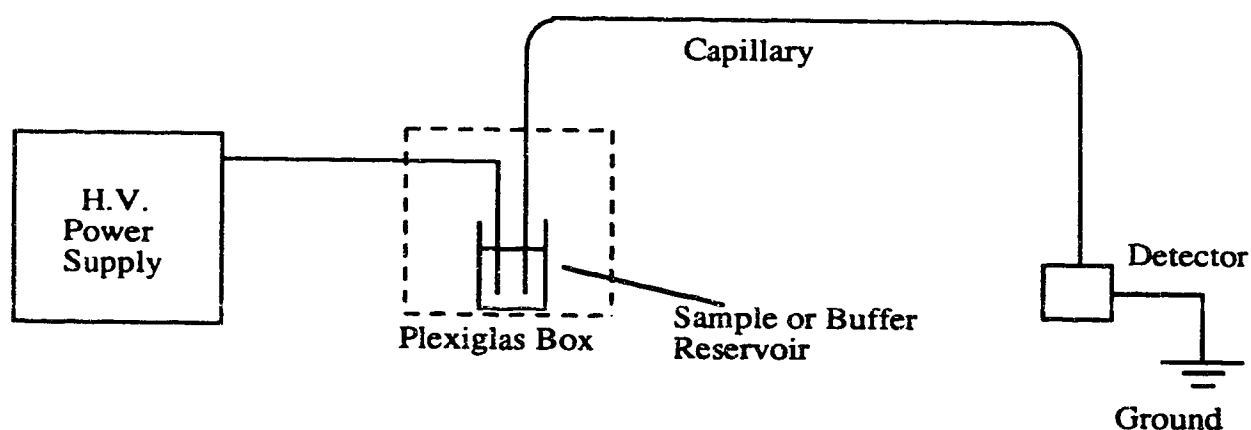


Fig. 1.2 Block diagram of a capillary electrophoresis system

1.2.1 Zeta (ζ) potential

When the capillary wall contacts an ionic solution, e.g. the buffer solution used in CZE, excess charges are produced by ionization of surface functional groups of the capillary wall (silanol groups, in the case, of fused silica capillary), these excess charges will lead to

different orientations for the molecules at the solid-liquid interface compared with the molecules in the bulk solution. Figure 1.3a shows the interaction of ions at the solid-liquid interface in a fused silica capillary. IEP is an analogy of the inner Helmholtz plane, the negative charges are formed from the ionization of surface functional groups; OHP represents the outer Helmholtz plane, which is the stagnant double layer. The diffuse layer is formed because of the thermal agitation in the solution, which extends from the OHP to the bulk of the solution[14]. Because the diffuse layer is further away from the surface charges, this layer is mobile. The sum of the potential differences from OHP to the bulk solution along the Y axis is defined as the ζ potential[15], as shown in Fig. 3b. The value of the ζ potential is different for different ionic species and for different capillary wall materials.

1.2.2 Electroosmosis

When an electric field is applied to the capillary along the X axis (Fig. 1.3), the cations (or, more generally, the counterions of the surface charge) in the diffuse layer will migrate toward the cathode (or anode, determined by the charge of ions in the diffuse layer). Because all of the cations are solvated in the diffuse layer, as illustrated in Figure 1.3, when they move, they will bring along the solvent molecules as well, so the solution in the capillary moves. This flow of solution induced by counterion movement is called electroosmosis. The flow rate of electroosmosis is determined by the value of the ζ potential, and can be calculated by:

$$v_{eo} = \mu_{eo} \times E \quad (1.1)$$

where v_{eo} is the electroosmotic flow rate, E is the electric field, and μ_{eo} is the electroosmosis mobility of a certain ionic species, which is determined by the ζ potential:

$$\mu_{eo} = \frac{\epsilon}{4 \pi \eta} \zeta \quad (1.2)$$

where ϵ is the dielectric constant of the solution and η is the viscosity.

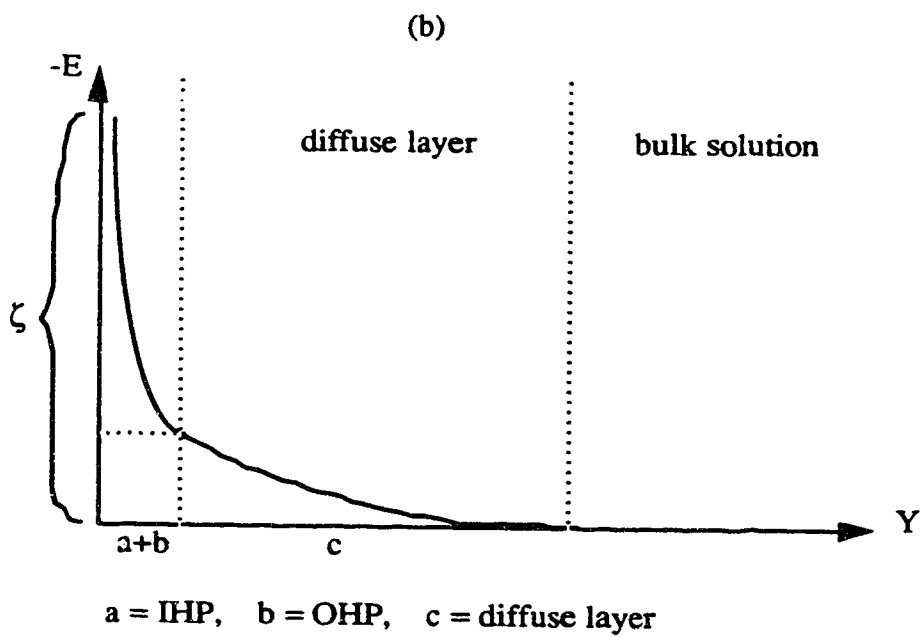
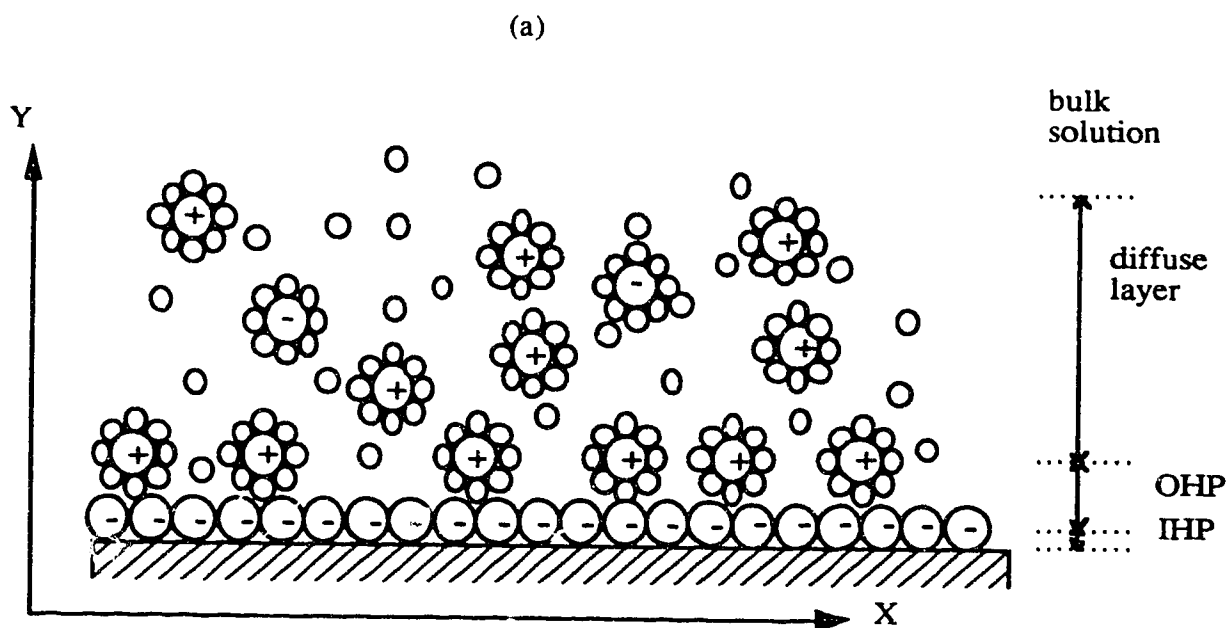


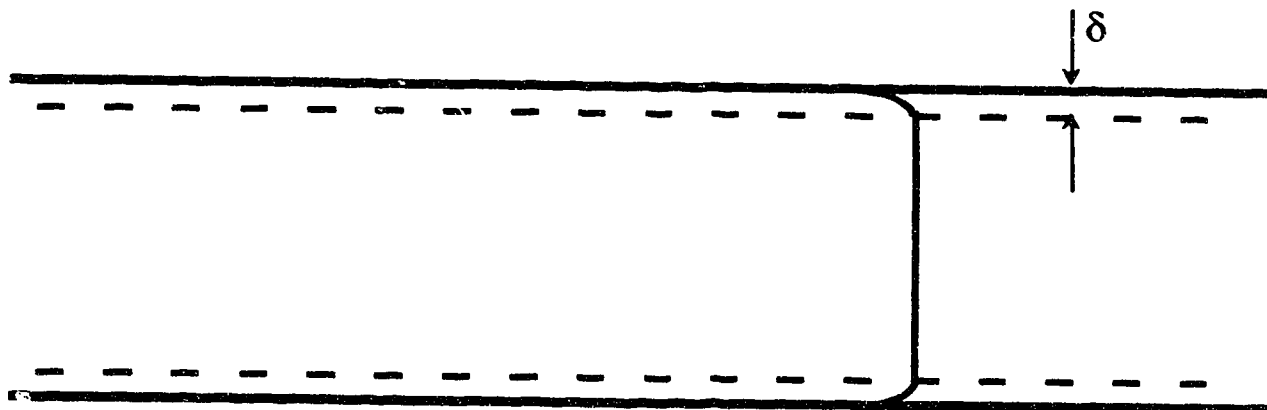
Fig. 1.3 Solid-liquid interface at the wall of capillary in CZE and zeta potential.

1.2.3 The flow profile

The thickness of the electric double layer is determined by the ionic strength of the electrolyte in the solution, according to Debye-Hückel theory.

$$\frac{l}{\kappa} = \frac{3 \times 10^{-8}}{\sqrt{\text{ionic strength}}} \text{ (cm)} \quad (1.3)$$

Where l/κ is the thickness of the diffuse layer. For solutions with electrolyte concentration ranging from 10^{-2} M to 10^{-6} M, the double layer will be from 3 to 300 nm in thickness. Since most of the time the double layer is very thin, the electroosmotic flow usually originates in the vicinity of the capillary wall. Because there is no stationary phase in the capillary, the flow profile will be flat, as long as the capillary radius is more than 7 times the thickness of the double layer[16]. The flat flow profile greatly reduces the band broadening during the separation process. Fig 1.4 shows a illustration of a flat flow profile in capillary electrophoresis.



δ is the thickness of the diffuse layer

Fig. 1.4 Flat flow profile in CE; the curved part is the double layer, which is usually a few nanometers in thickness and can be neglected in practice.

1.2.4 Electrophoretic migration

The migration of ions under an electric field in a solution is called electrophoretic migration. The migration velocity of the ions in electrophoresis is given by:

$$v_{ep} = \mu_{ep} \times E = \frac{\mu_{ep} V}{L_c} \quad (1.4)$$

where μ_{ep} is the electrophoretic mobility, E is the electric field as defined before, V is the driving voltage used in electrophoresis, and L_c is the length of capillary.

The time of the electrophoretic migration t_m can also be calculated:

$$t_m = \frac{L_c}{v_{ep}} = \frac{L_c^2}{\mu_{ep} V} \quad (1.5)$$

It can be seen that the electrophoretic migration time is proportional to the square of the length of capillary when the same voltage is applied.

1.2.5 The flow rate in CZE

In capillary zone electrophoresis, both electrophoretic migration and electroosmotic flow should be considered in the separation process. The velocity of sample flow from one end to the other will be determined by:

$$v = \frac{(\mu_{ep} + \mu_{eo}) V}{L_c} \quad (1.6)$$

and the time necessary for the sample to move from one end of the capillary to the other in this process is:

$$t = \frac{L_c^2}{(\mu_{ep} + \mu_{eo}) V} \quad (1.7)$$

In these two equations the mobility is a combination of the electrophoretic mobility and the electroosmotic mobility. It is clear that, if μ_{eo} is greater than μ_{ep} for every solute, then all the sample components will be eluted at the same end of the capillary.

1.2.6 Separation efficiency

The band broadening contributed by diffusion during the separation can be calculated from the Einstein's law of diffusion:

$$\sigma^2 = 2 \times D \times t = \frac{2 D L_c^2}{(\mu_{ep} + \mu_{eo}) V} \quad (1.8)$$

where σ^2 is the variance induced by longitudinal diffusion, D is the diffusion coefficient of the solute, and t is the time allowed for the sample to diffuse, which is the retention time of the sample in CZE.

When diffusion is the dominant factor for band broadening in CZE, which mostly is the case, the number of theoretical plates can be calculated by:

$$N = \frac{L_c^2}{\sigma^2} = \frac{(\mu_{ep} + \mu_{eo}) V}{2 D} \quad (1.9)$$

where N is the number of theoretical plates. We can see, from equation 1.8, that the number of theoretical plates is independent of the length of capillary.

Standard methods can also be used to estimate the number of theoretical plates,

$$N = 5.54 \left(\frac{t_r}{W_{1/2}} \right)^2 \quad (1.10)$$

where t_r is the retention time for a certain solute and $W_{1/2}$ is the full peak width at half height.

1.2.7 Resolution

There are two kinds of flow in capillary zone electrophoresis as discussed before. Electroosmosis is not specific, the whole solution inside the capillary moves when an electric field is applied. Ions of different kinds are separated only by the differences in their electrophoretic migration. The resolution of two solutes in CZE is given by:

$$R = \frac{1}{4} N \frac{\Delta v}{v^*} \quad (1.11)$$

where R is the resolution, N is the average theoretical plates, Δv is the difference in the moving velocity of the two solute zones, and v^* is the average zone velocity.

Substituting equation (1.6) and (1.9) into equation (1.11), gives:

$$R = \frac{\sqrt{2}}{8} (\mu_{ep,1} - \mu_{ep,2}) \left[\frac{V}{D (\mu_{ep}^* + \mu_{eo})} \right]^{\frac{1}{2}} \quad (1.12)$$

where $\mu_{eo,1}$ and $\mu_{ep,2}$ are the electrophoretic mobilities for the two solutes and μ_{ep}^* is the average electrophoretic mobility.

The resolution can also be estimated by the same equation in chromatography:

$$R = \frac{t_{r,1} - t_{r,2}}{\frac{1}{2} (W_1 + W_2)} \quad (1.13)$$

where $t_{r,1}$ and $t_{r,2}$ are the retention times for solute 1 and solute 2 respectively, W_1 and W_2 are the base-line peak-widths in unit of time.

1.2.8 Discussion

For a separation technique, it is highly desirable that the instrument has a high number of theoretical plates, high resolution and a short time for separation. Equation (1.6) shows that the time will be shorter with higher electrophoresis voltage and a shorter capillary; equation (1.8) shows that the number of theoretical plates will be higher when higher voltage is applied and is independent of the capillary length; and equation (1.11) shows that the resolution is proportional to the square root of the separation voltage. From these statements it can be concluded that, theoretically, a short capillary plus high voltage will produce an extremely good separation efficiency. However, there are some practical limitations that have to be considered. The electrical heating and the establishment of a parabolic temperature gradient across the tube are the principal limitations to the use of high voltages and short capillaries. The ability of the capillary to dissipate the heat, which is generated by passing of electrical current per unit length of the capillary, is given by[17]:

$$\frac{P}{L_c} = \frac{r^2 V^2 K C}{L_c^2} \quad (1.14)$$

where P is the power generated by the electrical current, L_c is the capillary length, K and C

are the molar conductance and concentration of the buffer solution, respectively, r is the radius of the capillary, and V is the voltage applied in electrophoresis.

This equation shows that better heat dissipation requires longer length capillary with a smaller radius, lower ionic strength, and lower applied voltage. Many conditions have to be considered when choosing a suitable length of capillary and voltage for electrophoresis regarding the separation time, separation efficiency and heat dissipation.

On the other hand, using capillaries with smaller radius is often advantageous in CZE. The parabolic temperature gradient is minimized because of the diffusion of the solute across the small cross section of capillary tube; the medium is stabilized against convective flow by the wall effect, and the heat dissipation is enhanced due to the increased surface-to-volume ratio.

1.3 Micellar electrokinetic capillary chromatography

Micellar electrokinetic capillary chromatography (MECC) is a modified technique of capillary zone electrophoresis [18, 19]. In CZE, neutral molecules can not be separated because their electrophoretic mobility is zero in an electric field. Adding micellae into the system offers a pseudostationary phase in the capillary tube, which allows the neutral molecules to be separated due to the differential distribution of the different neutral molecules in the added micellar phase. In addition, because surfactant is added to the system, there is less chance of solute being adsorbed on the capillary wall, tailing in some analyte peaks can be reduced.

1.3.1 The principle of MECC

Adding surfactant into the buffer solution used in capillary zone electrophoresis is an important modification to CZE. The separation of neutral molecules is realized while the

advantages of the CZE format[18-20] is retained. When the concentration of the ionic surfactant added exceeds the critical micelle concentration (cmc), the monomers of surfactant form roughly spherical aggregates called micellae. Usually the hydrophobic tails of these surfactants orient toward the centre of the micelle with the charged heads pointing toward the surface. If more surfactant is added, there will be more micellae formed, while the concentration of monomer remains at about cmc.

The surfactant mostly used in MECC is sodium dodecyl sulfate (SDS), which is an anionic surfactant. After SDS is added into the buffer solution, two phases exist inside the capillary: one is the aqueous phase, the other is micellar phase. Because of the orientation of the surfactant molecules, the surfaces of the SDS micellae have a large negative net charge. Under the electric field, these micellae have a large electrophoretic mobility toward the anode. At the same time, most aqueous buffer solutions have strong electroosmotic flow toward the cathode. Usually, the magnitude of the electroosmotic mobility of the solution is higher than electrophoretic mobility of the micellae, so the micellae will still move toward the cathode, but with a slower flow rate. The neutral molecules will partition between the two phases, and they can be separated if their solubility in the micellar phase is different. If the solute is more soluble in the micelle, it moves slower due to the longer time spent in the micellar phase; if the solute is less soluble in the micellar phase, it moves faster, for it spends more time in the aqueous phase.

In conventional chromatography, the sample species partition between stationary phase and mobile phase and the retention of a solute can be described by the retention time and the capacity factor:

$$t_r = (1 + k') t_0 \quad (1.15)$$

and

$$k' = \frac{t_r - t_0}{t_0} \quad (1.16)$$

where t_r is the retention time, t_0 is the void time, and k' is the capacity factor, which is the ratio of the total moles of solute in the stationary phase to those in the mobile phase.

The situation is not the same in MECC, because the solutes partition between two mobile phases. For neutral molecules, t_0 refers to the elution time for the aqueous part of the buffer solution, and t_r refers to the retention time for the micellae. Equations (1.15) and (1.16) have to be modified to describe the retention of solutes in MECC⁽¹⁸⁾:

$$t_r = \frac{(1 + k'') t_0}{1 + \left(\frac{t_0}{t_{mc}}\right) k''} \quad (1.17)$$

and

$$k'' = \frac{t_r - t_0}{t_0 \left(1 - \frac{t_r}{t_{mc}}\right)} \quad (1.18)$$

where k'' is used for capacity factor to emphasize the difference from conventional chromatography; t_0 and t_{mc} are the retention times of the aqueous and micelle phases, respectively. The terms $[1 + (t_0/t_{mc})k'']$ and $[1 - t_r/t_{mc}]$ in equations (1.17) and (1.18) account for the moving pseudostationary phase. If the t_{mc} goes to infinity, equation (1.17) and (1.18) will be the same as the equations used for conventional chromatography. The parameters t_0 and t_{mc} can be determined by injecting methanol, which is assumed to be insoluble in the micellae, and Sudan III, an organic dye which is totally solvated in the micellar phase.

Resolution in MECC is given by:

$$R = \frac{N^{\frac{1}{2}}}{4} \left(\frac{\alpha - 1}{\alpha} \right) \left(\frac{k_2''}{k_2'' + 1} \right) \left(\frac{1 - \frac{t_0}{t_{mc}}}{1 + \left(\frac{t_0}{t_{mc}}\right) k_1''} \right) \quad (1.19)$$

where α is the selectivity factor (k_2''/k_1''), N is the average number of theoretical plates, and the last term of this equation accounts for the pseudostationary phase. If the t_{mc} is infinity, equation (1.19) will have the same form as conventional chromatography.

1.3.2 Parameters affecting efficiency in MECC

Based on equations (1.17), (1.18) and (1.19), we can see some factors that could affect the number of theoretical plates, N , and the resolution, R . Retention time, t_r , can be

affected through t_0 and t_{mc} , by the changes in applied voltage, column dimensions, buffer concentrations, temperature, surfactant concentrations, etc. The voltage, time and other conditions of sample injection can also affect N .

In addition to the factors mentioned above, the resolution, R , will also be affected by the selectivity α , while α is determined by the kind of surfactant used in MECC, and by the pH of the aqueous buffer solution. The pH determines whether the solute will be neutral molecules and selectivity α is determined by the partition coefficient of each solute which has lot to do with the charges the molecules have. In general terms, the total plate height H for MECC can be given by the expression[21, 22]:

$$H = H_L + H_S + H_{M,m} + H_{M,c} + H_T \quad (1.20)$$

where the H_L is the longitudinal diffusion, H_S is the resistance to mass transfer in pseudostationary phase, $H_{M,m}$ is the resistance to mass transfer in mobile phase (intermicelle), $H_{M,c}$ is the intracolumn resistance to mass transfer in mobile phase, and H_T is the thermal dispersion. Van Deemter type plots of plate height versus applied voltage can be constructed to describe the effects of parameters on separation efficiency.

1.3.3 Discussion

Usually neutral species are separated by HPLC, micellar LC and size exclusion chromatography (SEC). MECC offers an important alternative for this kind of separation with superior separation efficiency in very short time. It is an interesting hybridization of CZE, HPLC, micellar LC, and SEC. The separation window is determined by t_0 and t_{mc} , which means samples start to be eluted from t_0 , which is the time needed for aqueous buffer to elute, and end at the time of t_{mc} , the time needed for micellae to elute.

MECC also has the ability to separate ionic species. The interaction between ionic species and micellae can be electrostatic attraction or repulsion and the hydrophobicities of the solutes. Of course, the same as in CZE, these ionic solutes will also experience electrophoresis and electroosmosis. The mechanism for the separation of ionic species in

MECC is more complicated. MECC has been successfully used for separation of amino acids and proteins in this research group[23-25].

References:

1. Haglund, H. and Tiselius, A., *Acta Chem. Scand.*, (1950), **4**: p. 957.
2. Hjerten, S., *Chromatographic Reviews*, (1967), **9**: p. 122.
3. Everaerts, F.M. and Hoving, K.W.M.L., *Sci. Tools*, (1970), **17**(1): p. 25.
4. Jorgenson, J.W. and Lukacs, K.D., *Anal. Chem.*, (1981), **53**(8): p. 1298.
5. Jorgenson, J.W. and Lukacs, K.D., *Science (Washington, D. C.)*, (1983), **222**(4521): p. 266.
6. Kuhr, W.G., *Anal. Chem.*, (1990), **62**(12): p. 403R.
7. Wallingford, R.A. and Ewing, A.G., *Adv. Chromatogr. (N. Y.)*, (1989), **29**, p. 1.
8. Kuhr, W.G. and Monnig, C.A., *Anal. Chem.*, (1992), **64**: p. 389R-407R.
9. Mikkers, F.E.P., Everaerts, F.M., and Verheggen, T.P.E.M., *J. Chromatogr.*, (1979), **169**: p. 11.
10. Wallingford, R.A. and Ewing, A.G., *Anal. Chem.*, (1987), **59**(4): p. 678.
11. Wallingford, R.A. and Ewing, A.G., *Anal. Chem.*, (1988), **60**: p. 1972.
12. Ewing, A.G., Wallingford, R.A., and Olefirowicz, T.M., *Anal. Chem.*, (1989), **61**(4): p. 292A.
13. Rice, C.L. and Whitehead, R., *The Journal of Physical Chemistry*, (1965), **69**(11): p. 4017.
14. Bard, A.J. and Faulkner, L.R., *Electrochemical Methods*. 1980, Jhon Wiley, New York.
15. Adamson, A.W., *Physical Chemistry of Surfaces*. 2 ed. 1967, Interscience, New York, Chapter 4.
16. Stevens, T.S. and Cortes, H.J., *Anal. Chem.*, (1983), **55**: p. 1365.
17. Lukacs, K.D. and Jorgenson, J.W., *J. High Resolut. Chromatogr. Chromatogr. Commun.*, (1985), **8**(8): p. 407.

18. Terabe, S., Otsuka, K., Ichikawa, K., Tsuchiya, A., and Ando, T., *Anal. Chem.*, (1984), **56**(1): p. 111.
19. Burton, D.E., Sepaniak, M.J., and Maskarinec, M.P., *J. Chromatogr. Sci.*, (1986), **24**(8): p. 347.
20. Terabe, S., Otsuka, k., and Ando, T., *Anal. Chem.*, 1985. **57**: p. 834.
21. Foley, J.P., *Anal. Chem.*, (1990), **62**, 1302 .
22. Sepaniak, M.J. and Cole, R.O., *Anal. Chem.*, (1987), **59**(3): p. 472.
23. Waldron, K.C. and Dovichi, N.J., *Anal. Chem.*, (1992), **64**: p. 1396.
24. Zhao, J.Y., Chen, D.Y., and Dovichi, N.J., *J. Chrom.*, 1992. **608**: p. 117.
25. Zhao, J.Y., Waldron, K.C., Miller, J., Zhang, J.Z., Harke, H., and Dovichi, N.J., *J. Chrom.*, 1992. **608**: p. 239.

Chapter 2. High Sensitivity Fluorescence Detectors*

The ultrasmall sample volume used in capillary electrophoresis requires high sensitivity detectors. Different kinds of detectors can be employed for this purpose. Mass spectrometry[1, 2], electrochemistry[3-5], UV-Visible absorbance [6, 7], radioactive isotopes[8], laser induced thermo-optical absorbance techniques[9-12] and laser induced fluorescence[13-15] are among the most often used detection methods.

Laser induced fluorescence is particularly interesting because the detection sensitivity extends to near the single molecule level in favorable cases. A detection limit of 10^{-21} mole has been reported for amino acids labeled with fluorescein isothiocyanate, separated by capillary electrophoresis[14]. The high sensitivity detector introduced here is also a fluorescence detector.

2.1 Low cost, high sensitivity laser induced fluorescence detection

Fluorescence detection is often adapted for use in capillary electrophoresis because of its high sensitivity. Laser light is most amenable to focusing in small areas, which leads to very high mass sensitivity for fluorescence detection. Different kinds of lasers, such as helium cadmium lasers[16-19] and argon ion lasers[14, 20, 21] have been used extensively by different groups. Some criteria must be met in choosing the laser. First, for sensitive detection, the laser intensity must be stable, so that the performance of the detector is only limited by shot noise in the fluorescence signal. Second, the wavelength of the laser must match the absorbance spectrum of the analyte.

Since most analytes do not fluoresce, labeling the sample with fluorescent dyes is often necessary. The samples most frequently used in this respect can be different biochemical molecules like amino acids, peptides, proteins, oligonucleotides and DNA

* Part of this chapter has been published in *Journal of Chromatography*, 559 (1991) 237-246

molecules. Many derivatization strategies have been employed including dansyl (DNS)[22], o-phthal-aldehyde (OPA)[23], naphthalenedialdehyde (NDA)[24], fluorescein isothiocyanate (FITC)[25], and fluorescamine[17]. In this chapter, another fluorescent label, tetramethylrhodamine isothiocyanate (TRITC), will be used as an example in high sensitivity fluorescence detection.

TRITC, as a fluorescent label, was first used in immunology in 1962[26]. The maximum absorption of TRITC, with a relatively wide band, is centered at about 555 nm in water solution, and the maximum fluorescence is centered at about 573 nm. The absorption and fluorescence spectra have been measured and are shown in Figures 2.1 and 2.2. The absorption spectrum was measured with a UV-Vis spectrophotometer (8451A Diode Array Spectrophotometer, Hewlett Packard), and the fluorescence spectrum was measured with a fluorescence detector (Heath), when the sample (TRITC solution) was excited at the wavelength of 555 nm.

The advantages of TRITC conjugates in immunology studies was demonstrated by Brandtzaeg in 1977[27]. Anionic-exchange fractions of IgG labeled with FITC, TRITC, RB200SC, and rhodamine B isothiocyanate (RBITC) were tested on different substrates, and the resultant fluorescence was evaluated. Conjugations with TRITC were found to be three times more sensitive than FITC on a molar basis. In addition, there was negligible fading of emitted light, and negligible tissue autofluorescence at the excitation wavelength.

TRITC has been used to label molecules with molar weight larger than 10,000 in fluorescence microscopy, but has not been used in amino acid determination at the time of this study. Using TRITC as a label should have the following advantages:

- 1) High sensitivity amino acid determination.
- 2) Can be excited by a low cost green He-Ne laser.
- 3) Might be used in Edman degradation analysis of amino acid sequence in proteins and peptides.
- 4) Can be used as a label for DNA segments in DNA sequencing.

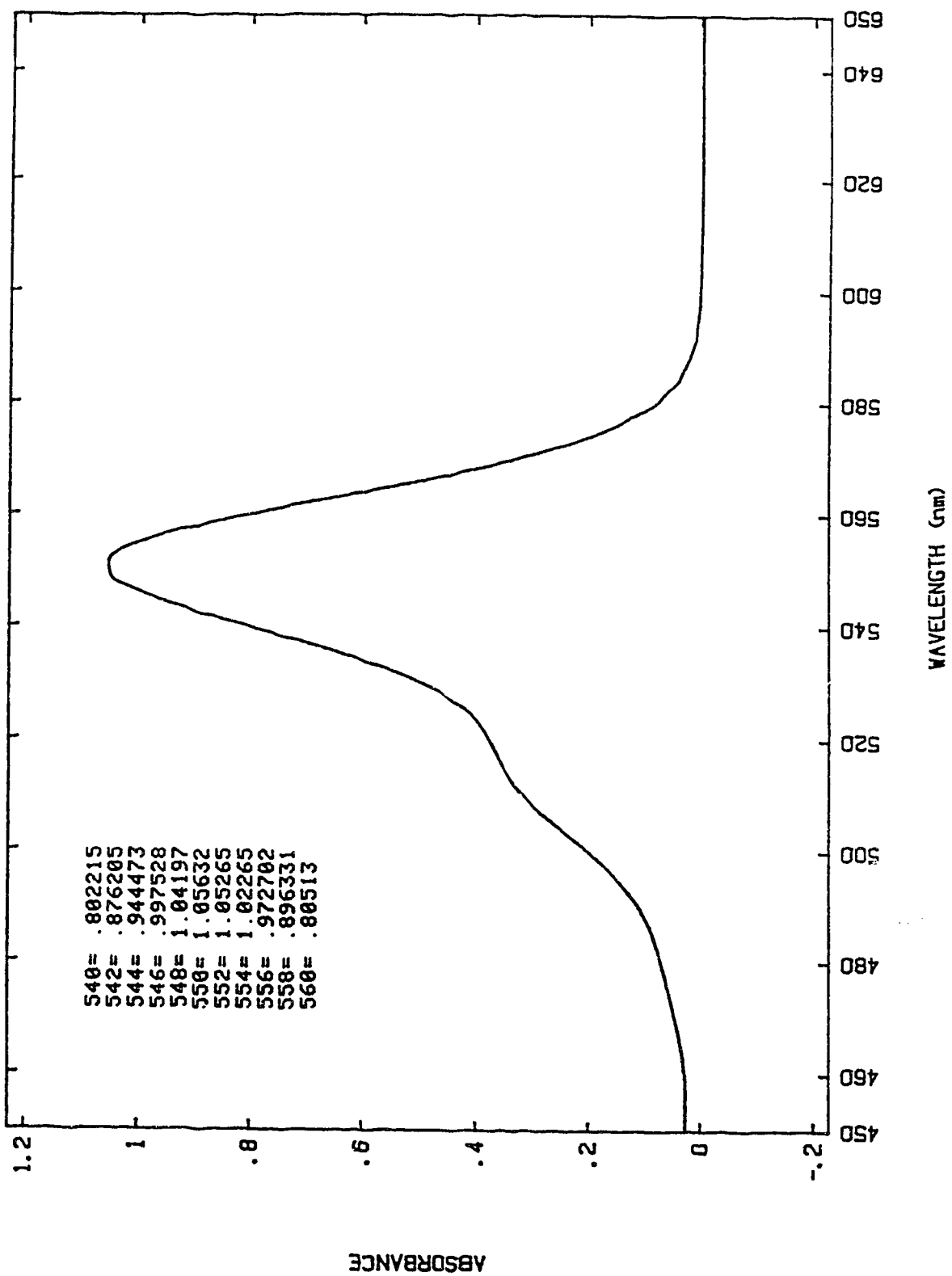


Fig. 2.1 The absorption spectrum of TRITC

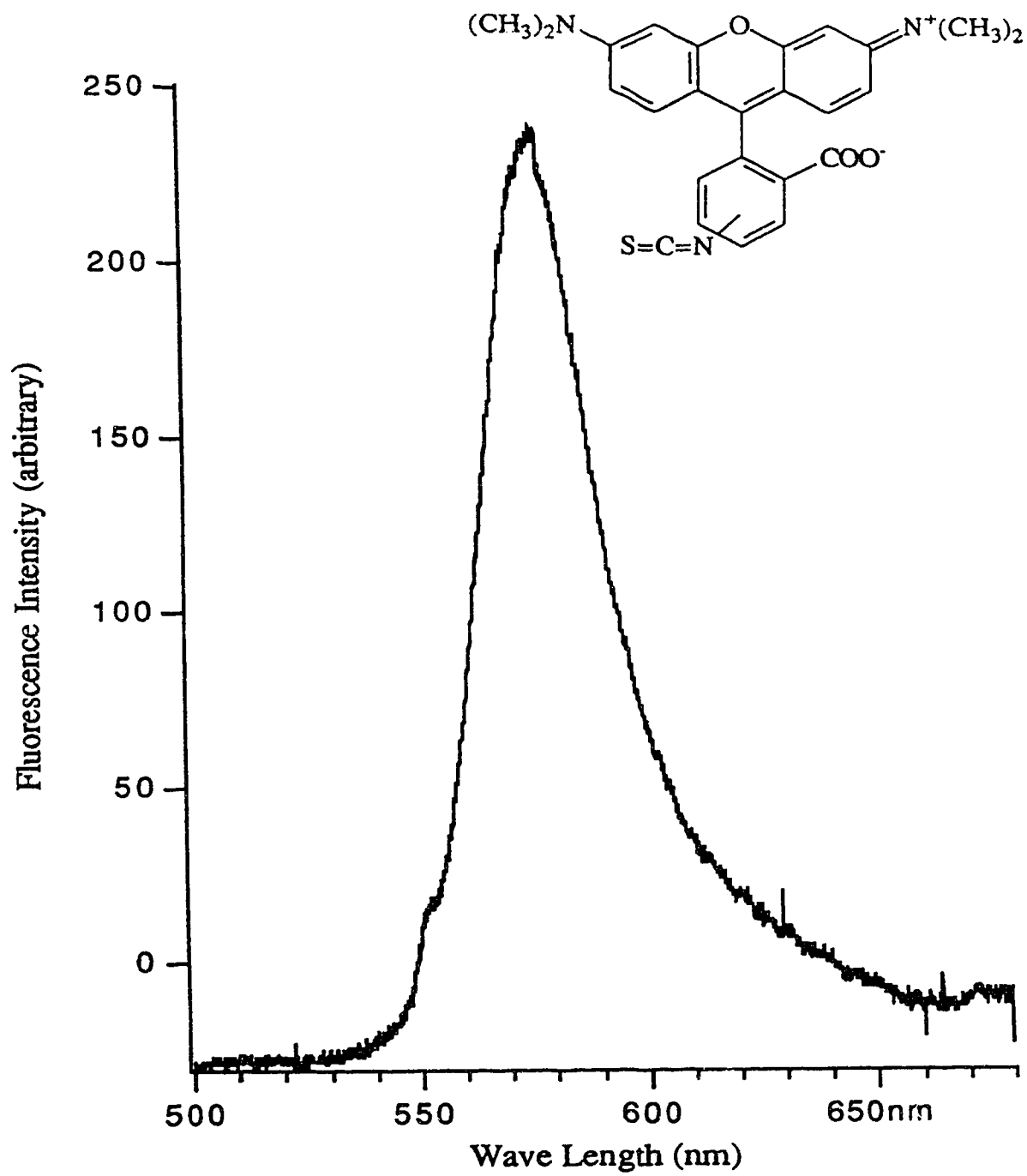


Fig. 2.2 The fluorescence spectrum of TRITC

Amino acids derivatized with TRITC have an absorbance maximum at about 555 nm in water solution. Because of the relatively wide absorption band, a low cost 543.5 nm wavelength He-Ne laser is a good match as an excitation source. Other criteria for choosing lasers are subtle. Raman scatter from the solvent and spatial mode quality of the laser need to be considered.

2.1.1 The Detector

A laser induced fluorescence detector (Figure 2.3) consists of a laser, a focusing lens, a sheath flow cuvette, collection optics, a spectral filter and a photodetector.

Optical design

The design of the system is guided by two principles. First, the instrument should use the minimum number of components to make it simple and robust. By reducing the components and by simplifying the instrument design, the cost, reliability, stability and ease of use for the instrument will be improved. Second, the instrument should be designed to maximize the collection of photons generated by fluorescence while minimizing the background signal intensity. To collect the maximum fluorescence signal while at the same time avoiding as much of the excitation source as possible, the collection optics were designed to be perpendicular to the laser beam.

The Laser

Helium-Neon lasers can be operated at a wavelength of 543.5 nm. The molar absorptivity of TRITC is quite high at this wavelength, about $82,000 \text{ M}^{-1}\text{cm}^{-1}$, although the maximum absorption occurs at 555 nm. This laser is very stable, relatively low cost, small in volume, easy to use, and has long lifetime. These properties are highly desirable

for an excitation source. The detailed information about the laser used in the fluorescence detector is listed in Table 2.1.

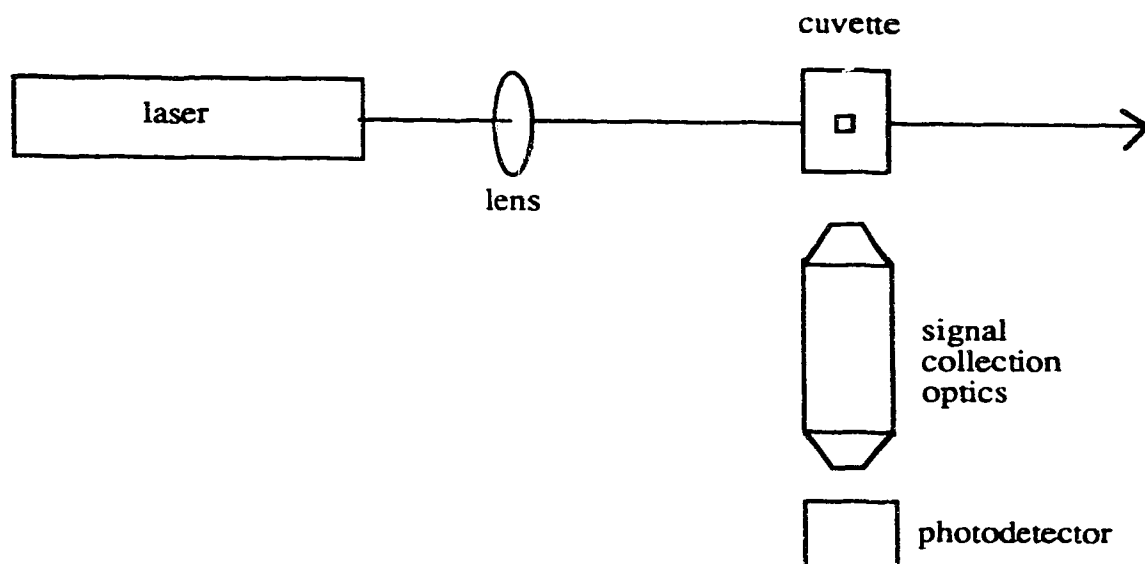


Fig. 2.3 Block diagram of the laser induced fluorescence detector

Although this laser operates at low power, 0.75 mW, high sensitivity fluorescence measurements are still possible. The relationship between laser power and fluorescence signal was discussed before [14]. Even though high power is valuable in fluorescence measurements, the power and irradiance (Wcm^{-2}) of the beam cannot be increased without bound. At high irradiance levels, optical saturation and photobleaching become significant. To avoid these problems, for highly fluorescent dye molecules, the laser irradiance should be held to a value less than 10^5 Wcm^{-2} at the sample. In the instrument developed here, the He-Ne laser produces an irradiance of about 100 Wcm^{-2} . This irradiance may not be the

optimized value, but because of the extremely low background, excellent detection limits can be obtained.

Table 2.1 Properties of 0.75 mW He-Ne laser used in the experiment

| | | | |
|---|-----------------------------|---|------------------|
| Manufacturer | Melles Griot | Model Number | 05LGR173 |
| Wavelength (nm) | 543.5 | TEM ₀₀ Power(mW) | 0.75 |
| Beam Diameter mm at e ⁻² points | 0.75 | Beam Divergence(Mrad, full angle) | 0.92 |
| Beam Amplitude Noise(%RMS, 0- 100 kHz) | 0.5 | Long term Amplitude stability (% change in a day) | 2.5 |
| Polarization | Random | Electrical Input | 2750 Vdc, 6.5 mA |
| Special Features | Hard Sealed Construction | | |

The sheath flow cuvette

To avoid extra-column band broadening, on-column detection seems to be most appropriate in capillary electrophoresis. However, fluorescence detection using the capillary as the detection chamber is difficult. Light scattering generated by the air- column and column-sample interfaces results in large background signals in fluorescence detection. This scattered light can be reduced in several ways. First, an obscuration bar can be introduced in the plane perpendicular to the capillary surface to block much of the scattered light[28]. Unfortunately, much of the fluorescence will also be blocked by this bar.

Second, the capillary can be tilted with respect to the laser beam and the detection optics[29], so that the scattered light is deflected away from the collection optics. Third, the capillary can be tilted at Brewster's angle, and a polarized laser beam can be used so that the scattered light originated at the air-column interface is extinguished[30]. Unfortunately, in each case aberrations will inevitably degrade the fluorescence signal, because it is necessary to image the fluorescence through the curved capillary wall. In every case, light scattering originating at the column-sample interface will contribute significantly to the background fluorescence signal.

Rather than detecting fluorescence directly on the capillary, it is possible to use a sheath-flow cuvette (Figure 2.4) for fluorescence detection[13]. The capillary is introduced into a 200 μm square sheath flow chamber constructed from good optical quality quartz. A sheath stream, provided by a high stability syringe pump, surrounds the sample stream at the exit of the capillary. The outer diameter of the capillary is 189 μm . At the very low flow rates employed in electrophoresis, the flow inside the capillary is laminar. The sheath stream has the same composition as the separation buffer and is connected to electrical ground to complete the circuit for the electrophoresis. Because the sample and the sheath have identical composition, no light scatter occurs at their interface, greatly reducing the background signal. The size of the sample stream is determined by both the relative volumetric flow rates of the sample and sheath stream[31] and the diffusion rate of the analytes into the sheath stream.

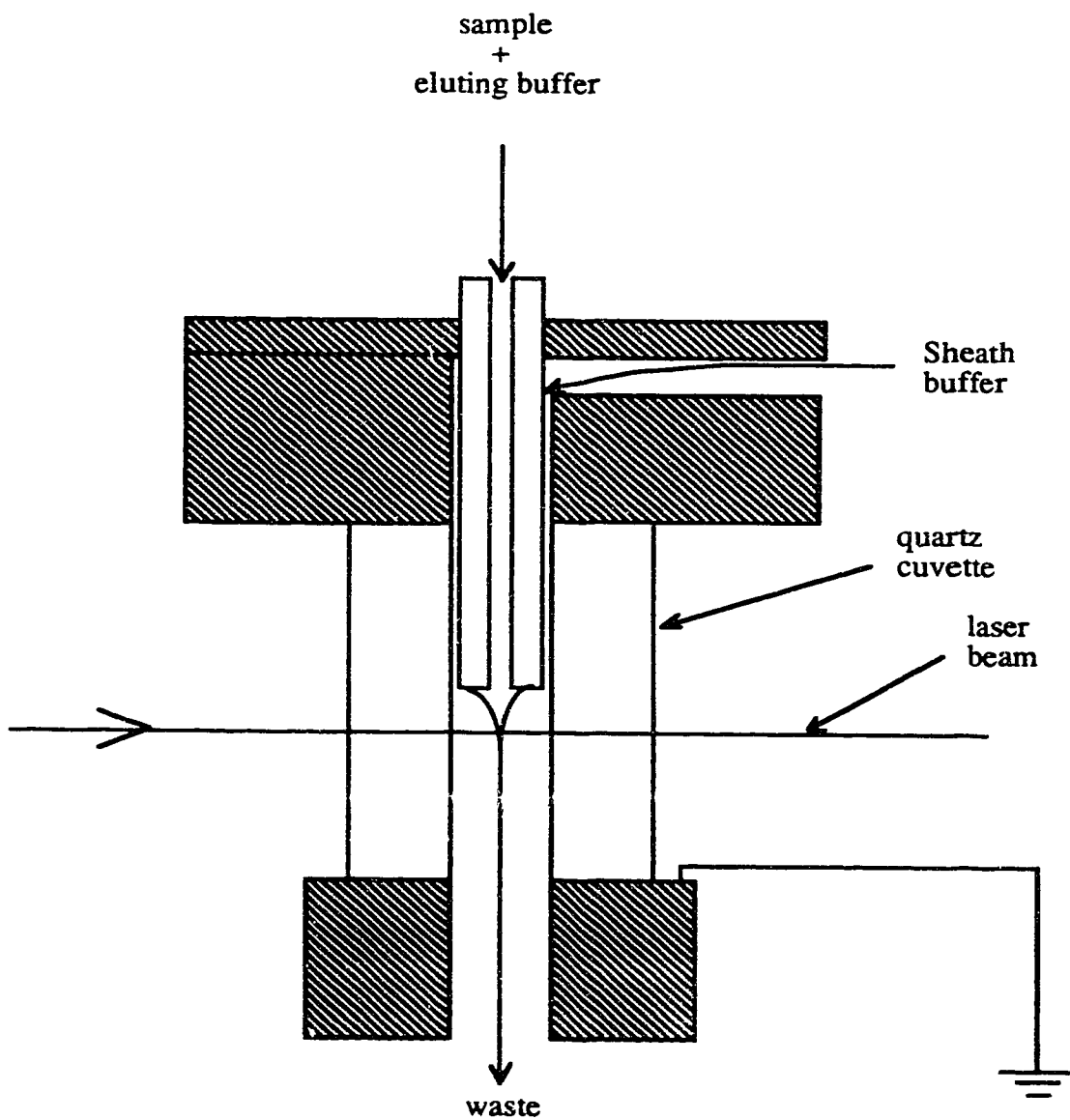


Fig. 2.4 The capillary and sheath flow cuvette in laser induced fluorescence detection.

Collection optics

The fluorescence generated from the illuminated sample stream must be collected with high efficiency, while scattered light reaching the detector must be minimized in order to obtain optimum detection limits. The fraction of light collected by a lens is related to its numerical aperture, N.A., and the refractive index of the surrounding medium, n , and is given by [14]:

$$\text{Collection Efficiency} = \sin^2 \left[\frac{\arcsin (N.A. / n)}{2} \right] \quad (2.1)$$

where a collection efficiency of 1 implies that the lens collects all of the photons emitted by the molecules. Usually, the lens is surrounded by air and $n = 1.0$. A lens with a numerical aperture of 1 will collect half of the light emitted by the sample. The collection efficiency may also be presented in terms of ray f-number which is equal to $1/(2N.A.)$. One of the best systems to obtain high collection efficiency is a microscope objective.

To choose a microscope objective, other conditions regarding the sheath flow cuvette have to be considered. Fluorescence must be imaged from a small region in the center of the sheath flow cuvette. However, the cuvette is equipped with relatively thick windows, typically 2 mm, which requires the use of an objective with a working distance of greater than 2 mm. Unfortunately, few microscope objectives are designed with both high numerical aperture and long working distances. The objective chosen had a numerical aperture of 0.45 and a working distance of 4.2 mm. Collection efficiency is about 5%. Expensive objectives with higher numerical aperture and the required working distance are available for optimizing the system in future work.

A pinhole is placed in the image plane of the objective lens to isolate the image of the illuminated sample region while rejecting light scattered from the cuvette walls. The size of the pinhole matches the size of the image of the illuminated region. For a 20 μm diameter sample stream with a 18 \times objective lens, a pinhole of 400 μm in diameter is used.

If the pinhole is too small, part of the signal will be blocked, yet if the pinhole is too big, the background may be increased.

Spectral Filter

If the appropriate laser wavelength has been chosen, the fluorescence will have a minimal spectral overlap with Raman and Raleigh scatter. Either a monochromator or a spectral filter may be used to spectrally isolate the fluorescence from the background scattered signal. A spectral filter is favored in this case for simplicity and high transmission at the selected wavelength.

Some interference filters are specially designed to allow a weak fluorescence signal to pass while discriminating an intense background of excitation light. These filters are designed with six interfering cavities which create a nearly rectangular passband with extreme out of band rejection. Full band-width at one part per million of transmittance is merely twice the full width at half height of the maximum transmission. With full-widths at half-height from 10 to 100 nm, this bandpass profile allows detection of low level signals within 10 nm from a very strong background. Using these filters, wide emission bands can be isolated from their excitation source.

The spectral filter used in this detector is a interference filter with a bandpass from 570 to 610 nm, which provides high transmission in this region (>70%). The spectrum of this filter is shown in Figure 2.5. It was placed between the objective lens and the pinhole so that the light from the microscope objective converges slowly and produces negligible deviation in the spectral band pass.

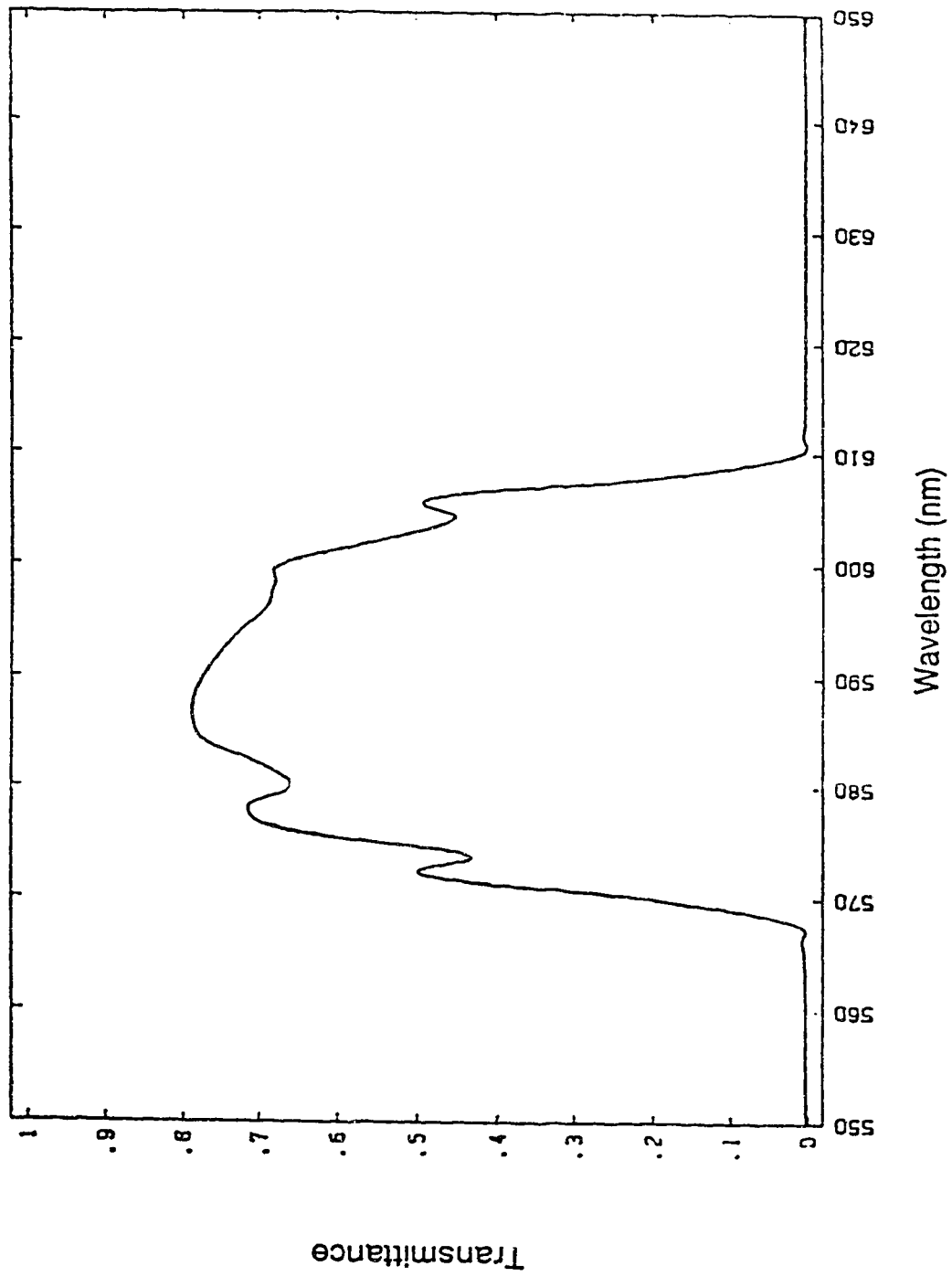


Fig. 2.5 Spectrum of the interference filter 590DF40.

Photodetector

At the maximum emission of TRITC and TRITC-amino acid derivatives, about 570 to 580 nm, multi-alkali type photomultiplier tubes produce good results. The photomultiplier tube chosen for this work was a Hamamatsu R1477. The quantum efficiency of this tube is about 14% at the wavelength of 575 nm. The quantum efficiency and cathode radiant sensitivity of the R1477 tube are shown in Figure 2.6; other properties are listed in Table 2.2.

2.1.2 Experimental section

Electrophoresis

The electrophoresis system is basically the same as systems described in Chapter 1. A 50 μm inner diameter fused silica capillary (Polymicro Technology) was used for separation. The length of the capillary was 92 cm. A 30 KV power supply (Spellman) was used to drive the electrophoresis. A platinum electrode provided electrical contact with the eluting buffer at the high-voltage, injection end of the capillary. This end of the capillary was enclosed within a safety-interlock equipped Plexiglas box. The detector end of the capillary was inserted into a sheath flow cuvette that was held at ground potential (see section 2.1.1). The sheath fluid was pumped by a high-pressure syringe pump (Isco) at a flow rate of 0.5 mL/h. The sample injection was done at 1 KV for 10 s. For a capillary length of 92 cm, and a retention time of 10 min. and 40 s., the injection volume is 0.94 nL (the calculation of injection volume will be discussed in detail in chapter 3). The electrophoresis was operated at a 30 KV driving voltage.

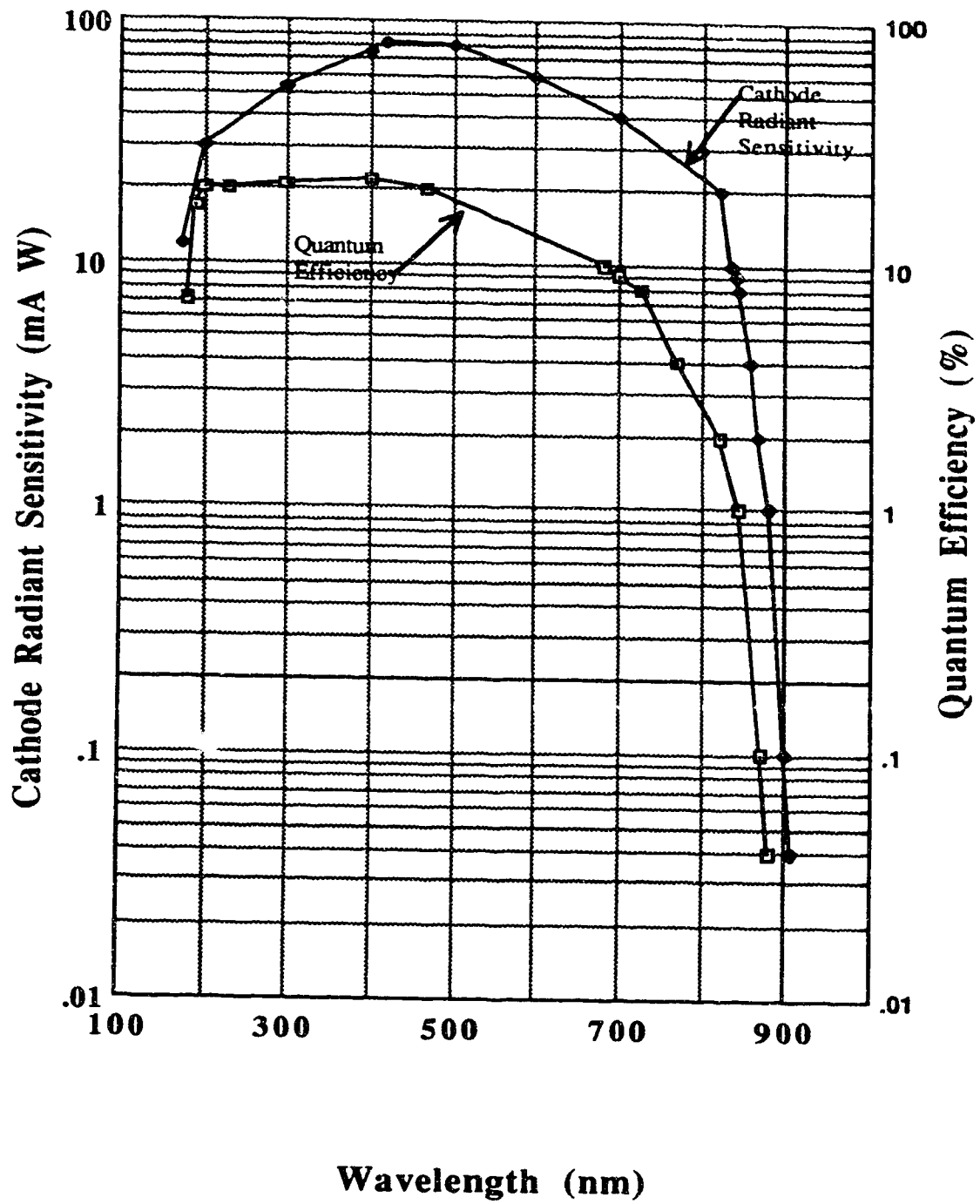


Fig. 2.6 Typical spectral response for R1477 photomultiplier tube --From data sheet.

Table 2.2 General properties of R1477 photomultiplier tube

| | | | |
|---|-------------|---|----------|
| Spectral Response Range(nm) | 185--900 | spectral response peak wavelength (nm) | 450 |
| Photocathode Material | Multialkali | Window Material | UV glass |
| Dynode Structure/No. of stages | CC/9 | Socket | E678-11A |
| Max. Anode to Cathode Voltage | 1250 | Anode to Cathode Supply Voltage (Vdc) | 1000 |
| Max. Average Anode Current (mA) | 0.1 | Cathode Sensitivity Min. Luminous ($\mu\text{A}/\text{lm}$) | 350 |
| Cathode Sensitivity Typ. Luminous ($\mu\text{A}/\text{lm}$) | 375 | Cathode Sensitivity Blue Typ. ($\mu\text{A}/\text{lm-b}$) | 10.0 |
| Cathode Sensitivity Red/White Ratio Typ. | 0.35 | Cathode Sensitivity Radiant typ. (mA/W) | 80 |
| Anode Sensitivity Min. Luminous (A/lm) | 1000 | Anode sensitivity Typ. Luminous (A/lm) | 2000 |
| Anode Sensitivity Radiant Typ. (A/W) | 420000 | Current Amplification Typ. | 5300000 |
| Typ. Anode Dark Current (after 30 min.) (nA) | 2 | Max. Anode Dark Current (after 30 min.) (nA) | 50 |
| Typ. rise time (ns) | 2.2 | Typ. Electron Transit Time (ns) | 22 |

Optics

The optical system was constructed on an optical bread board (Melles Griot). Fluorescence was excited by a 0.75 mW helium-neon laser (GreNe, Melles Griot) with a wavelength of 543.5 nm. The beam was focused with a 25 mm focal length (5×) microscope objective (Melles Griot) into the cuvette. Fluorescence was imaged with an 18×, 0.45 numerical aperture (NA) microscope objective (Melles Griot) onto a 400µm radius pinhole. The collected light was filtered with a 570 to 610 nm band pass interference filter (Omega Optical) and was detected with a photomultiplier tube (Hamamatsu). The output signal of the photomultiplier tube was conditioned with a 0.1 s RC filter and sent to the strip chart recorder.

Alignment of the fluorescence detector

The main idea in aligning the detector is to focus the laser beam exactly at the sample stream and to ensure that the fluorescence spot is exactly at the working distance of the microscope objective. To make the work easier, the laser beam and all the centers of the optical elements were set at a certain height above the optical table.

The arrangement of the optical elements is shown in Figure 2.7. To align the system, first, the laser beam was reflected by two mirrors and directed to the focusing lens. Then the 5× microscope objective, acting as a focusing lens, focuses the laser beam onto the waist of the sample stream. The image of this illuminated spot is then collected by the microscope objective, which is set at 90° angle to the laser beam. The image is then filtered by the interference band pass filter to get rid of background. The filtered sample image is then focused on the pinhole. The dash-lined box in Figure 2.7 represents a black box, which is used to keep the room light from entering the fluorescence light path. The objective, filter and pinhole were simply mounted on mirror stands. The cuvette, which was mounted on an xyz translation stage, was positioned so that the laser beam could pass through its center at a right angle to the cuvette surface. During alignment, a rhodamine B

solution, with a concentration of $8 \mu\text{M}$, goes through the capillary. The sheath flow rate is set at 0.5 mL per hour. When the fluorescence spot is imaged onto the pinhole, the photomultiplier tube is placed behind the pinhole so that the fluorescence signal passing through the pinhole can be directed to the window of the PMT.

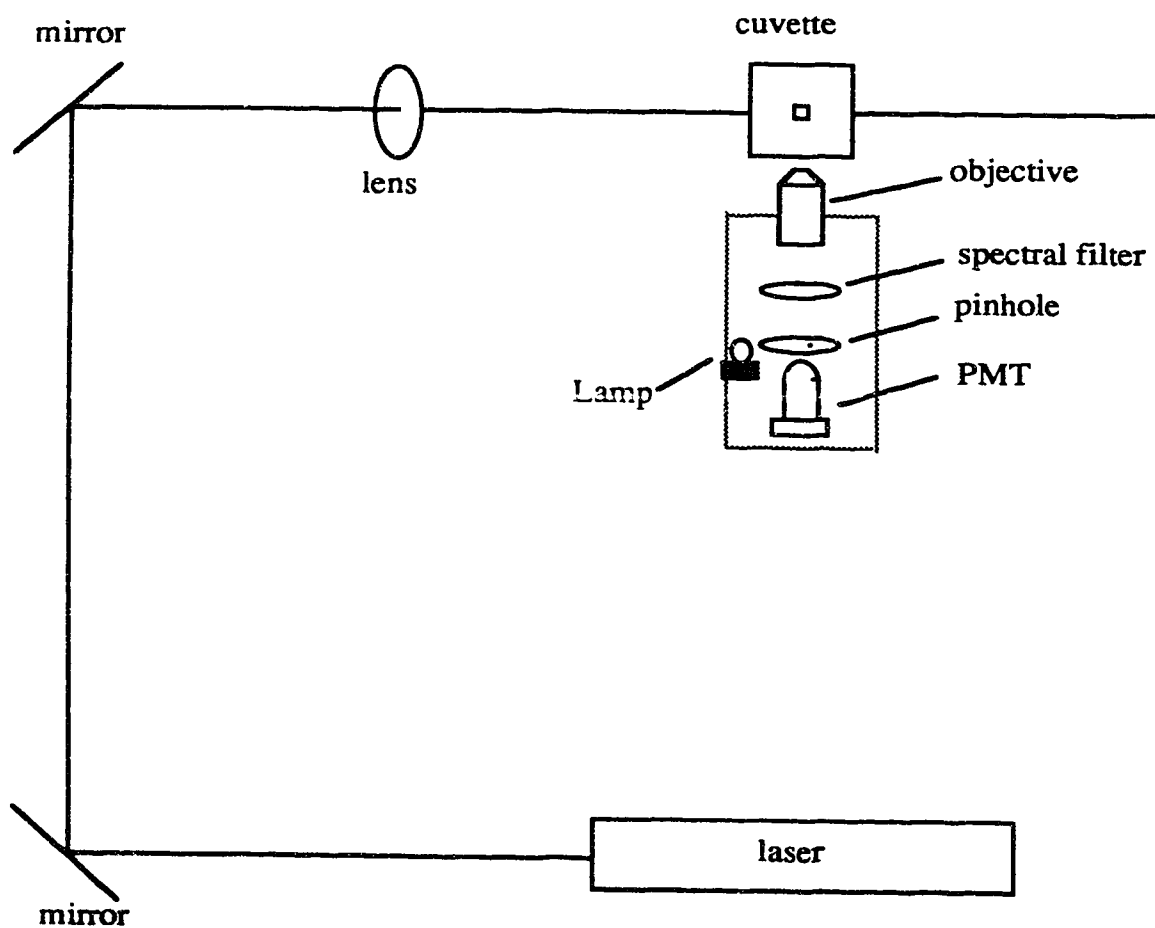


Fig. 2.7 Arrangement of the optical elements

Because there are very few optical elements that needed to be adjusted in this system, the system is very stable. In addition, simply by changing the laser and the spectral filter, the instrument can be used for the determination of other fluorescence materials.

An alternative alignment strategy was also used to simplify the steps of alignment. At the time of alignment, a small battery powered lamp was slid to a position just behind the pinhole, at the same time, the light path to the detector window was blocked to protect the PMT. A microscope was placed on the other side of the cuvette and aligned to be able to see the image of the pinhole. When the image of the lamp lit pinhole is clear and superimposed with the clear image of the fluorescent sample spot, the system is aligned. The lamp was moved out of the fluorescence light path after the system was aligned, as illustrated in figure 2.7.

Reagents

Tetramethylrhodamine-5-isothiocyanate (TRITC, isomer G, from Molecular Probes) was used to characterize the system. A TRITC solution, 1.6×10^{-5} M, was prepared in acetone as a stock solution. The stock solution was diluted with 5 mM borate buffer, with 10 mM sodium dodecyl sulfate (Aldrich) added in the buffer solution, pH = 9.0, to the desired concentration before injection into the capillary. The eluting buffer is 0.5 mM borate buffer, with 10 mM SDS added in the buffer, pH = 9.0, and this solution will be called the eluting buffer for simplicity through this chapter. For alignment, a rhodamine B (99%, Aldrich) solution, 7.9×10^{-4} M, was also prepared in acetone, and diluted to the desired concentration with the eluting buffer.

2.1.3 Results and Discussion

A calibration curve for TRITC was done to determine the detection limit. The injection volume for TRITC solution was 0.94 nL, the concentrations were from

2.56×10^{-10} M to 6.40×10^{-11} M. The slope of the calibration curve is 1.032×10^{11} mV/M, or 4.06×10^9 mV/M, the correlation coefficient is 1.00, and the curve originated from (0,0). The standard deviation of the background signal, σ , is 8.97×10^{-3} mV, and 3σ equals to 2.69×10^{-2} mV, which was obtained by collecting 100 data points, 1 point per second by a digital multimeter (195 System DMM, Keithley), when the PMT was operated at 1200 V. The limit of detection can be calculated by $3\sigma/(\text{slope})$, which is 6.6×10^{-12} M. For a injection volume of 0.94 nL, this detection limit corresponds to 3,700 molecules of TRITC, which was the best detection limit reported for capillary electrophoresis in 1990.

Further improvement can be expected if the noise level can be reduced, and the signal-to-noise ratio can also be improved. The limiting noise was found to be the thermal dark current of the PMT operated at high voltage. This can be improved if a cooling system is employed to keep the PMT at a low and constant temperature. Other improvements that could be done include optimizing the position of fluorescence detection, optimizing the sheath flow rate, and using a capillary with smaller diameter. The next section will describe detectors with improvement in design and performance.

2.2 Improving detection limits by using a cooled PMT

When the laser power is relatively high, for example, 20 mW to 50 mW, the main source of noise is scattered laser light, and the noise contributed by dark current is negligible. However, when a low power laser is used, as the one described in section 2.1, 750 μ W, the amount of scattered photons reaching the PMT is very small, due to the excellent optical quality of the sheath flow cuvette combined with appropriate interference filter which blocked the laser light. In this situation, dark current becomes significant. There are two problems related to operating a PMT at room temperature. First, dark current increases the background; it is difficult to reach the shot noise limited condition with a PMT operating at room temperature when a low power laser is used. Second, the current

flowing through the PMT base causes a temperature rise in the vicinity of the PMT and thus increases the dark current. Cooling the PMT will reduce the background. The effect of cooling the PMT on dark current is demonstrated in figure 2.8. The figure shows the process of cooling the PMT from room temperature (about 22°C) to -15°C.

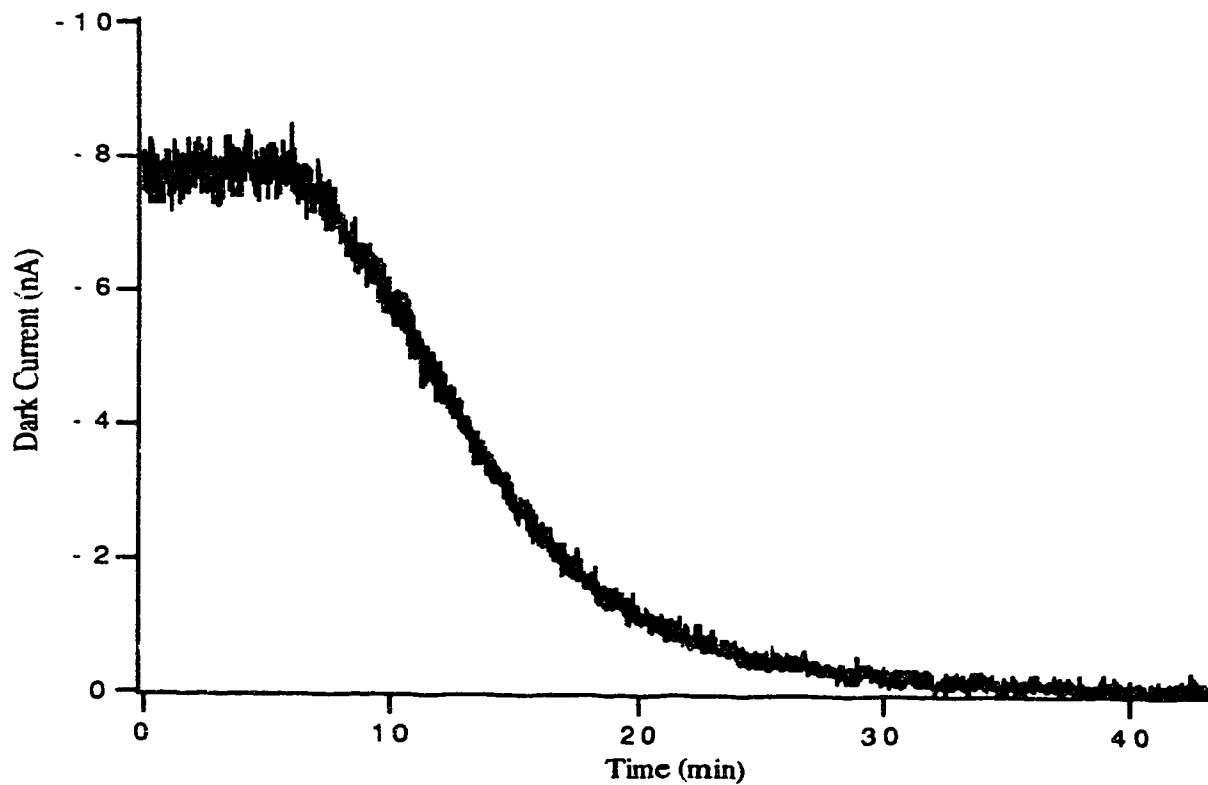


Fig. 2.8 The effect of cooling a PMT on PMT dark current. Both the background and the noise on the background are reduced.

2.2.1 Experimental Section

A 10- μm inner diameter, 48 cm long capillary (Polymicro, Arizona, USA) was used for the separation. The buffer was 5-mM borate (pH 9.0), 10-mM sodium dodecyl sulfate; SDS was added to eliminate peak tailing in the electropherogram. Samples were injected electro-kinetically for five seconds at 1 kV potential, corresponding to 30 pL of sample. The electrophoresis proceeded at a potential of 30,000 V.

2.2.2 Detector

A 0.75 mW helium-neon laser beam ($\lambda = 543.5 \text{ nm}$) (Melles Griot, Ontario, Canada) was focused with a 4 \times microscope objective about 200- μm below the exit of the capillary in a sheath flow cuvette with a 200- μm square flow chamber and 2-mm thick windows. Fluorescence was collected at right angles with a 18 \times , 0.45 numerical aperture objective (Melles Griot) and imaged onto a 0.8-mm diameter pinhole. A single interference filter (590 nm center, 40 nm band pass, model 590DF35, Omega Optical, Vermont, USA) was used to block scattered laser light. Fluorescence was detected with a Hamamatsu (California, USA) R1477 photomultiplier tube, operated at 1000 V and cooled to -15 $^{\circ}$ C with a Products for Research (Massachusetts, USA) PMT cooler.

2.2.3 Results and Discussion

In this detector, which is similar to that used in flow cytometry, the sample flows as a narrow stream in the center of a 200- μm square flow chamber, surrounded by a sheath stream of buffer solution. The high optical quality windows of the cuvette produce at least two orders of magnitude less light scatter than does an on-column detector. Also, by transferring the analyte to the moving sheath stream, the linear velocity, and hence the

illumination time of the analyte, is the same. Keller's group has reported high sensitivity detection for neat solutions of highly fluorescent dyes [32, 33]. Recently, Keller's group has reported, and Mathies' group has confirmed, detection of single phycoerythrin molecules in neat solution with a single spectral channel fluorescence detector [34, 35].

The argon ion laser ($\lambda = 488, 514.5 \text{ nm}$) is used by most investigators for excitation of fluorescence in capillary electrophoresis. However, the laser is rather expensive (~US\$10,000) and requires forced air cooling. An interesting alternative excitation source for fluorescence excitation is the helium-neon laser (the so-called GreNe laser) operating in the green at 543.5 nm. The laser is low cost (~US\$1,000) and features the same construction as the conventional red helium-neon laser. Six conventional red helium-neon lasers have been in operation in this laboratory for six to eight years with no tube failures; the green helium neon should have similar life-time. The laser produces quite low output power (0.75 mW) with excellent spatial coherence and good noise characteristics. Finally, the beam is easily focused to a 10- μm radius spot for fluorescence applications.

Tetramethylrhodamine isothiocyanate (TRITC) is well suited for application in laser-induced fluorescence detection. The molecule has molar absorptivity of about 85,000 $\text{L mol}^{-1} \text{ cm}^{-1}$ at the green helium-neon laser wavelength. Keller reports that the molecule has a fluorescence quantum yield of 15% and a photodestruction yield of 5×10^4 . Under conditions of complete photobleaching, the molecule is expected to produce at least 30,000 fluorescent photons, a factor of four greater than the signal produced by fluorescein [34].

A sheath flow cuvette is used as a post-column fluorescence detector to minimize background light scatter. Further reduction in the background signal comes from the relatively long excitation wavelength and low power excitation beam (750 μW). With this detector, the major contribution to background signal was dark current produced by the photomultiplier tube. This contribution to the background signal is minimized by cooling the photomultiplier tube to -15°C .

The detection limit of this detector for TRITC was determined in a free zone electrophoresis system. The relative standard deviation ($n = 5$) in peak height for a 1.28×10^{-10} M TRITC solution was 10%. Figure 2 presents a zone electropherogram of an injection of 4 zmol of analyte corresponding to 2,300 analyte molecules. A linear calibration curve, $r = 0.986$, was constructed from 6.4×10^{-11} M to 2.56×10^{-10} M TRITC. The detection limit, three standard deviations above the background signal, was 300 analyte molecules or 500 yoctomoles (1 yoctomole = 1 ymol = 10^{-24} mol). Note that the data were not conditioned beyond that provided by the 0.1 second time-constant filter; appropriate digital filtering would undoubtedly improve detection performance. Also, use of a higher power laser would undoubtedly improve detection limits further.

The major components used in the experiment (laser, high voltage power supply, optical breadboard, sheath flow cuvette, photomultiplier tube power supply, and photomultiplier tube cooler) have a total cost of about US\$8,000. It is possible to construct a simple, modest cost instrument with excellent analytical performance.

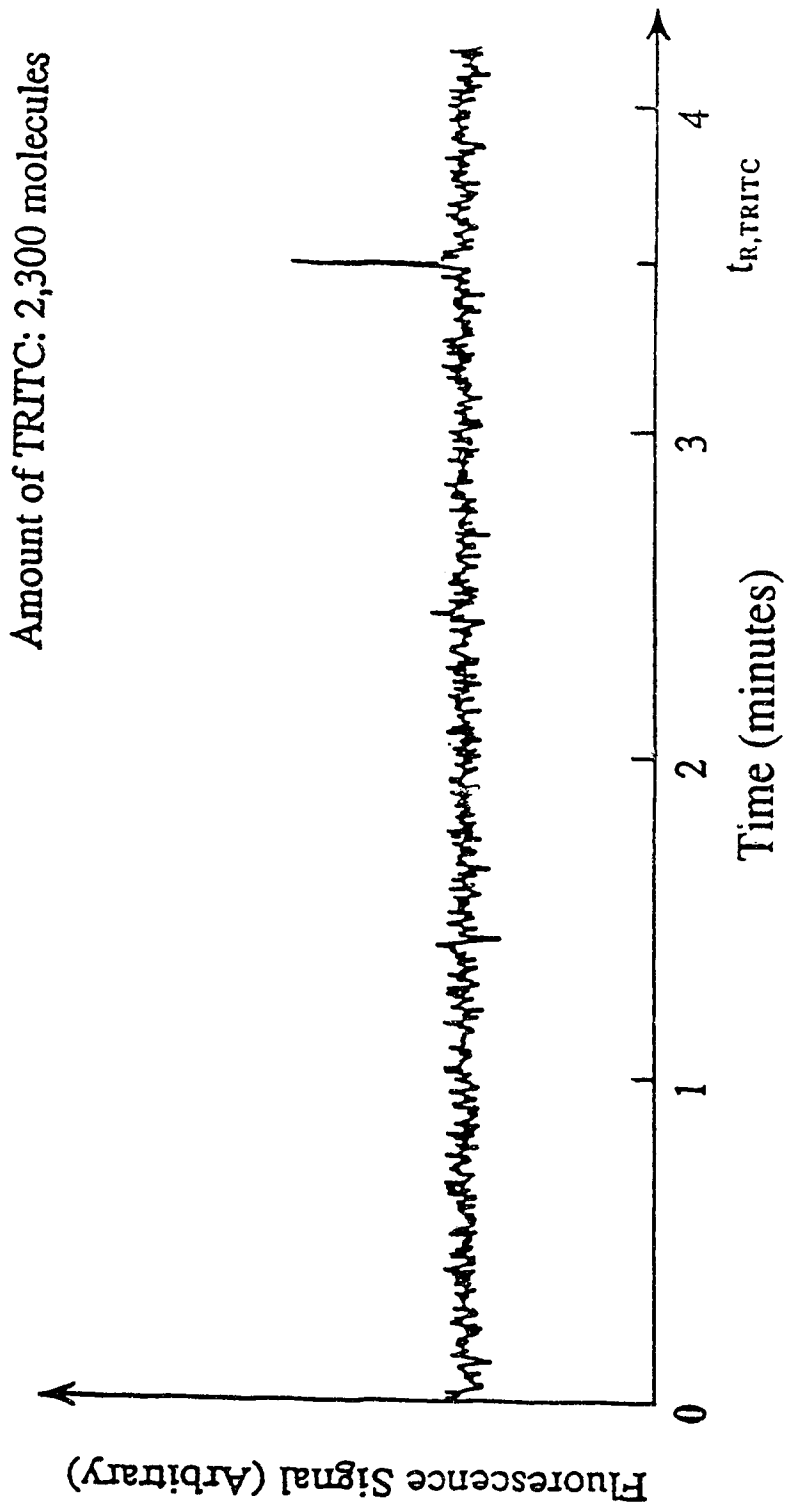


Fig. 2.9 Capillary free zone electropherogram of 4 zmol (2300 molecules) of tetramethylrhodamine isothiocyanate.

2.3 Improving the detection limits by redesigning the sheath flow cuvette and fluorescence collection system

From equation 2.1, the collection efficiency increases as the numerical aperture (N.A.) of the microscope objective increases. Table 2.3 lists collection efficiencies[14] for different N.A. values. However, a larger numerical aperture usually means a shorter working distance of the objective. For a 2 mm thick cuvette wall, it is hard to find a microscope objective with a large N.A. (> 0.45) without significantly increasing the cost. To be able to use market available low cost , large N.A. objectives, the thickness of the sheath flow cuvette has to be reduced.

Table 2.3 Collection efficiencies of lenses with different numerical apertures[14]

| | | | | | | | | | | |
|-----------------------|-------|-------|-------|-------|-------|-------|-------|-------|-------|-------|
| Numerical Aperture | 0.1 | 0.2 | 0.3 | 0.4 | 0.5 | 0.6 | 0.7 | 0.8 | 0.9 | 1.0 |
| Collection Efficiency | 0.003 | 0.010 | 0.023 | 0.042 | 0.067 | 0.100 | 0.140 | 0.200 | 0.280 | 0.500 |

A new sheath flow cuvette is used in the redesigned fluorescence detector. The cuvette has 1 mm walls and a 200 μm inner chamber, the length of the cuvette is 1 cm. A 60 \times , 0.7 N.A. microscope objective (Universe Kogaku (America), Inc., NY, USA) is used to collect fluorescent light. The working distance for this objective is 1.44 mm, the distance from the center of the cuvette to the outside of the cuvette wall is 1.1 mm. Considering the difference in refractive indices between the cuvette wall and air, as illustrated in Fig. 2.10, working distance is a few hundred micrometers longer for an object in the center of the cuvette than the working distance for an object exposed in air. At the same time, the solid angle from where the fluorescence is collected may be reduced.

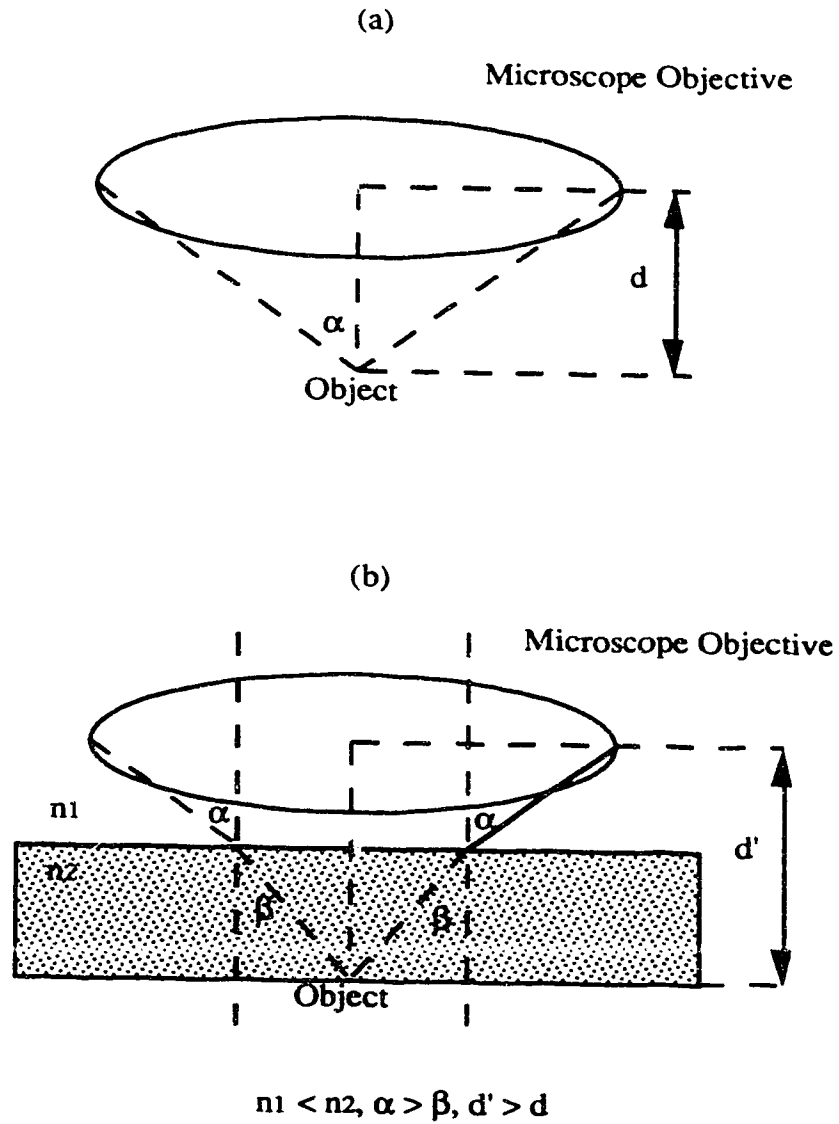


Fig. 2.10 The difference between the working distances of an microscope objective when the object is located in different media. (a) Both the objective and the object are in the air. (b) The objective is in the air, but the object is in another media which has a greater refractive index than air

The relatively long working distance of the microscope objective makes it easier to design the detection system and the relatively large numerical aperture makes it possible to collect more fluorescent light from the illuminated sample.

The detection system

The detection system is similar to the system illustrated in fig. 2.7. The optical system was constructed on an optical bread board (Melles Griot). A 1.0 mW helium-neon laser (GreNe, Melles Griot) with a wavelength of 543.5 nm was used instead of the 0.75 mW laser used in Section 2.1.2. The beam was focused with a 25 mm focal length, 5× microscope objective (Melles Griot) into the cuvette. Fluorescence was imaged by the new 60×, 0.7 numerical aperture microscope objective (Universal Kogaku) onto an iris which was adjusted so that the fluorescent light is allowed to go through, while the scattered light is rejected. The collected light was filtered with a 570 to 610 nm band pass interference filter (Omega Optical) and was detected with a photomultiplier tube (Hamamatsu). The output signal of the R1477 photomultiplier tube was collected by a photon counter (C1230, Hamamatsu) and digitized by a Macintosh IIsi computer. The program used to collect data is written in LabView[®], which is a graphic language.

Experimental Section

The electrophoresis is driven by a Spellman CZE1000R high voltage power supply. 4.13×10^{-3} M rhodamine 6G was prepared in ethanol, then diluted to 4.13×10^{-11} M by 5 mM borate buffer with 10 mM S.D.S., pH = 9.2. The capillary used was 10 μ m I.D., 140 μ m O.D., and 40 cm in length. The sheath flow was previously driven by a high-pressure syringe pump (Isco), but the line of products was discontinued by Isco at the time of constructing this sheath flow cuvette system. New good quality pumps would cost around \$5,000 to \$10,000. An inexpensive alternative was found to drive the buffer sheath. A

250 mL wash bottle was filled with buffer solution, the buffer level was set to be a few centimeters higher than the buffer level in the waste container. Because of the siphon effect, the sheath buffer will flow through the cuvette by gravity; because it is not step motor driven, the flow is very smooth, with no pulses which may disturb the fluorescence signal. The sheath flow rate can be controlled by adjusting the buffer level in the wash bottle while keeping the buffer levels in the injection vial and waste cell constant. The level difference was set at 7 cm in this case.

Results and Discussion:

The sample was injected at 500 V for 5 seconds, the electrophoresis was performed at 30,000 V, and the retention time of TRITC was about 3 minutes. Fig. 2.11 shows electropherograms of repeated injections of 400 molecules of rhodamine 6G into a capillary (the first electropherogram is a blank). The detection limits can be calculated by an equation often used in chromatography [36] and well suited in capillary electrophoresis*:

$$C_{\text{LOD}} = K_{\text{LOD}} h_n C_s / h_s \quad (2.2)$$

where C_{LOD} is the concentration detection limit, K_{LOD} is a constant determined by the length of time of the electropherogram and the full width at half height of the analyte peak, h_n is the largest noise fluctuation (either positive or negative) observed in the piece of electropherogram interested, and h_s/C_s is the analyte peak height per unit amount of analyte.

* This equation is derived from an extension of the Bienayme-Tchebycheff inequality. The Bienayme-Tchebycheff inequality, $P_n(|h_n| \geq ks_n) \leq 1/k^2$, states that the probability (P_n) that a fluctuation ($|h_n|$) exceeds the standard deviation (s_n) by a factor of k is not greater than $1/k^2$. This relationship applies to all fluctuations, since no assumptions about the distribution of the fluctuations underlie its derivation. However, the maximum values of the probability predicted by commonly used distribution functions. A relationship that better approximates such distributions is the Camp-Meidell extension of the Bienayme-Tchebycheff inequality, $P_n(|h_n| \geq ks_n) \leq 4/9k^2$. It introduces only the following restrictions: That the noise distribution be unimodal, i.e., that it be a monotonically decreasing function on both sides of its one mode, and that assumptions be made about the predominance of large deflections on either side of the baseline. This latter assumption, which implies that noise distribution's mode corresponds to the baseline, is one that is often made when little is known about the nature of the noise distribution. Equation 2.2 is derived from this extension of the inequality[36].

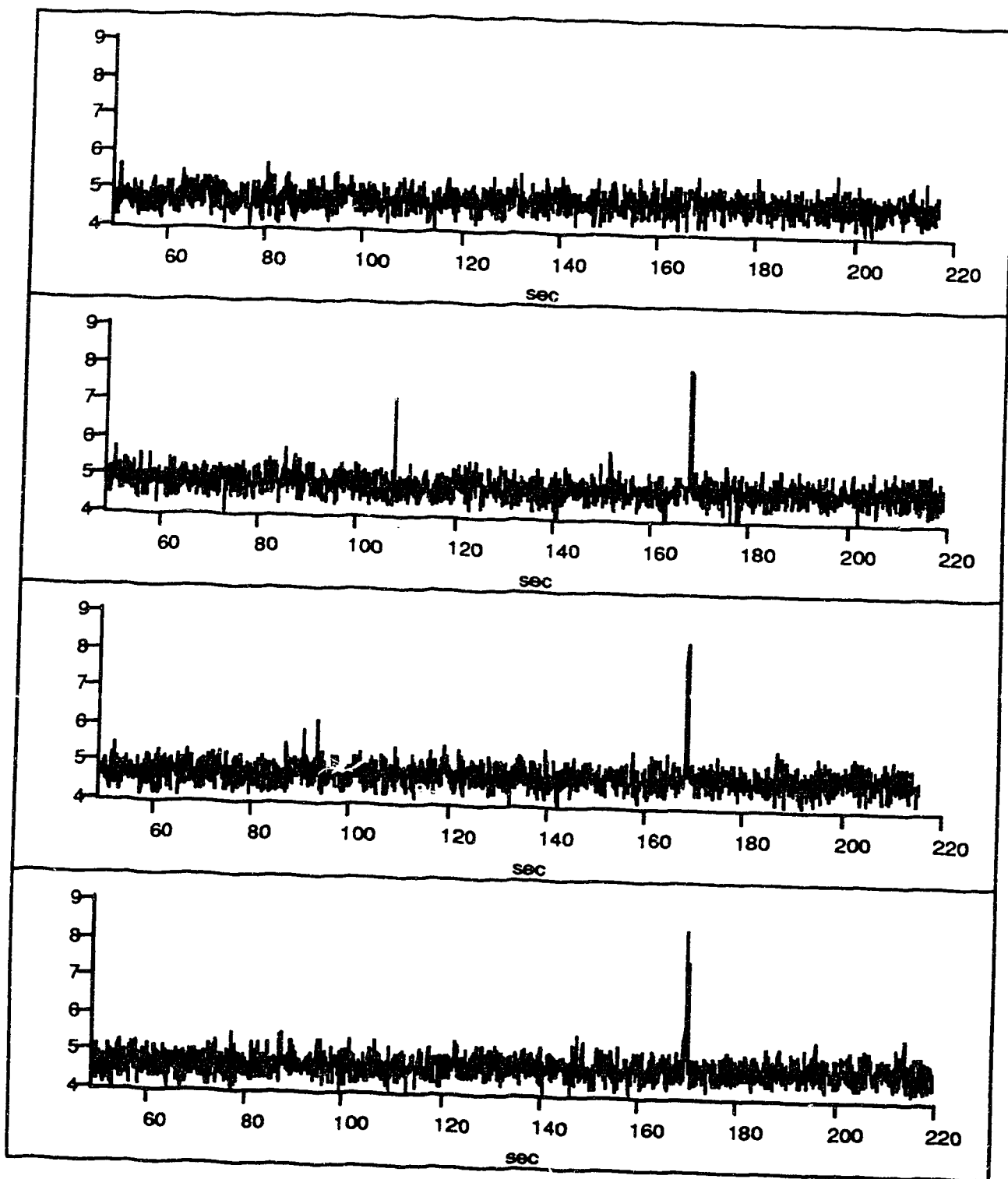


Fig. 2.11 Electropherograms of repeated injections of 300 molecules of rhodamine 6G into a capillary.

Some values of the constant K_{LOD} are listed in table 2.4. The electropherograms show that the rhodamine 6G peaks are very sharp, the full width at half height is usually 0.5 seconds or shorter. Data was collected for more than 220 seconds, so K_{LOD} for $N=100$ is used, where N is the length of the electropherogram (220 s) divided by the FWHM (0.5). The capillary volume is 33 nL and the injection volume is about 16 pL. Assuming each injection injects 400 molecules (the actual amount may vary because of sampling error), the detection limit is around 60 molecules.

Table 2.4 Some values of the constant K_{LOD} at different N^* values

| N | 10 | 20 | 50 | 100 |
|-----------|--------|--------|--------|--------|
| K_{LOD} | 1.9718 | 1.4309 | 0.9194 | 0.6536 |

* N is obtained by using the length of the electropherogram divided by the full width at half height of the analyte peak.

Since the data was collected in the digital form by a computer, digital signal processing like smoothing, Fourier transform low pass filtering, or time domain filtering can be easily performed. Figure 2.12 shows one of the electropherograms from Fig. 2.11, and the results of binomial smoothing operations. Electropherogram (a) is the raw data, the detection limit is 59 molecules, electropherogram (b) is the result of 3 times smoothing, the detection limit is 42 molecules, and electropherogram (c) is the result of 5 times smoothing, the detection limit is 40 molecules.

With the help of Fourier transform, it is possible to transform a time domain data to frequency domain. Figure 2.13 shows the real part of a Fast Fourier transform of the same electropherogram.

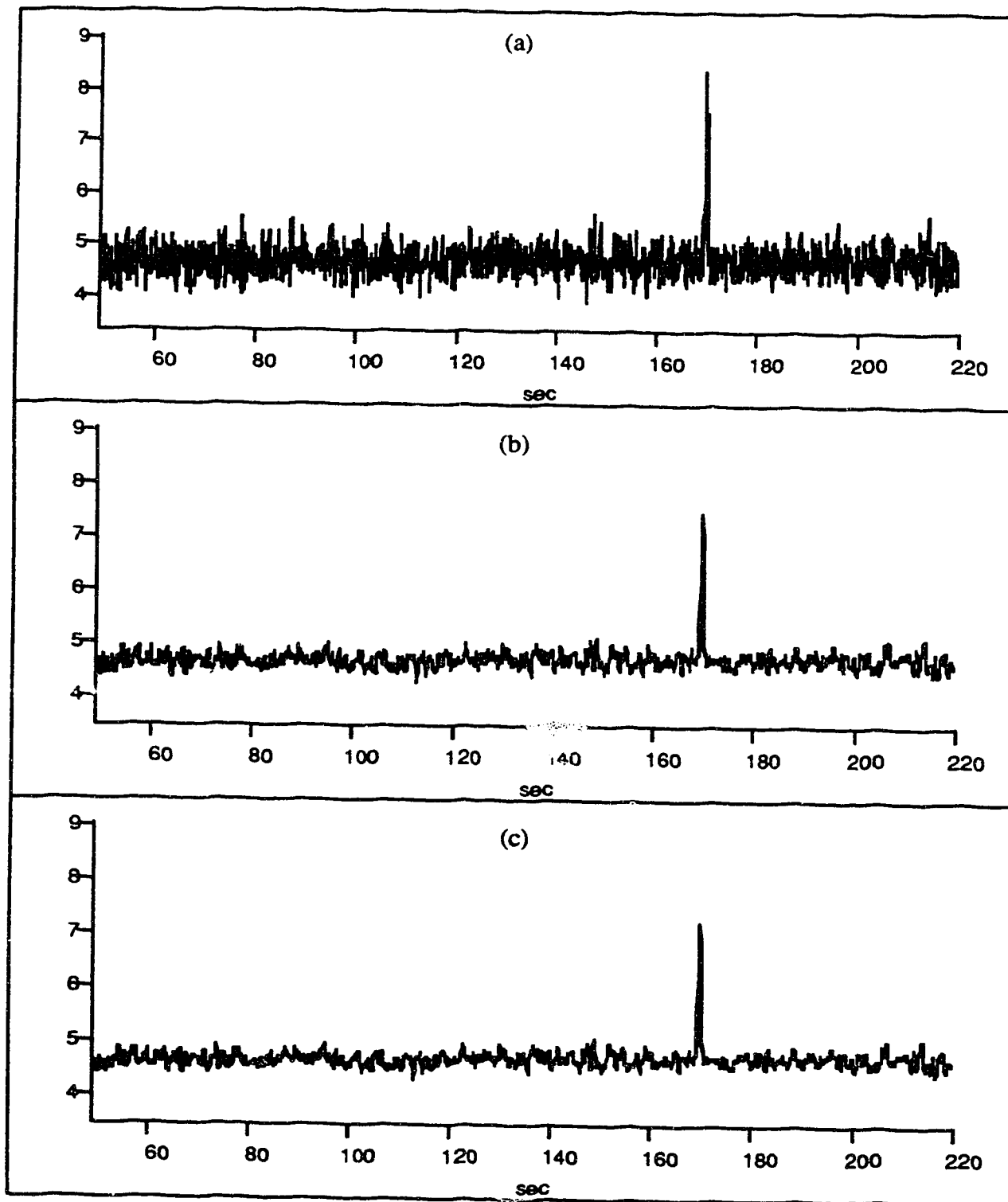


Fig. 2.12 (a) one of the electropherograms in Fig. 11, (b) the results of 3 times binomial smoothing, and (c) the results of 5 times binomial smoothing.

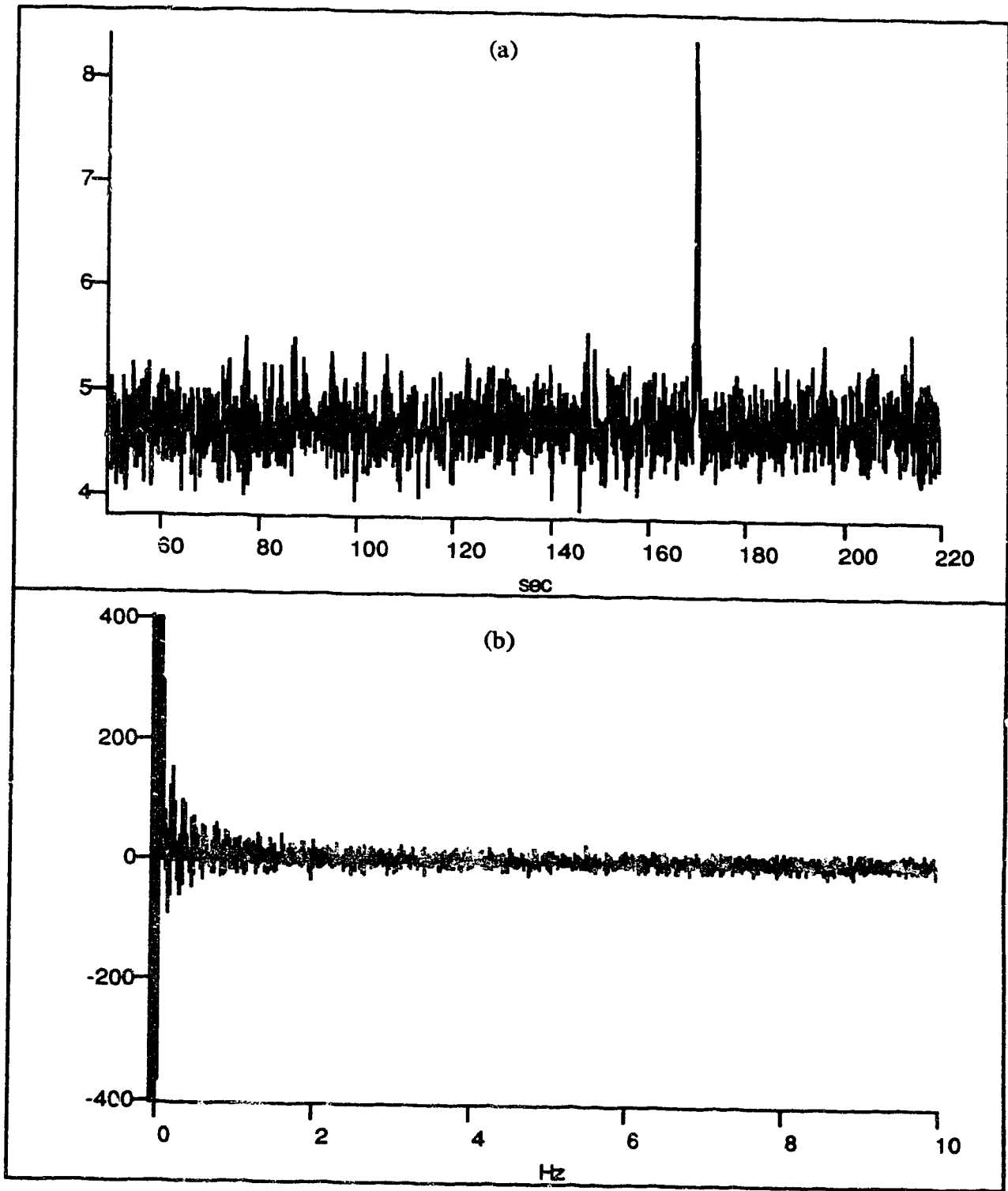


Fig. 2.13 The real part of a Fast Fourier transform of the same electropherogram as Fig. 2.12 (a).

From the Fourier transform of the time domain data shown in Fig. 2.13, the noise characteristics can be determined. In this case, the signal peak mainly contributes to the lower frequency part of the transform result. At frequencies above 1 Hz, there appears to be some noise added to the signal. When the frequency is higher than 2 Hz, the components are mainly noise. With the help of Fourier transform, appropriate digital filters can be designed for different data so that most noise can be rejected in the frequency domain while reserving as much signal component as possible. Because the signal components are mainly at low frequency, the filter is designed to start at 1 Hz with an order of 2, which means the filtering function is gradually reduced to zero. The difference among low pass filters with different orders of filtering is shown in fig. 2.14. The smaller slope in the filter will allow the signal components higher than 1 Hz to pass through the filter while gradually cutting off the noise components at higher frequency. Lower order filtering also avoids side lobes caused by truncation of the transformed data.

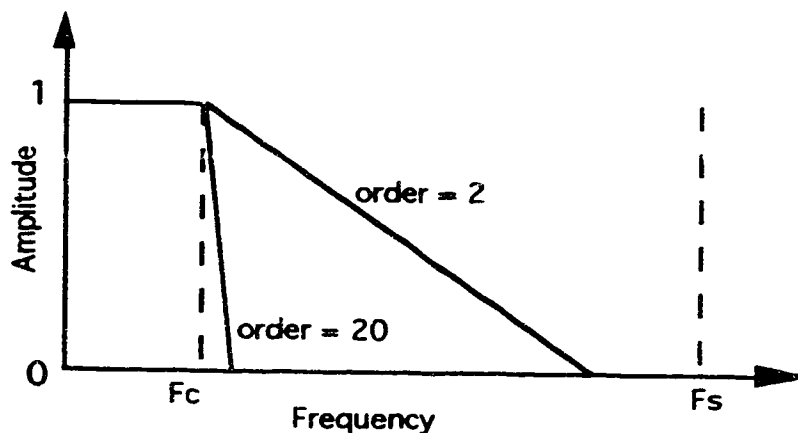


Fig. 2.14 An illustration of a low pass frequency domain digital filter, F_s is the sampling frequency and F_c is the cut off frequency of the filter.

Figure 2.15 shows the effect of Fourier transform low pass filtering. Fig 2.15 (a) shows the same electropherogram as Fig. 2.13 (a), the detection limit is 59 molecules; Fig. 2.15 (b) shows the filtered electropherogram, the cut off frequency of the filter equals to 1 Hz, and the order equals to 2, the detection limit for the filtered data is 40 molecules.

Another way of digital signal processing is Savitzky-Golay type time domain filtering. The correlation* of two signals is equivalent to multiplication of their Fourier transforms. Therefore, correlating the electropherogram to a Gaussian shaped function gives a time domain filtering, which is equivalent to a perfectly designed filter in the frequency domain of the Fourier transform provided the Gaussian function has a the same standard deviation as the signal peaks. Figure 2.16 shows an example of designing a Savitzky-Golay time domain filter. Fig. 2.16 (a) shows a normalized peak from an electropherogram; Fig. 2.16 (b) shows a Gaussian shaped filter function, with the standard deviation adjusted so that the shape of the filter is very close to the real signal response. Using this class of filters gives the best results in digital signal processing, as illustrated in Fig. 2.17. Another electropherogram is used in this figure: Fig. 2.17 (a) is the raw data, the detection limit is 53 molecules; Fig. 2.17 (b) is the resultant electropherogram from time domain filtering by a Gaussian shaped filter, the detection limit is 32 molecules. With this system, both rhodamine 6G and tetramethylrhodamine isothiocyanate were tested; the detection limits were around 30 molecules of injected sample. These were the best detection limits in the history of capillary electrophoresis in 1991. With the new sheath flow cuvette, better microscope objective, more powerful laser and digital signal

* Correlation is the relationship between a signal and a delayed version of another (or the same) signal. If $V_1(t)$ is one function and $V_2(t)$ is another function, t is a variable delay, for cross correlation:

$$C_{1,2}(\tau) = \lim_{T \rightarrow \infty} \frac{1}{2T} \int_{-T}^{+T} V_1(t) V_2(t-\tau) dt \quad (2.3)$$

and for autocorrelation:

$$C_{1,1}(\tau) = \lim_{T \rightarrow \infty} \frac{1}{2T} \int_{-T}^{+T} V_1(t) V_1(t-\tau) dt \quad (2.4)$$

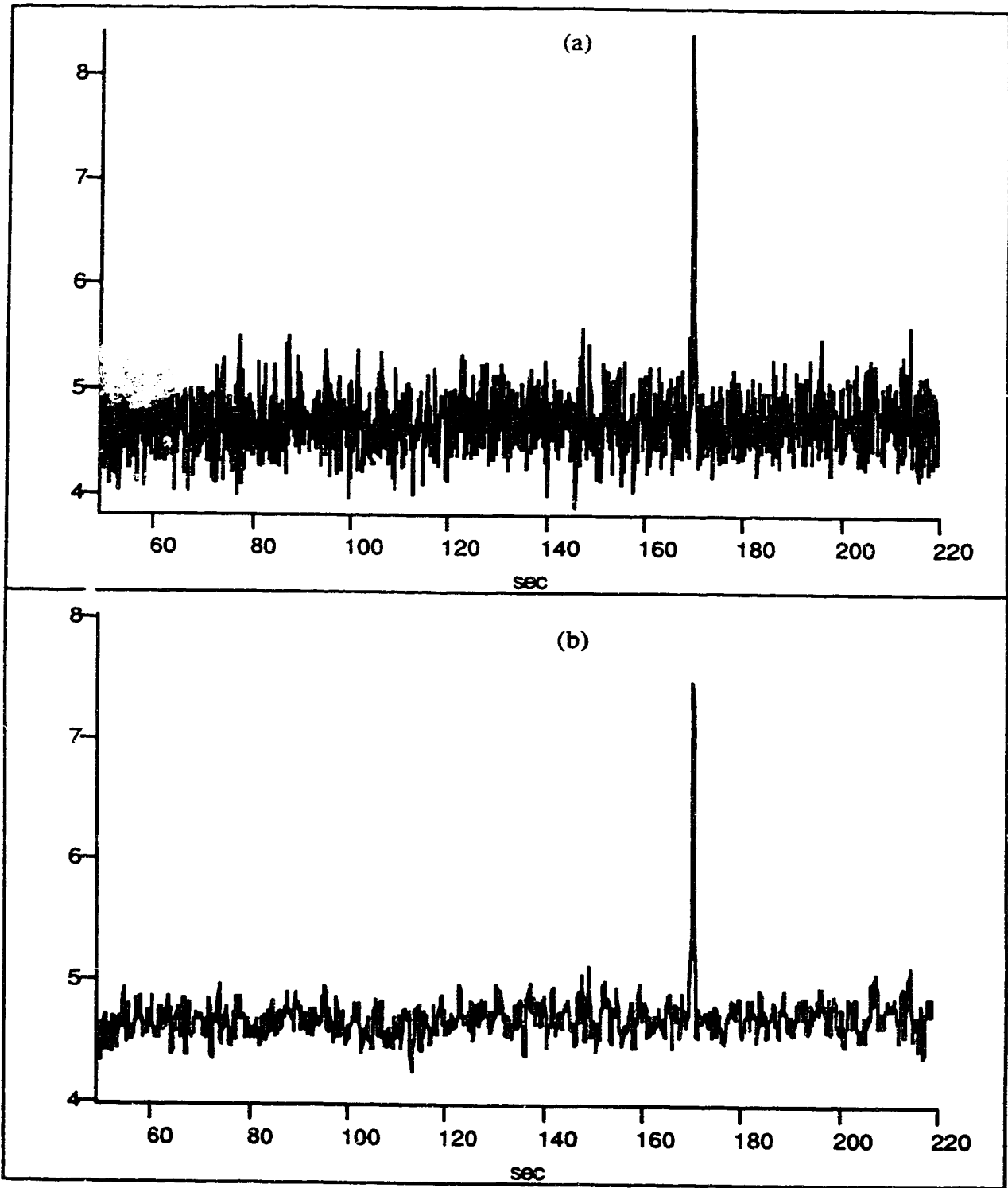


Fig. 2.15 The effect of Fourier transform low pass filtering. (a) raw data, (b) filtered data

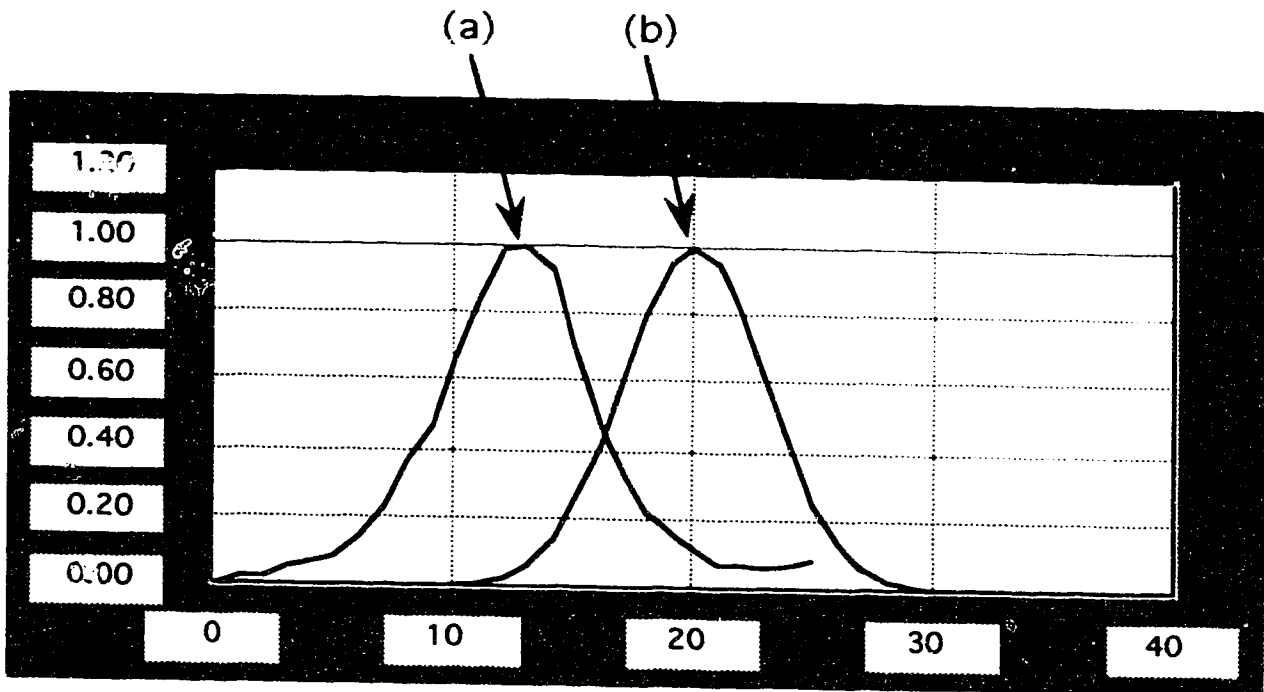


Fig. 2.16 (a) a normalized peak from an electropherogram; (b) a Gaussian shaped filter function, with the standard deviation adjusted so that the shape of the filter is very close to the real signal response. The standard Gaussian function is:

$$P_G(x, \mu, \sigma) = \frac{1}{\sigma \sqrt{2\pi}} \exp \left[-\frac{1}{2} \left(\frac{x - \mu}{\sigma} \right)^2 \right] \quad (2.5)$$

It is a continuous function describing the probability that from a parent distribution with a mean μ and a standard deviation σ , the value of a random observation would be x . The shape of the Gaussian can be adjusted to match the shape of the responding function of the signal .

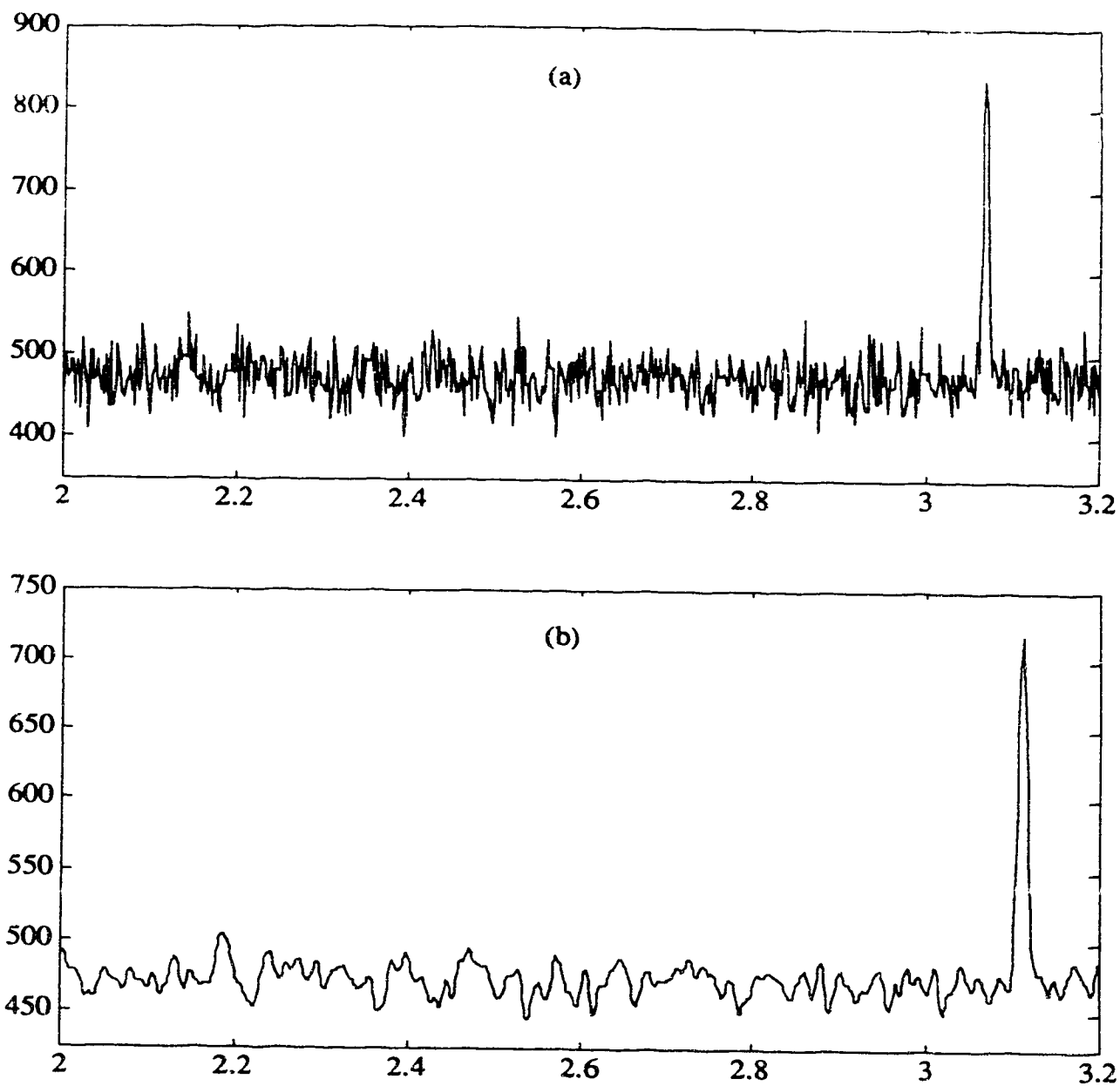


Fig. 2.17 Comparison of the original electropherogram and the resultant electropherogram after a Gaussian shaped time domain filter. (a) is the raw data, the detection limit is 53 molecules; Fig. 2.17 (b) is the resultant electropherogram from time domain filtering by a Gaussian shaped filter, the detection limit is 32 molecules. The horizontal axis is time in min., and the vertical axis is number of photons.

processing, the detection limits have been improved by a factor of 10 compared to the previous results.

2.4 Detection of single fluorescent molecules in capillary electrophoresis

Fluorescent signal is proportional to the laser power to a certain extent. Since the power of the Gre-Ne laser is relatively low (1 mW was the highest power laser commercially available in 1991), scattered light is not the determining noise. Reducing dark current by cooling the PMT improved the detection limits in fluorescence detection. In order to improve the detection limits further in this sheath flow cuvette system, a more powerful laser has to be used. The properties of the fluorescent dye also need to be considered so that the laser chosen has a wavelength matching or close to the maximum absorption of the dye. However, higher laser power will produce more stray light which leaks through the optical filter system and reaches the photo detector. As the laser power approaches 10 mW, the situation can be classified as background shot noise limited. In this case the noise is proportional to the square root of the background signal while the fluorescence signal is directly proportional to the laser power, until photo-bleaching of the dye molecules is significant. Another way to improve the detection limits will be to collect more signal. As more signal is collected, there will be more background also. However, in this background shot noise limited situation, signal to noise ratio will be improved as:

$$\frac{S}{N} \propto \frac{E_s}{E_b^{1/2}} \quad (2.6)$$

where E_s is the signal and E_b is the background.

Instrumentation

A new laser is used in this experiment. The laser is also a hard sealed He-Ne laser but operating at 594 nm (yellow). The power of this laser is 8 mW, which is much higher than the lasers used before. To increase the fluorescence collection efficiency, two microscope objectives are used which doubles the amount of fluorescence collected from the sample. The optical arrangement is shown in Fig. 2.18. The laser beam is directed by two mirrors into a focusing microscope objective. The beam is then directed into the sheath flow cuvette about 20 μm from the tip of the capillary. The beam waist is about 30 μm and the capillary inner diameter is 10 μm . These dimensions ensure that all sample molecules will pass through the laser beam, and with properly adjusted aperture, all sample molecules will pass through the volume being imaged. After going through the cuvette, the beam is absorbed by a beam collector. The sheath buffer is supplied by a 250 mL wash bottle seated on a lab jack. The buffer level is arranged to be 5 cm higher than the level in the waste cell. The fluorescence from the sample is collected on each side of the cuvette by two 60 \times , 0.7 N.A. microscope objectives and is directed into two photo detectors. In each photo detector, there is a interference filter which allows fluorescent light to pass through (about 85% transmission), while rejecting the scattered laser light and Raman bands from the solvent. An iris is placed at the plane where the probed volume is imaged. The iris, which is a spatial filter, is adjusted so that only the clear image of the fluorescence spot passes through while the fluorescence from the polyimide coating of the capillary and some more intense scatter from the edges of the cuvette are blocked. The output leads of the two PMTs (Hamamatsu, R1477) are connected to a summing circuit and digitized by a Macintosh Quadra 700 computer. The computer also monitors the current inside the capillary. The electrophoresis is driven by a Spellman CZE1000R high voltage power supply. The power supply is controlled by the same Macintosh computer. The sample

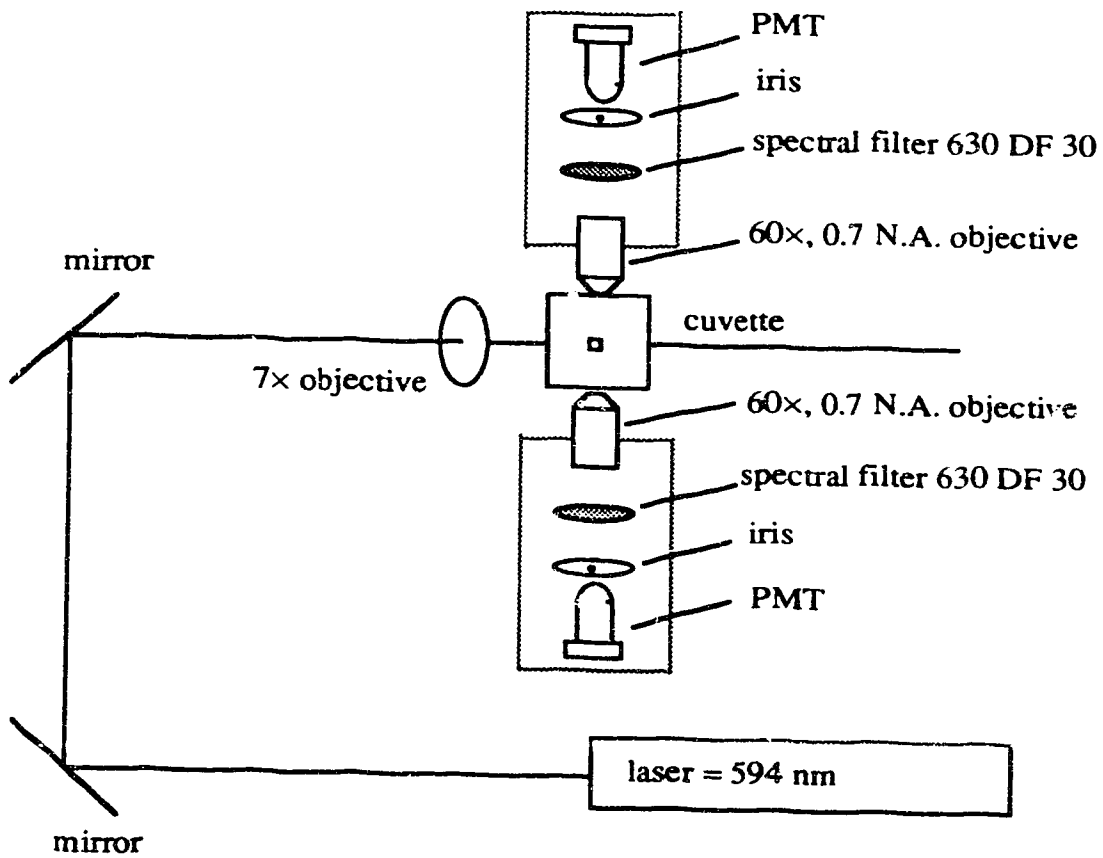


Fig. 2.18 The optical arrangement of the two channel fluorescence detector.

injection was controlled by the computer. Both the injection program and the electrophoresis voltage control program are programmed in LabVIEW®.

Experiment

A 10 μm I.D., 140 μm O.D. capillary is used; the length of the capillary is 45 cm. The buffer used in this experiment is 10 mM borate, 10 mM SDS, pH = 9.2. The sample is sulforhodamine 101, which is a precursor to Texas Red*. The absorption and emission spectra of sulforhodamine 101 are shown in Figure 2.19 and Figure 2.20. The maximum absorption is 586 nm ($107,000 \text{ cm}^{-1}\text{M}^{-1}$), which is very close to the laser wavelength (594 nm), and the fluorescence maximum is 607 nm. The sample is dissolved in ethanol and diluted to 3.8×10^{-13} with buffer before injecting into the capillary.

Results and discussion

Figure 2.21 shows an electropherogram for a 3.8×10^{-11} M sample injected at 500 V for 5 seconds. For a 10 μm I.D. capillary, 45 cm in length, the volume of the capillary is 35 nL. When 29,000 V is applied to the capillary, the sample retention time is around 245 seconds. Based on this information, the volume of injection can be calculated (this will be discussed in Chapter 5) to be 12 pL. On average, the injected sample solution contains 275 molecules of sulforhodamine 101. The detection limit calculated from this electropherogram is 5.7 molecules. The sample solution was further diluted to 3.8×10^{-12} M and the same volume of sample solution was injected into the capillary. The average amount of sulforhodamine is 28 molecules in 12 pL of 3.8×10^{-12} M solution. Fig 2.22 shows a few electropherograms of injection of 28 sulforhodamine 101 molecules into the

* Texas Red, which is Molecular Probes' registered trademark for sulfonyl chloride derivative of sulforhodamine 101, is the current standard for red dyes with spectra that minimally overlap with that of fluorescein. The quantum yield of Texas Red conjugates is intrinsically higher than that of TRITC or Lissamine rhodamine B. Because of this combination of characteristics, Texas Red conjugates are both brighter and have lower background than the conjugates of the other commonly used red fluorescent dyes if the correct filters are used.

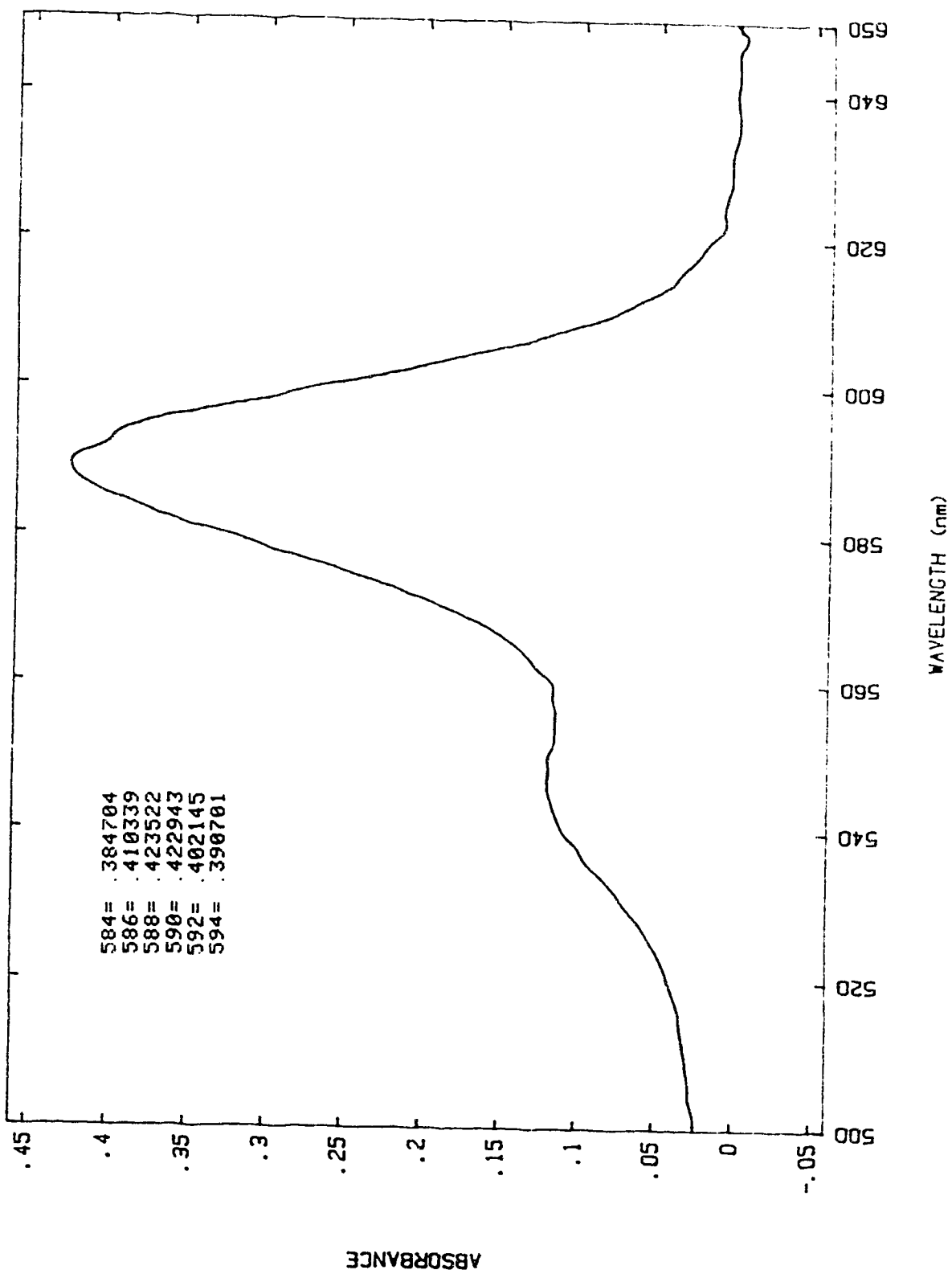


Fig. 2.19 The absorption spectrum of sulforhodamine 101

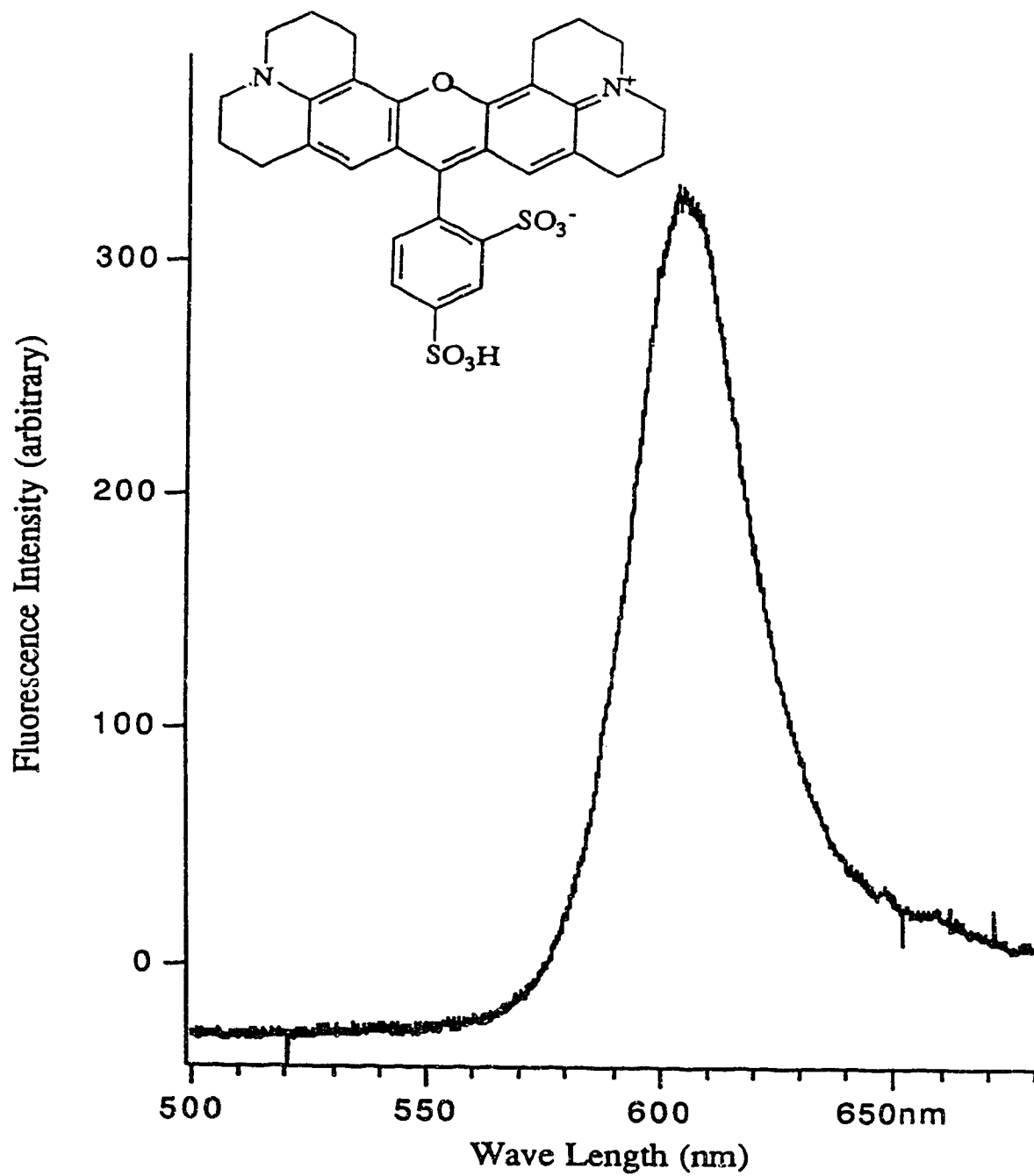


Fig. 2.20 The fluorescence spectrum of Sulforhodamine 101

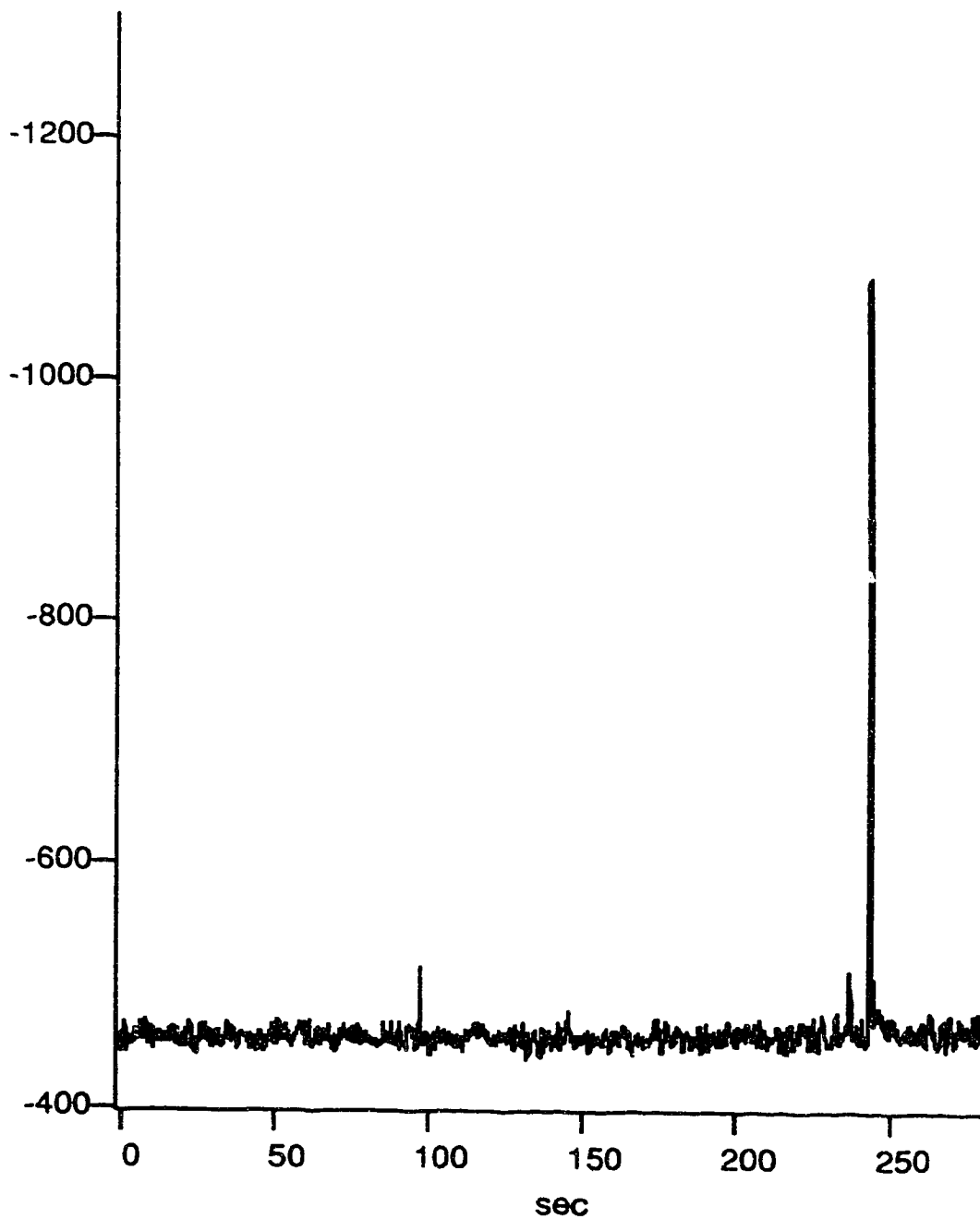


Fig. 2.21 Electropherogram of an injection of 275 molecules into the capillary

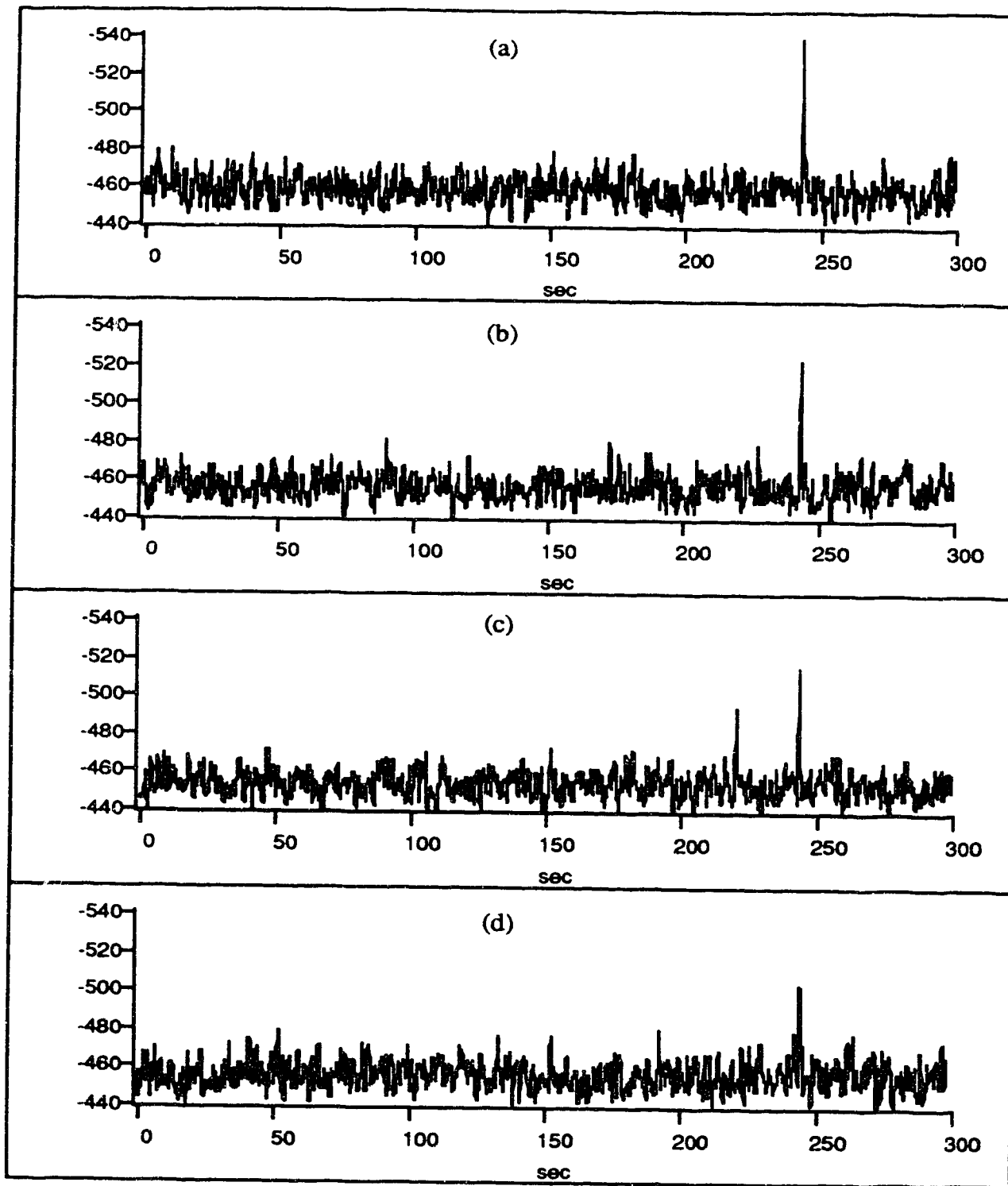


Fig. 2.22 Electropherograms of 28 molecules injected into the capillary

capillary. All data are smoothed. The detection limits in these electropherograms are: (a) 4.6 molecules, (b) 6.1 molecules, (c) 5.7 molecules and (d) 8.3 molecules. The sample was diluted again to 3.8×10^{-13} M, and volume of the injection was changed. The injections were performed at 5000 V for 3 seconds, which correspond to injection volumes of 74 pL. The average amount of sulforhodamine 101 was 17 molecules. Figure 2.23 shows a few unprocessed electropherograms of 19 molecules being injected into the capillary. Even the raw data shows the unmistakable peaks at the retention time of sulforhodamine 101. The detection limits calculated from these electropherograms are: (a) 8.0 molecules, (b) 6.4 molecules, (c) 4.6 molecules and (d) 5.1 molecules. The smoothed data are shown in Figure 2.24. The detection limits calculated from the smoothed data are: (a) 8.1 molecules, (b) 4.9 molecules, (c) 4.2 molecules and (d) 4.8 molecules. It is interesting to see that as the amount of sample decreases, smoothing or other kinds of data processing will not improve the signal to noise ratio significantly because of the very sharp peaks generated by very few molecules of the sample. The characteristics of a very sharp peak are very close to those of noise. The signal from the two PMTs is conditioned by a 0.5 sec RC low pass filter. In this 0.5 second integration time, there are random noise components and signal components integrated into one data point. If the time of a single molecule passing through the laser beam is known, the time constant of the low pass filter can be adjusted so that sufficient amount of the signal will be integrated while reducing the noise components during the period of integration. The background shot noise can therefore be reduced.

An experiment was done to determine the speed of the sample coming out of the capillary and passing through the laser beam. Polystyrene beads, 0.5 μm in diameter were used as a indicator in the buffer solution inside the capillary. The 2.5% 0.5 μm polystyrene latex was diluted 25000 times by eluting buffer, and then continuously driven through the capillary. This flow was stopped after 10 minutes, and the buffer with beads was replaced by a clean buffer solution. The clean buffer solution was also driven

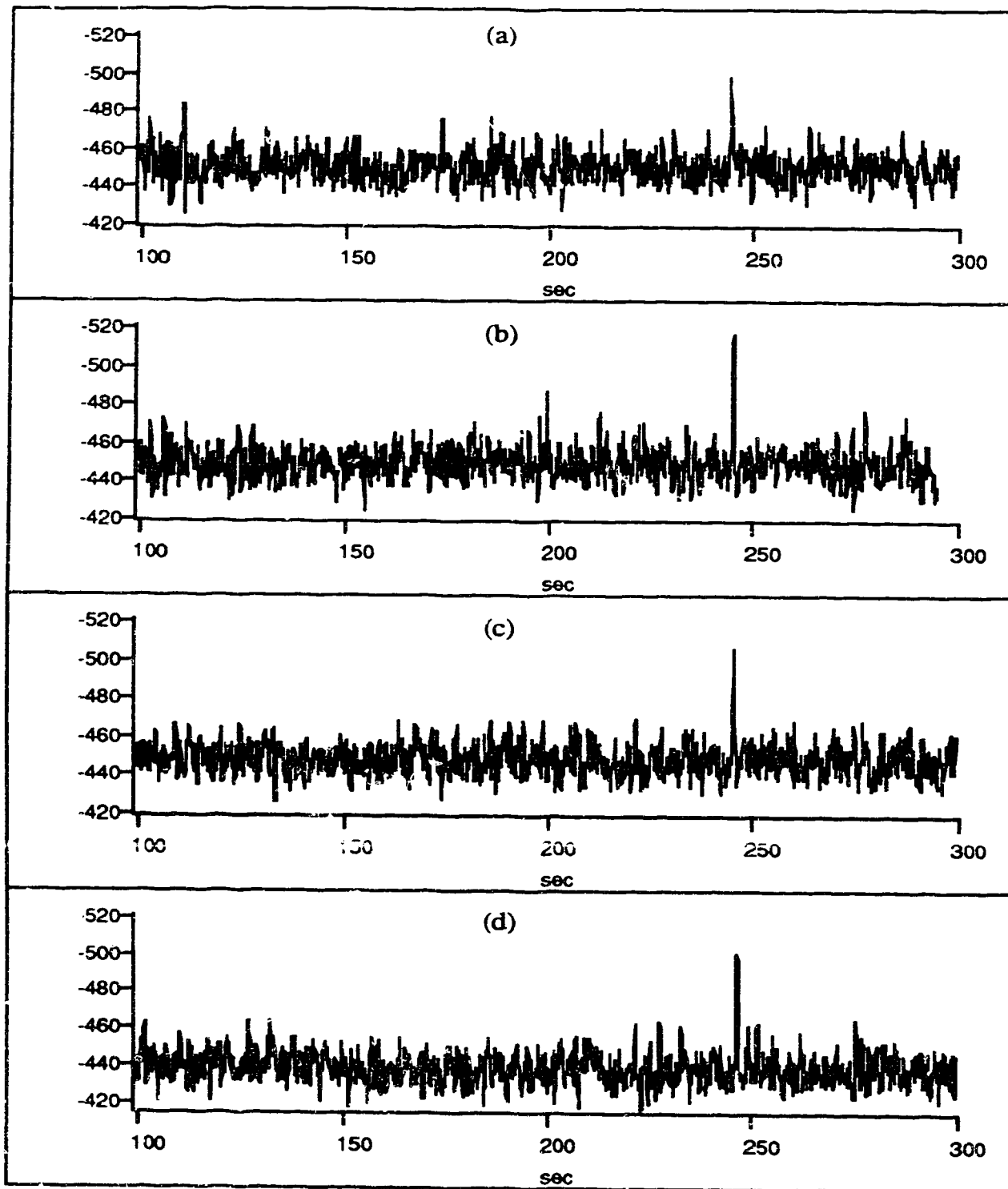


Fig. 2.23 Electropherograms of injection of 19 molecules into the capillary, raw data.

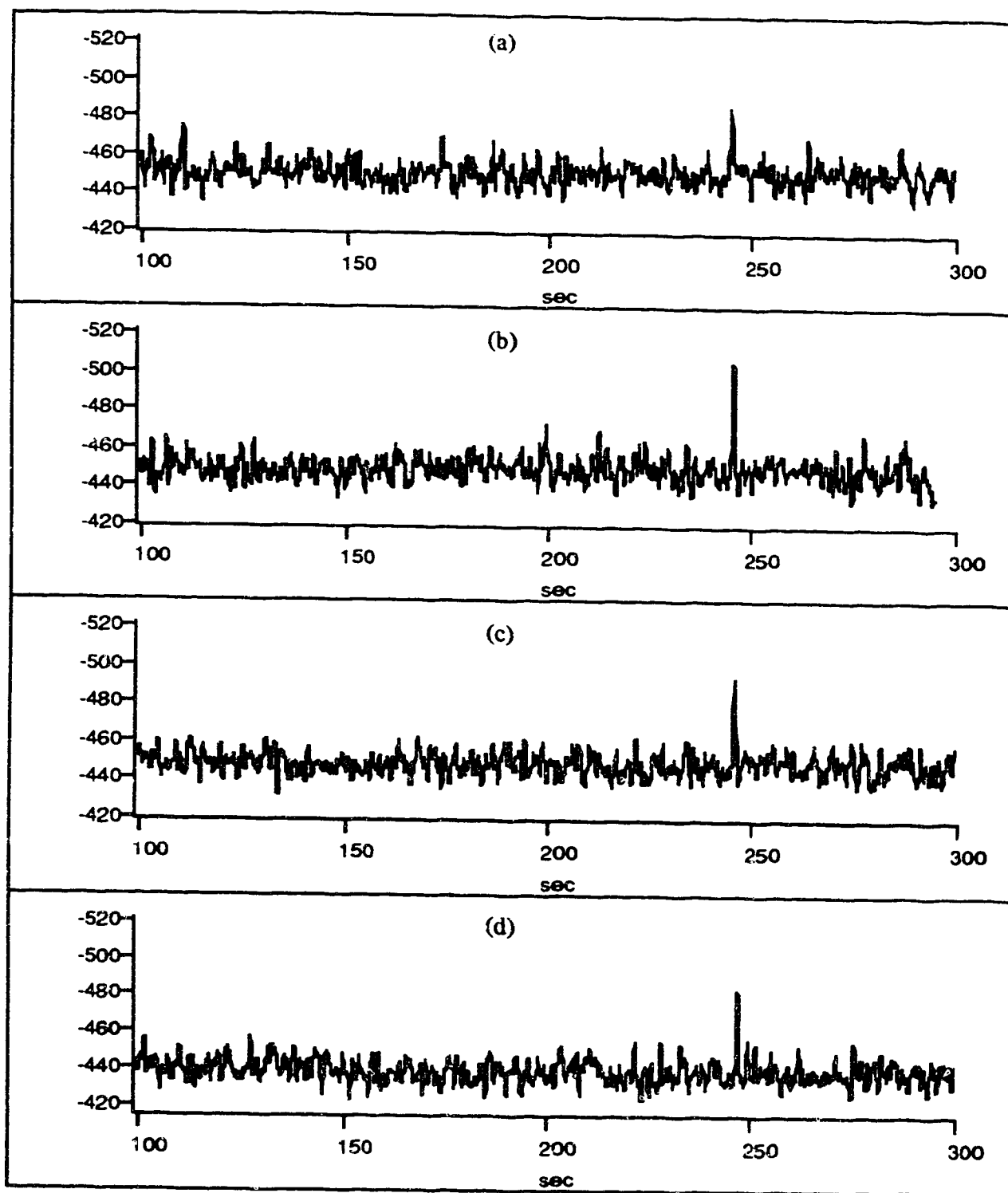


Fig. 2.24 Smoothed electropherograms of injection of 19 molecules.

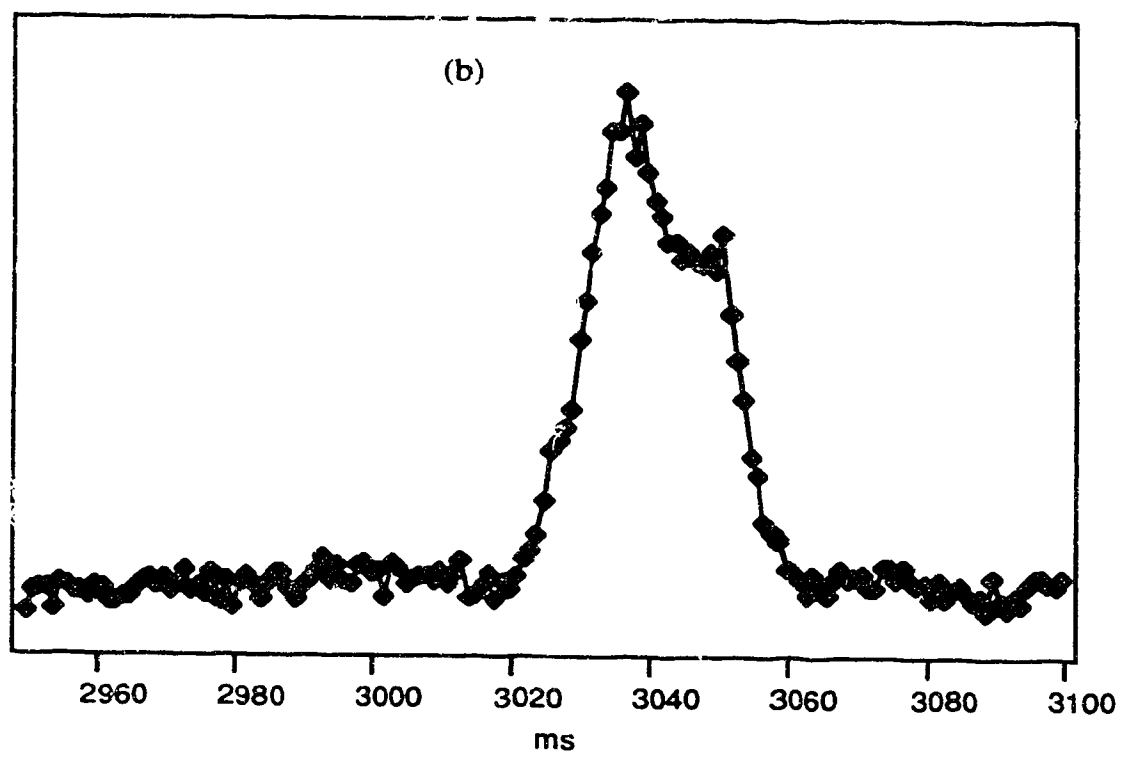
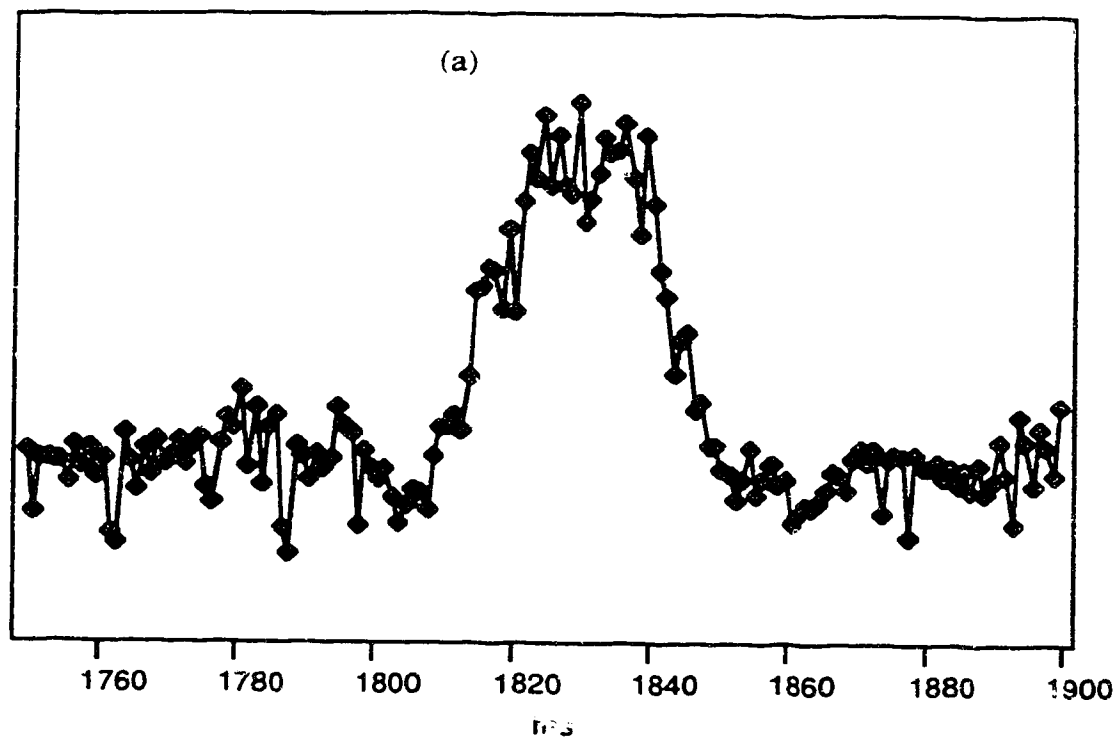


Fig. 2.25 The reflected light from $0.5 \mu\text{m}$ polystyrene beads.

continuously through the capillary for 10 minutes, then data collection was started. The ultra trace amounts of polystyrene beads left in the system were sufficient for the speed measurement. When the beads passed through the laser beam, the scattered laser light was collected by a microscope objective and sent to a PMT. The signal was digitized at 1000 Hz after going through a 1000 Hz low pass filter. Two segments of that data are shown in Figure 2.25. It took the beads around 40 milliseconds to clear the waist of the laser beam. This information about the time a molecule takes to pass the laser beam is extremely important. With this information, appropriate electronic filters can be chosen for single molecule detection, and appropriate sample concentration and sample flow rates can be used. The following experiments are designed based on the knowledge acquired from the previous ones.

To be able to detect single molecules in the solution, it is important to ensure that there will be times that only one molecule is present in the probed area. A 45 cm, 10 μm I.D. capillary has a volume of 35 nL. If the sample concentration is 3.8×10^{-13} M, then the total amount of the sulforhodamine 101 in the capillary is 1.33×10^{-20} mole, i.e., 8007 molecules. To be able to have one molecule present in the laser pass, the flow rate of the sample has to be smaller than 1 molecule per 40 milliseconds, or 25 molecules per second (41.5 yoctomoles/second, 1 yoctomole = 1×10^{-24} mole), which is equivalent to 109 pL/s of the 3.8×10^{-13} M sample being used. Electrophoresis is the only method that can accurately deliver this kind of flow rate.

A series of experiments were done to prove the detector described in this section is able to detect single molecules. The sample concentration was 3.8×10^{-13} M, the driving voltages of electrophoresis, retention times, volumetric flow rates and molecules per second flowing through the beam waist are listed in table 2.5.

Table 2.5 The experiments for single molecule detection

| | | | | | |
|-------------------------|------|-----|-----|-----|-----|
| CE Voltage (KV) | 5 | 10 | 15 | 20 | 25 |
| Retention time (s) | 1421 | 711 | 474 | 355 | 284 |
| Flow rate (pL/s) | 25 | 49 | 74 | 99 | 123 |
| Flow rate (molecules/s) | 6 | 11 | 17 | 23 | 28 |

The capillary was filled with sample solution and the electrophoresis was set at a certain driving voltage for 5 min. before data was collected to ensure the stability of the system. The data was then collected at 1000 Hz by the computer. After 30 seconds the polarity of the driven voltage was reversed to stop the sample flow. In order to keep the sample molecules from leaking out of the capillary, reversing the voltage is more efficient than turn off the driving voltage. A 1000 Hz low pass filter was used to condition the signal from the PMT. As a result, the first 30 seconds of the following series of data contains fluorescence signals from the sample molecules, and the following 40 seconds of data should be only background. Figure 2.26 shows data for a flow rate of 6 molecules per second in the first 30 seconds. The data is binomial smoothed 5 times. Some higher spikes are observed during the first 30 seconds, but it is difficult to say whether they are due to fluorescence signal until an autocorrelation is performed. Autocorrelation was performed on two separate sections of the electropherogram, each 2000 data points long (it would take too long to perform an auto correlation on 30000 data points). One section was taken from the first 30 seconds, and the second section from the latter part of the electropherogram. The results are shown in Figure 2.27 and 2.28. Figure 2.27 is the

autocorrelation of the background data. The result shows little correlation in this part. On the other hand, the autocorrelation of the signal part in Figure 2.28 shows a significant correlation (note the scale is different) with a delay time of about 60 ms. This means the spikes noticed in Fig. 2.26 have a peak width which is remarkably close to the time required for the sample molecules to travel through the laser beam. The next step in analyzing the data is to plot the histograms of the first 30 sec. and the last 30 sec. of data. Figure 2.29 is the histogram of the data from Fig. 2.26, signal is the histogram for the first 30 seconds and background is the histogram for the last 30 second (from 40 to 70 seconds). A significant shift in the maxima of the two histograms is noticed. In figure 2.30, three groups of histograms, each group from a different data set are compared. Figure 2.30(a) shows the same histograms as Fig. 2.29, with a 1000 Hz filter, (b) shows the histograms for data conditioned by a 100 Hz electronic low pass filter, and (c) shows the histograms from data conditioned by a 31.5 Hz filter. All three sets show a significant shift of the maxima of the histograms. This means the fluorescence signal was observed in all three situations. The shapes of the three groups are rather different. Although they are all Gaussian curves, the standard deviations are different, with the 31.5 Hz filter producing the smallest standard deviation. This is understandable because it is closer to the transit time of the fluorescent molecules through the laser beam. Based on this observation, further experiments were done using a 31.5 Hz filter.

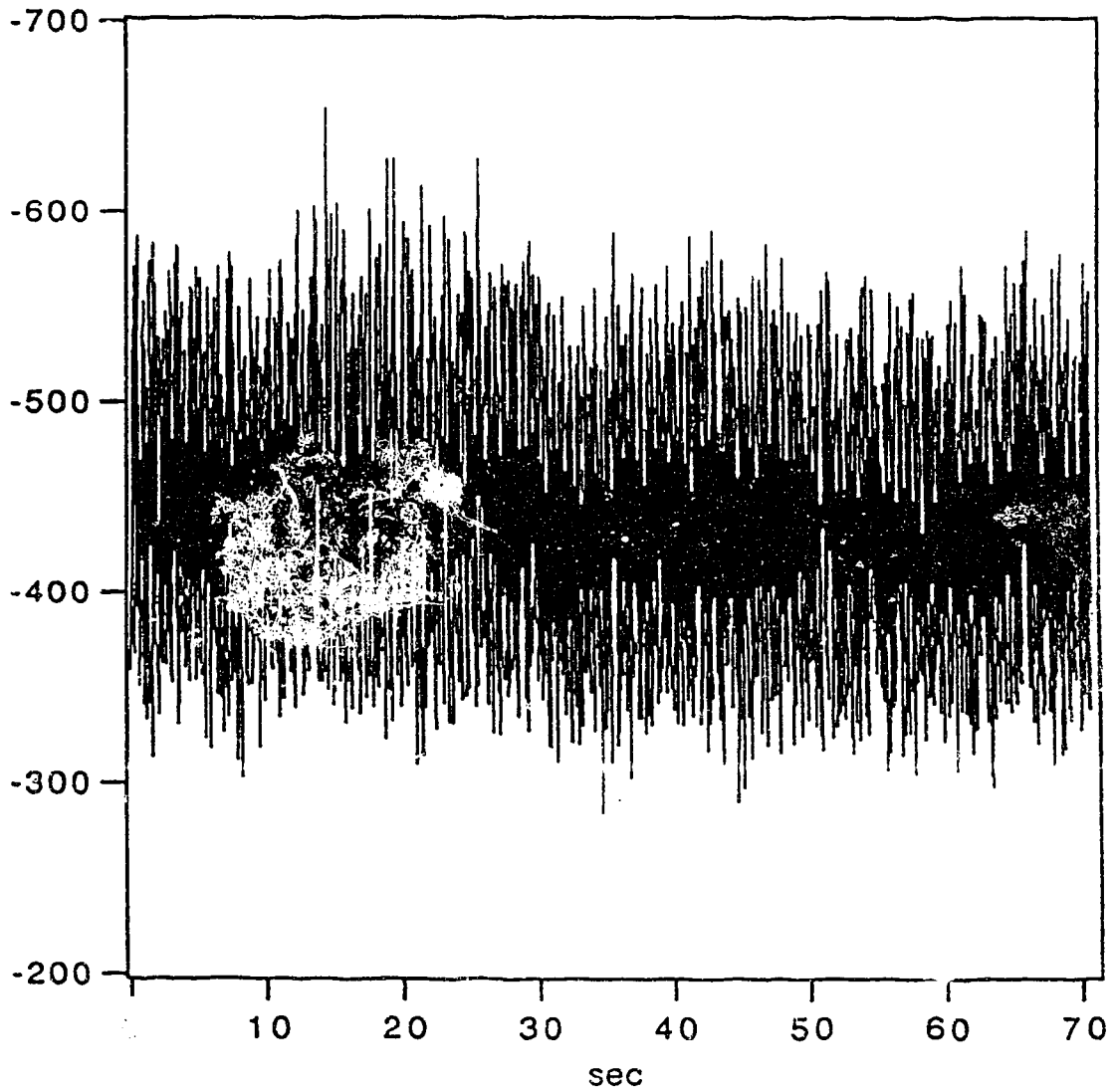


Fig. 2.26 Data for a flow rate of 6 molecules per second in the first 30 seconds. The polarity of the electrophoresis driven voltage is reversed after 30 seconds. The data is binomial smoothed 5 times.

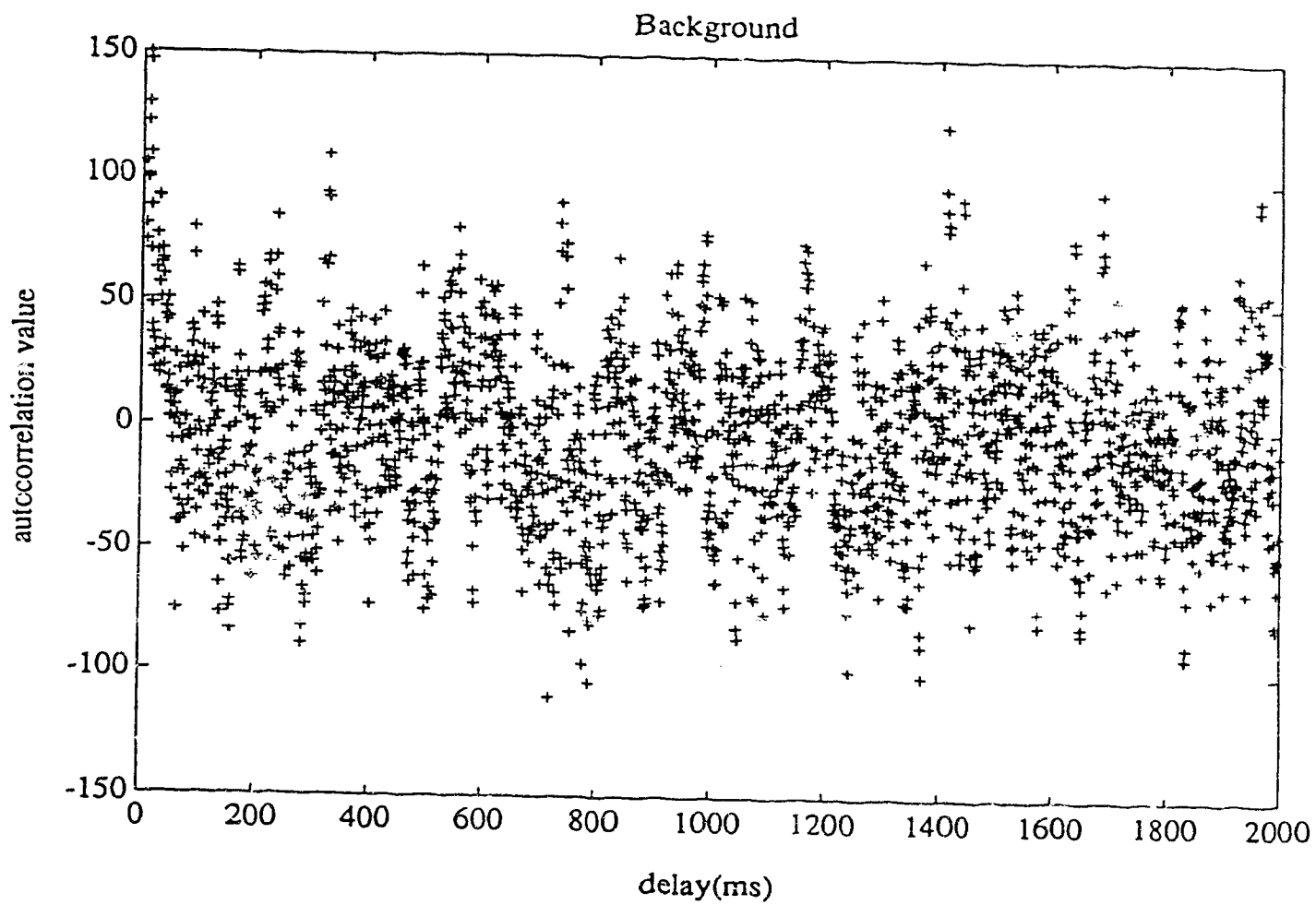


Fig. 2.27 Autocorrelation of a section of 2000 points from the background in Fig2.26.

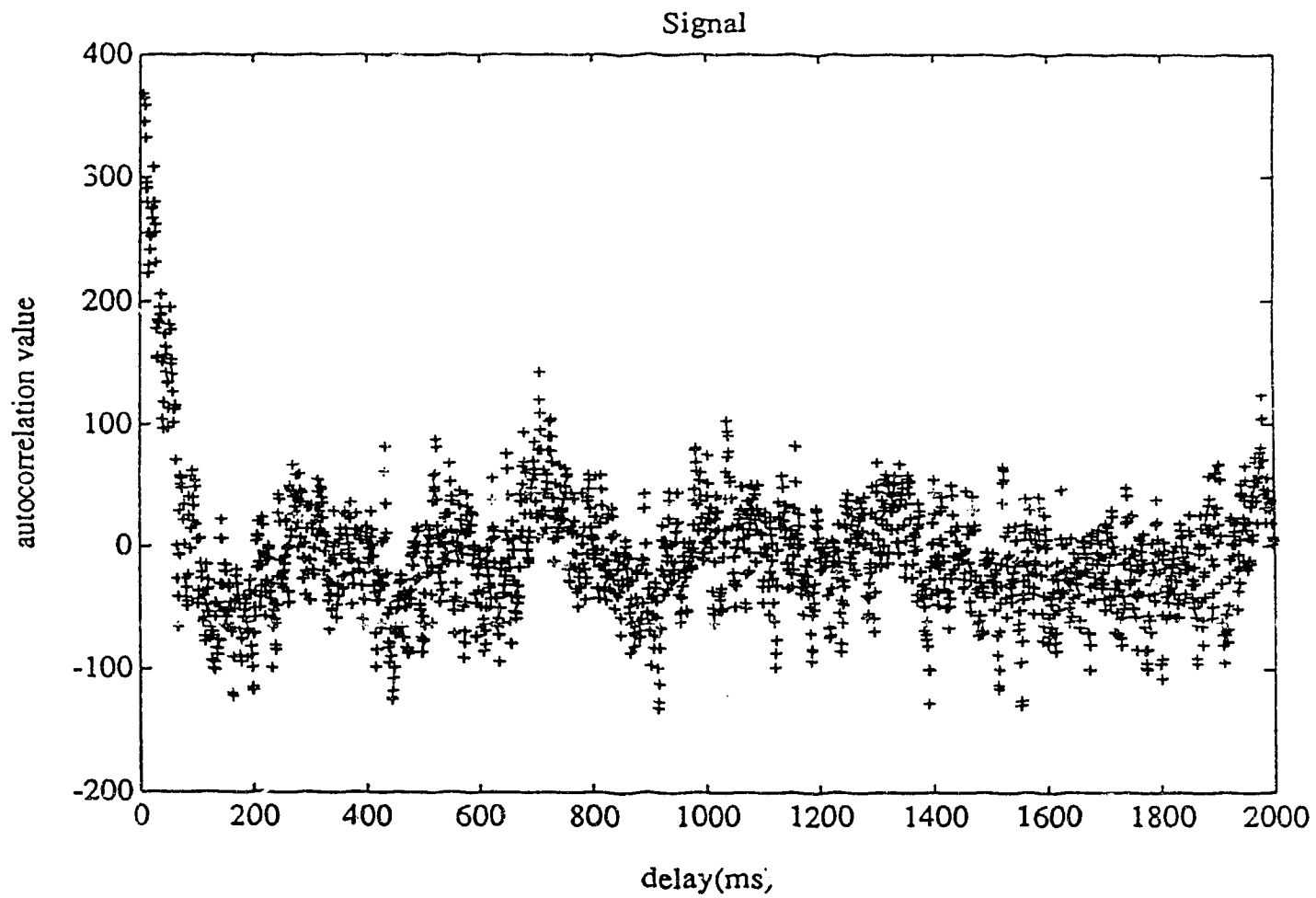


Fig. 2.28 Autocorrelation of a section of 2000 points from the signal in Fig. 2.26.

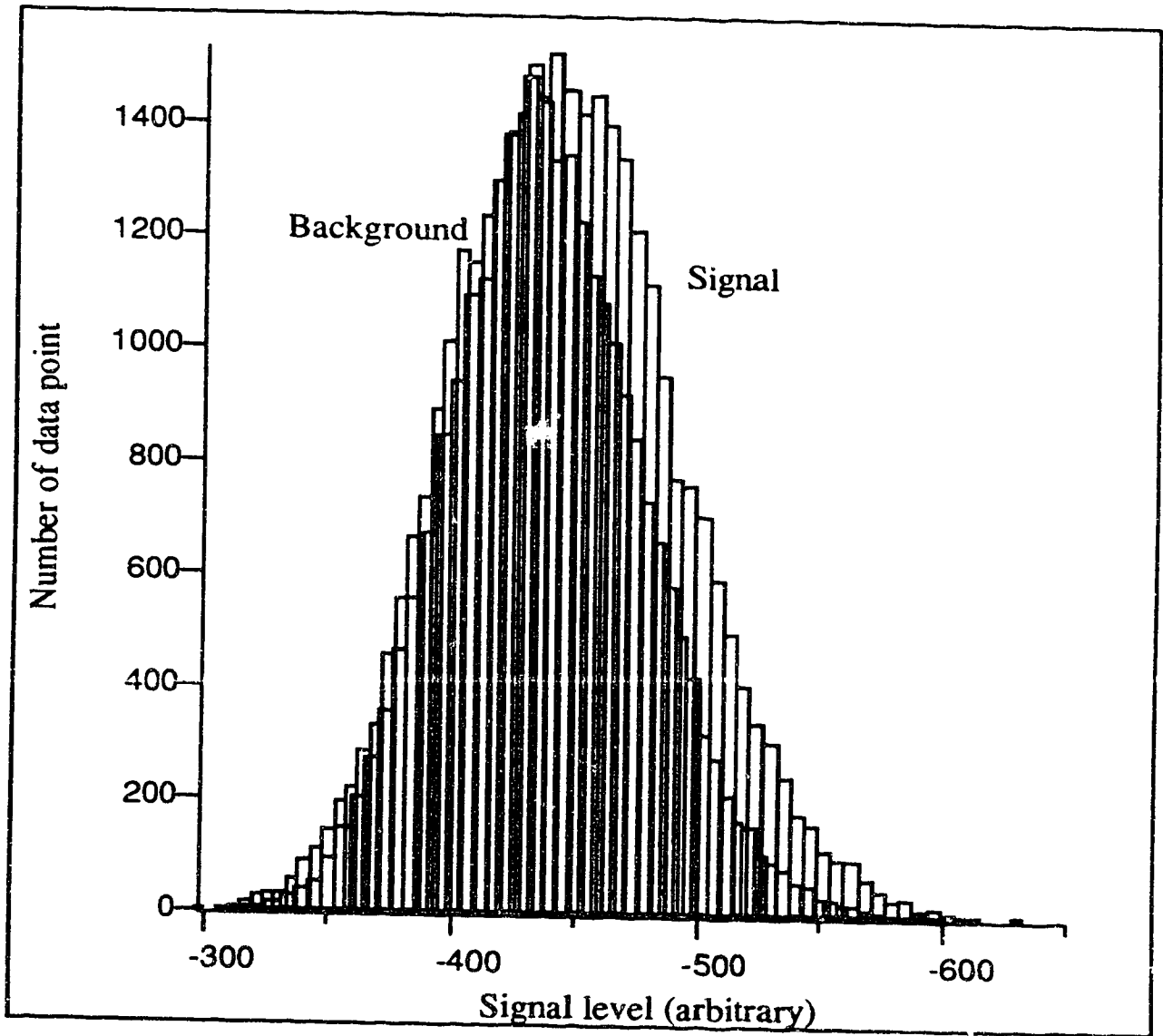


Fig. 2.29 The histogram of the data from Fig. 2.26. The signal part of the histogram is derived from the first 30 seconds with the sample flowing, and the background histogram is derived from the last 30 second (from 40 to 70 seconds) without the sample flowing. There is a significant shift of the maximum for the signal histogram.

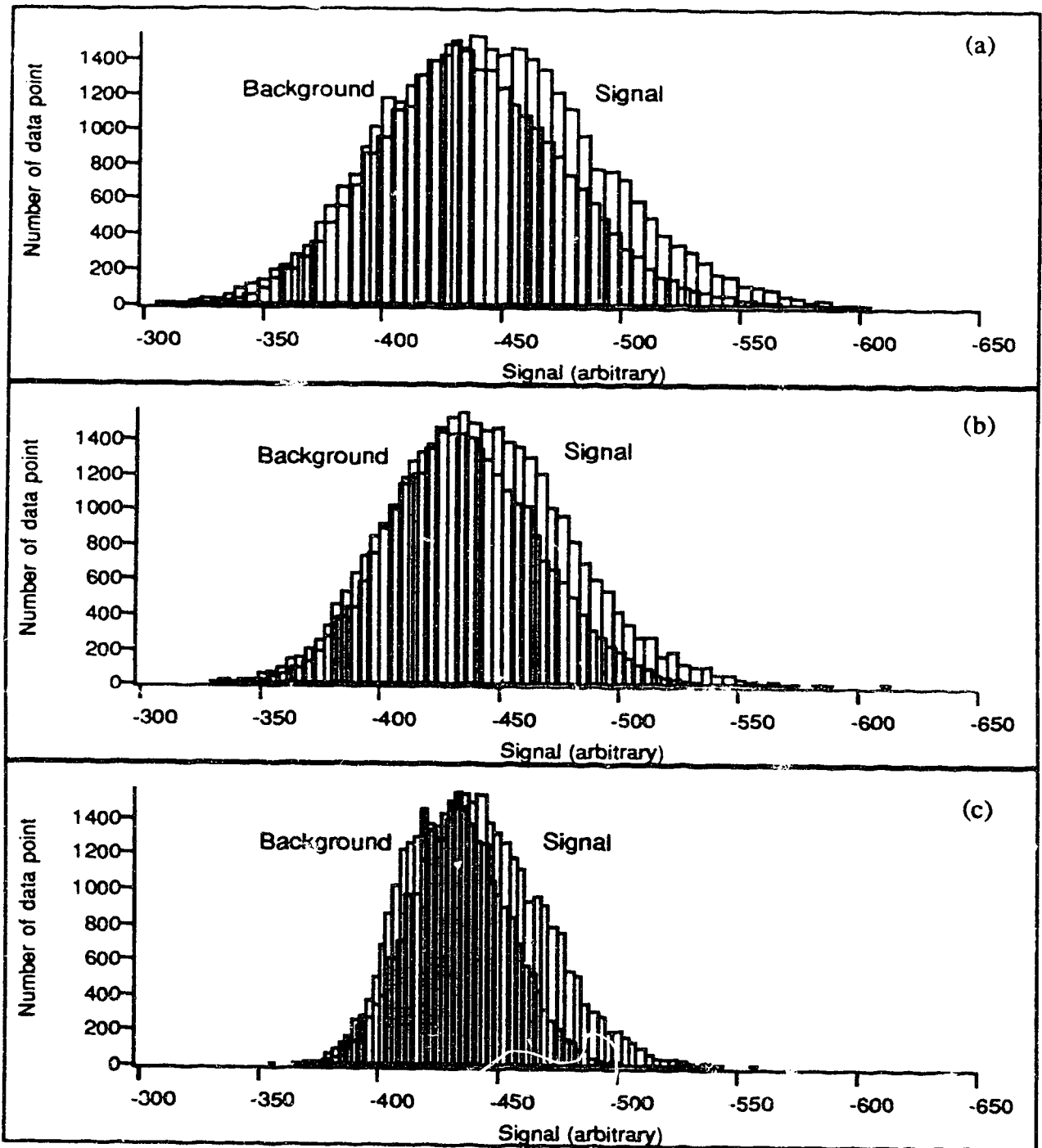


Fig. 2.30 Comparison of the histograms from three sets of data: (a) is from data conditioned by a 1000 Hz low pass filter, (b) 100 Hz filtered, and (c) 31.5 Hz filtered.

A series of data was taken for different flow rates of the sample solution. The different voltages used to drive the sample flow are listed in Table 2.5. In each case, data were collected during the first 30 seconds when sample was flowing and during the last 40 seconds when the polarity of the power supply was reversed in order to switch off the sample flow. The sample flow rates were controlled at 6, 11, 17, 23 and 28 molecules/s respectively. The digitization rate was 1000 Hz, the signal was conditioned with a 31.5 Hz low pass filter, and each electropherogram contains 70,000 data points. The histograms of the first 30,000 and the last 30,000 data points of each are plotted and shown in Figure 2.31.

From (a) to (e) in Figure 2.31, it is clearly shown that as the sample flow rate increases, the signal level also increases while the histograms of background signals in all five sets of histograms are very similar. As has been determined, the time for a single molecule to pass the laser beam is around 40 milliseconds. When the sample flow rate is 25 molecules per second, it should be expected that on an average, there will be one molecule on average in the laser beam. In Figure 2.31 (e) the flow rate is 28 molecules per second. It is a reasonable guess that the maximum of the histogram should be the signal level generated by a single molecule present in the laser beam. The single molecule signal level is located at about between 2σ to 3σ from the maximum of the Gaussian shaped background histogram. This suggests that the mean of the signal level of a single molecule is around 2 to 3 times the standard deviation of the background signal. Setting a threshold at the mean of the single molecule signal level, it is possible to count molecules flowing through the electrophoresis system.

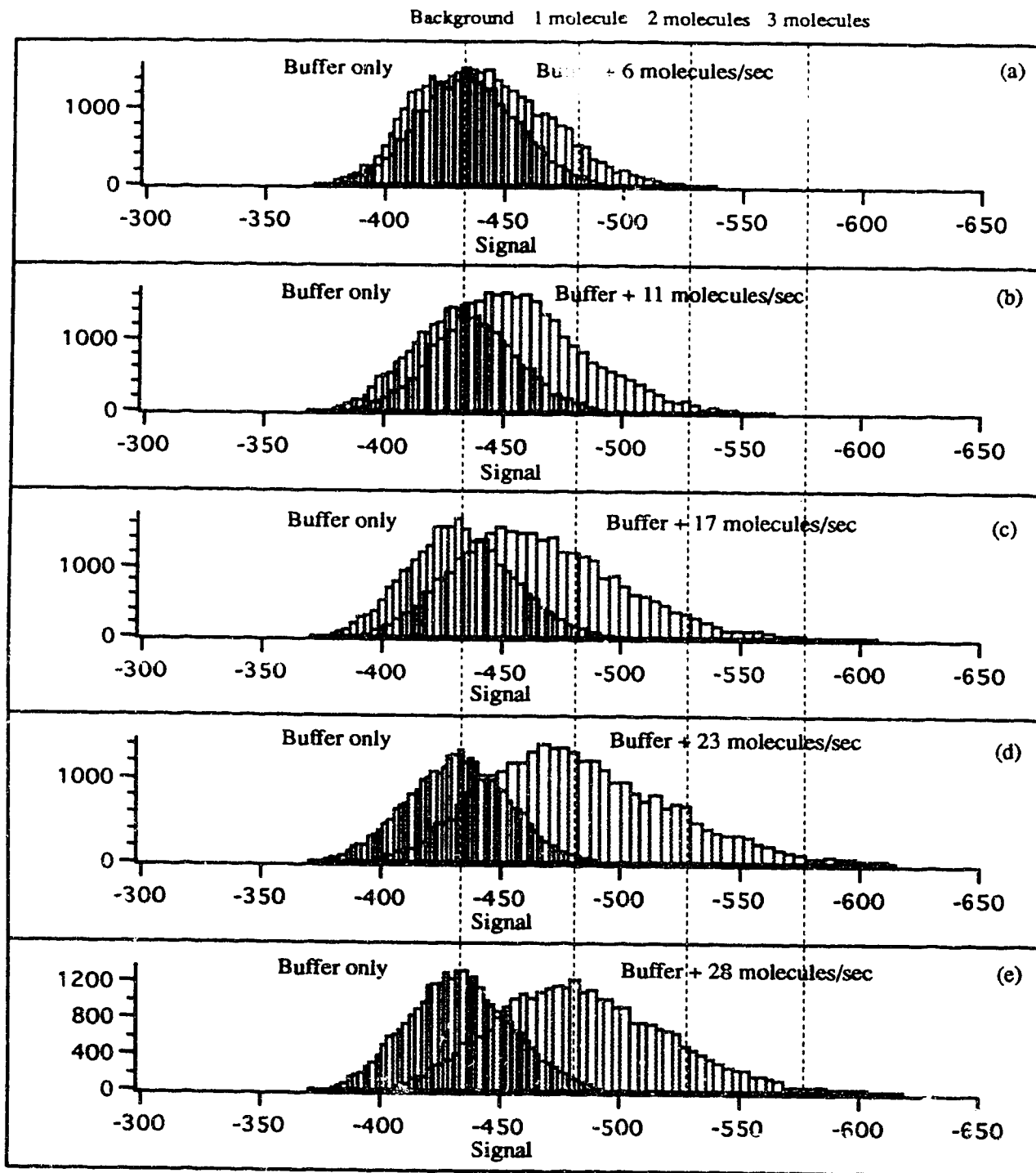


Fig. 2.31 The histograms of the data collected at different sample flow rate.

Counting analyte molecules is one of the ultimate goals for an analytical chemist. Based on the analysis on the histograms of the data obtained (Figure 2.31), it should be possible to make counting molecules a reality. By setting a threshold on the signal, it is possible to count the peaks above the threshold as signals generated by fluorescent molecules. However, there are two kinds of error when the signal level is close to the detection limit. The error of the first kind is claiming that an analyte molecule is absent when it is present. The error of the second kind is claiming that an analyte molecule is present when it is absent. When the threshold is set at the mean of the signal level generated by single molecules, the probability of the error of first kind is 50%.

The maximum of the signal distribution in Figure 2.31(e) is chosen as the threshold because on average there will be one molecule present in the laser beam when there are 28 molecules per second flowing through the laser beam. Another threshold is set at two times the difference of the first threshold from the mean of the background, and the third threshold is set at three times the difference. Any peak above the first threshold but below the second will be counted as one molecule; any peak above the second but below the third threshold is counted as two molecules; and any peak above the third threshold is counted as three molecules. Figure 2.32 shows a randomly chosen 8 second portion of the data which is the basis of the histogram in Figure 2.31(a). There were 6 molecules on average passing through the laser beam while the first 30 seconds of the data was collected. From the 8 second section, 48 counts are found (this is purely a coincidence). To compare with the background, another portion from the same run after the sample flow was stopped was also chosen randomly; 12 counts are found in this section (Figure 2.33). With this threshold, the false count rate from the background is high because the threshold is set relatively low. The error of the second kind is 25%, the error of the first kind is also 25%. The number of molecules is estimated as the number of counts while the sample is flowing subtracted by the number of counts from the blank.

The background ground count rate can be reduced by increasing the level of the threshold. Figure 2.34 shows the same data as Figure 2.32, with higher thresholds. There are 32 counts in 8 seconds in this case, and 7 counts in the portion when the sample flow was stopped (Figure 2.35). The experiment listed in Table 2.5 were repeated and all data were plotted the same way as shown in Figure 2.34 and 2.35 and the peaks were counted. The results are listed in Table 2.6. The average count rate after subtracting the average background count rate is 62% of the expected count rate calculated from the sample concentration and the volumetric flow rate. The average error of the first kind in this case is 38%, and the error of the second kind (false count) is 4% which is much smaller than the case when the threshold is set low. The actual count rate and the background count rate vs. expected count from each experiment are plotted in Figure 2.36.

When the sample flow rate is at 6 molecules per second, most fluorescence signal is generated by single molecules. The fact that the background corrected count rate is 50% of the expected count rate suggests that the adjusted threshold is at the mean signal level generated by single molecules. When the flow rate increases, there will be more two-molecule or three-molecule events. The signal generated by two or three molecules is much higher than 3σ of the background and there will be fewer errors of the first class. This may be the reason that the percentage of the background corrected count tends to increase as the sample flow rate increases.

With further improvement in instrumentation, the signal-to-noise ratio can be improved so that the signal from a single fluorescent molecule will reach the level that errors of both the first kind and second kind will be insignificant. Numerous applications of single molecule detection can be found in analytical chemistry and related fields. The second part of this thesis will demonstrate some applications of high sensitivity fluorescence detectors in high speed DNA sequencing.

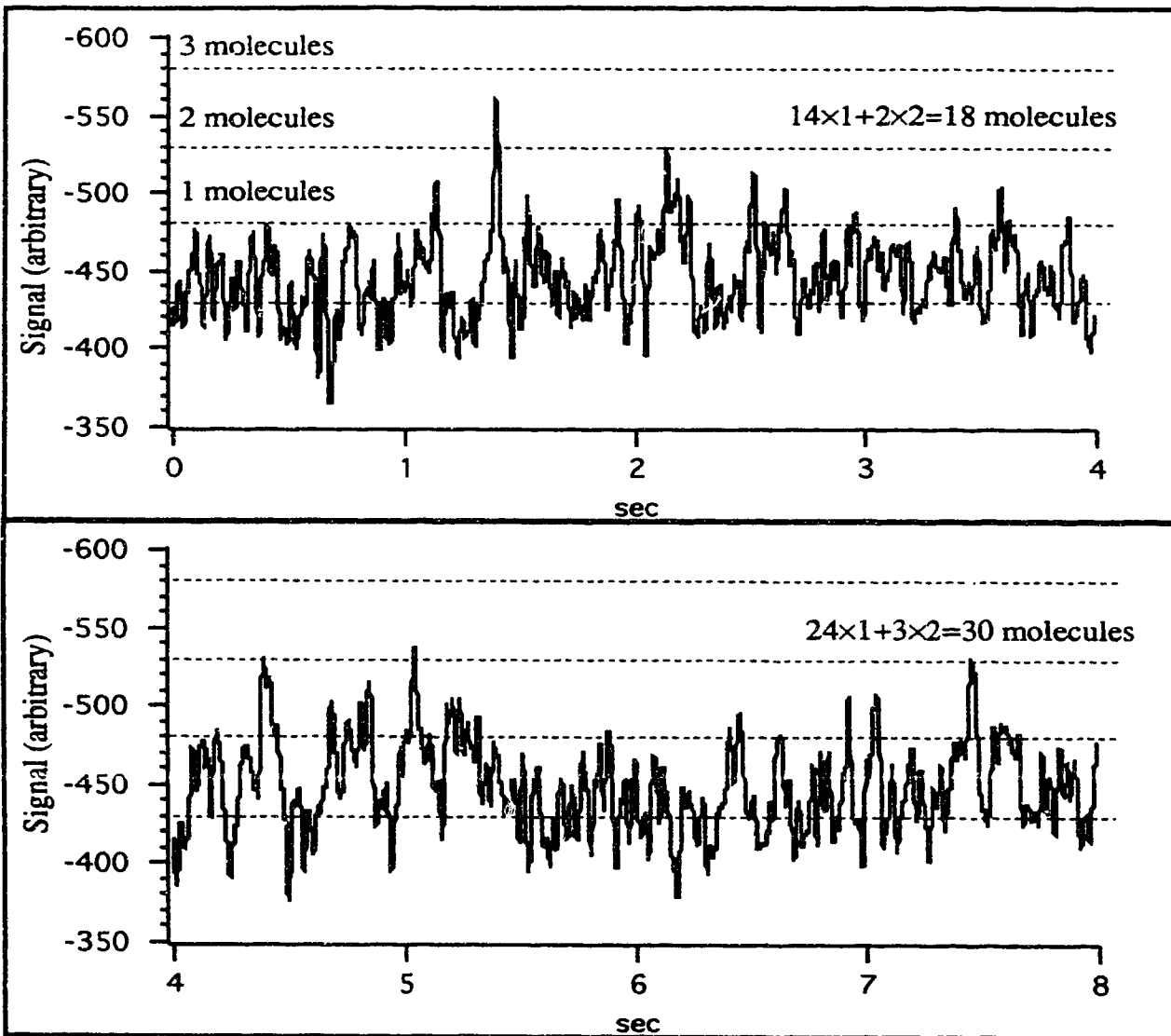


Fig. 2.32 A segment of data which was collected when the sample flow rate was 6 molecules per second.

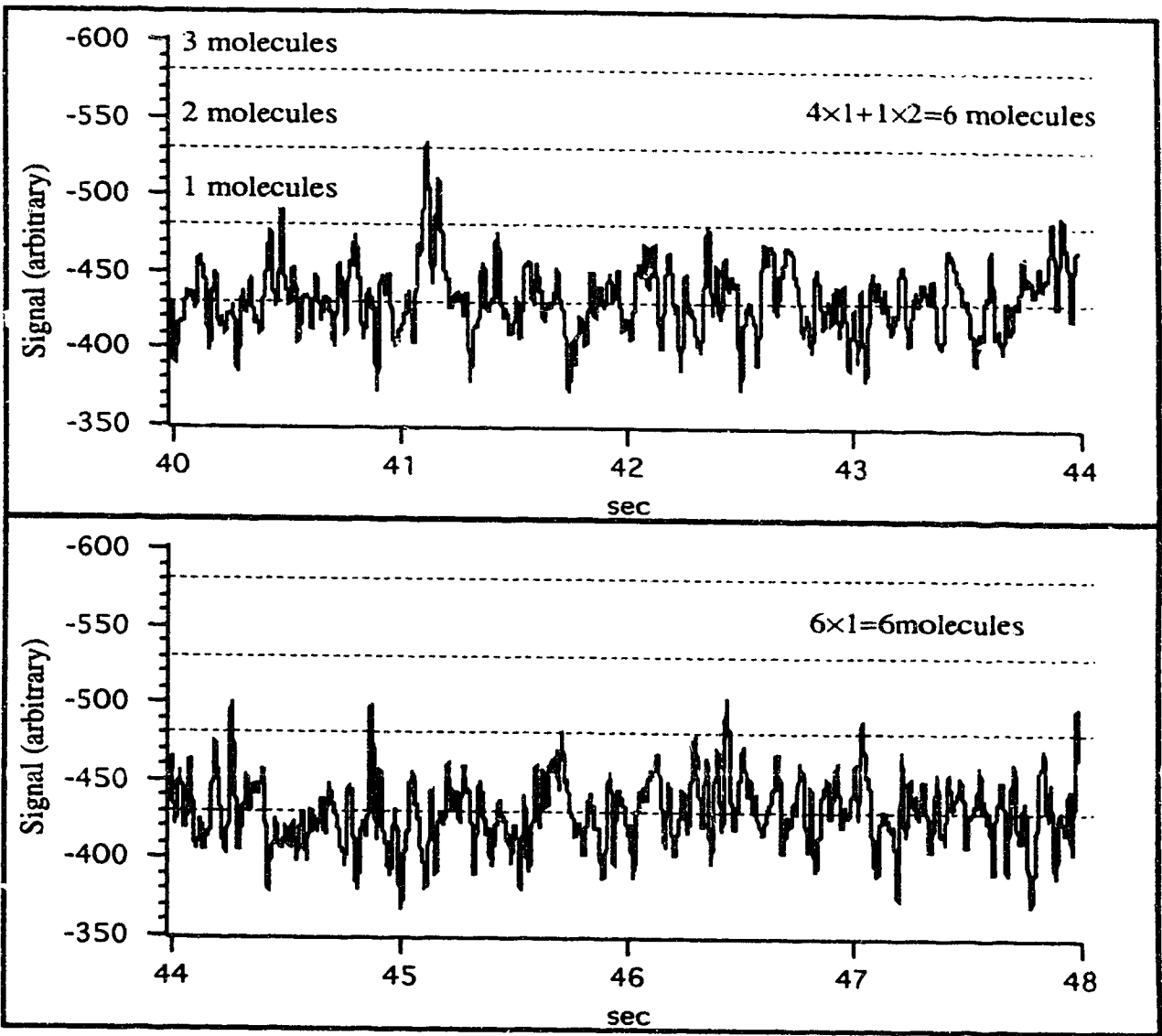


Fig. 2.33 A segment of data which is collected when there should be only buffer in the probed volume.

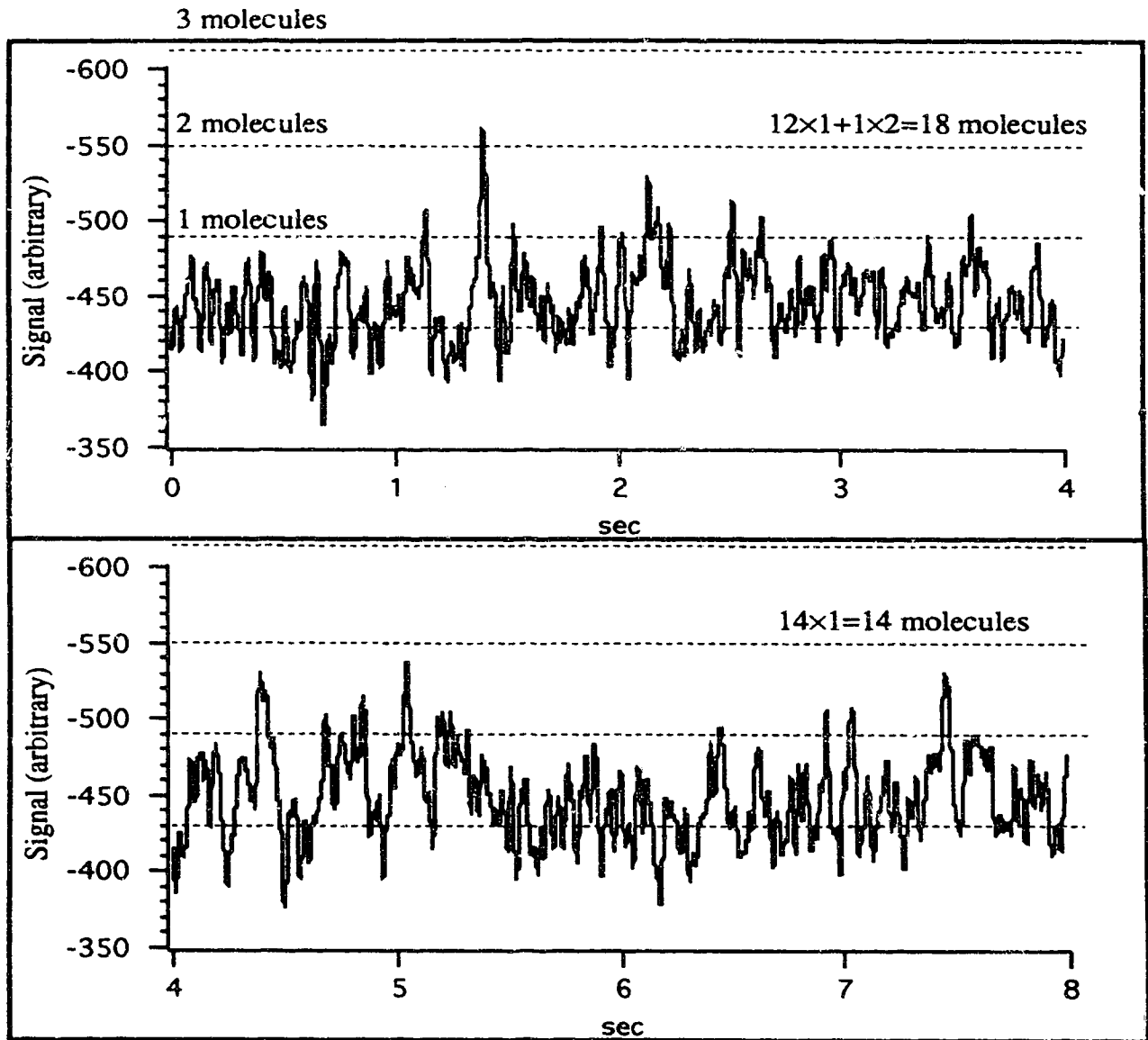


Fig. 2.34 Counting molecules based on the adjusted threshold, 6 molecules per second is expected.

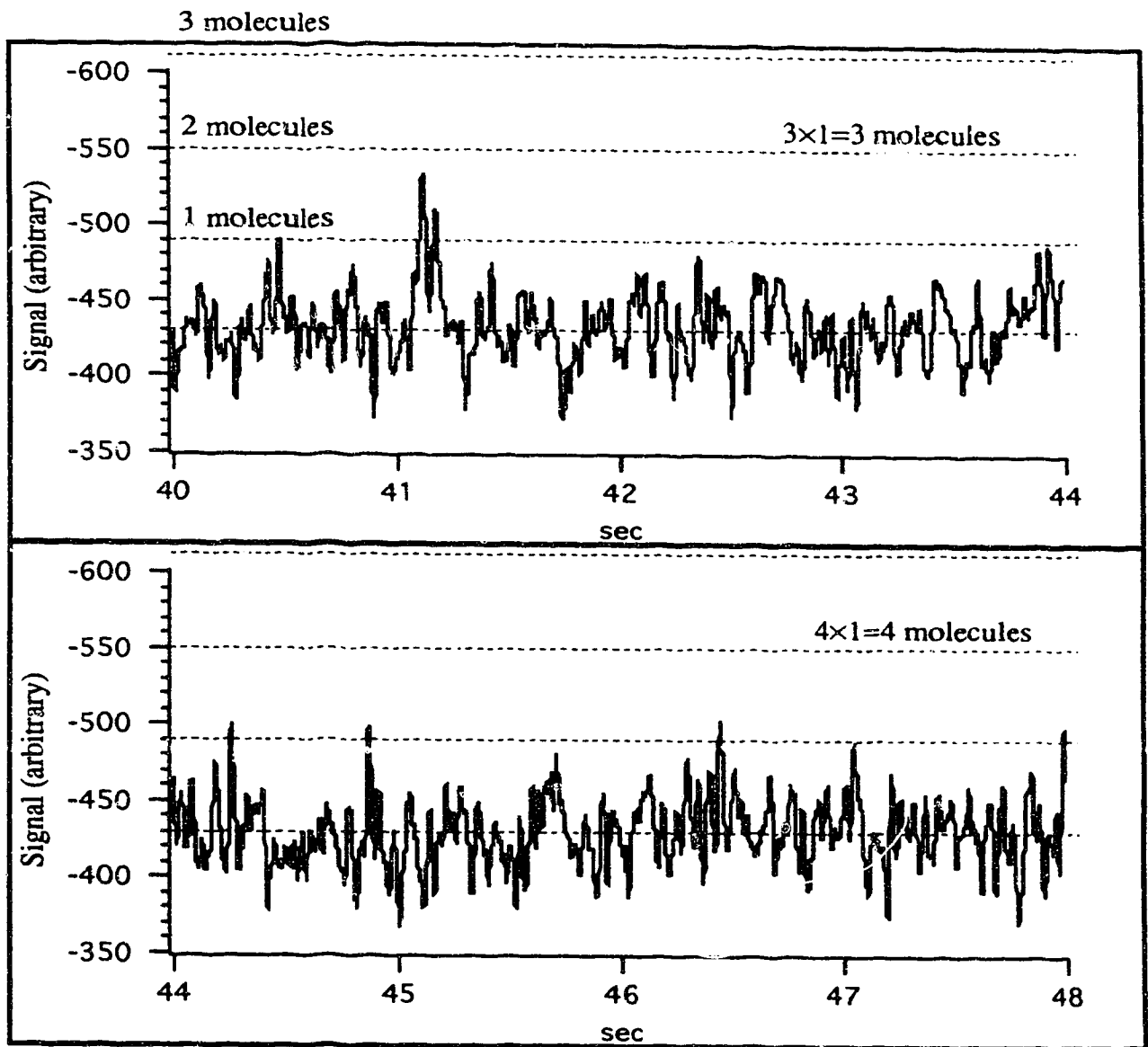


Fig. 2.35 Counting molecules based on the adjusted threshold, buffer only.

Table 2.6 The results of counting molecules at different flow rates.

| Expected (molecules/s) | Actual count (molecules/s) | Background count (molecules/s) | Background corrected (molecules/s) | Background corrected/expected |
|---------------------------|-------------------------------|--------------------------------------|--|----------------------------------|
| 6 | 3.6 | 0.6 | 3 | 0.5 |
| 6 | 3.6 | 0.6 | 3 | 0.5 |
| 11 | 8.4 | 0.7 | 7.7 | 0.7 |
| 11 | 7.5 | 1.5 | 6.0 | 0.545 |
| 17 | 10.4 | 0.8 | 9.6 | 0.565 |
| 17 | 11.6 | 0.8 | 10.8 | 0.635 |
| 23 | 17.1 | 0.5 | 16.6 | 0.722 |
| 23 | 16.3 | 0.7 | 15.6 | 0.678 |
| 28 | 18.7 | 0.6 | 18.1 | 0.646 |
| 28 | 21.7 | 0.7 | 21.0 | 0.75 |

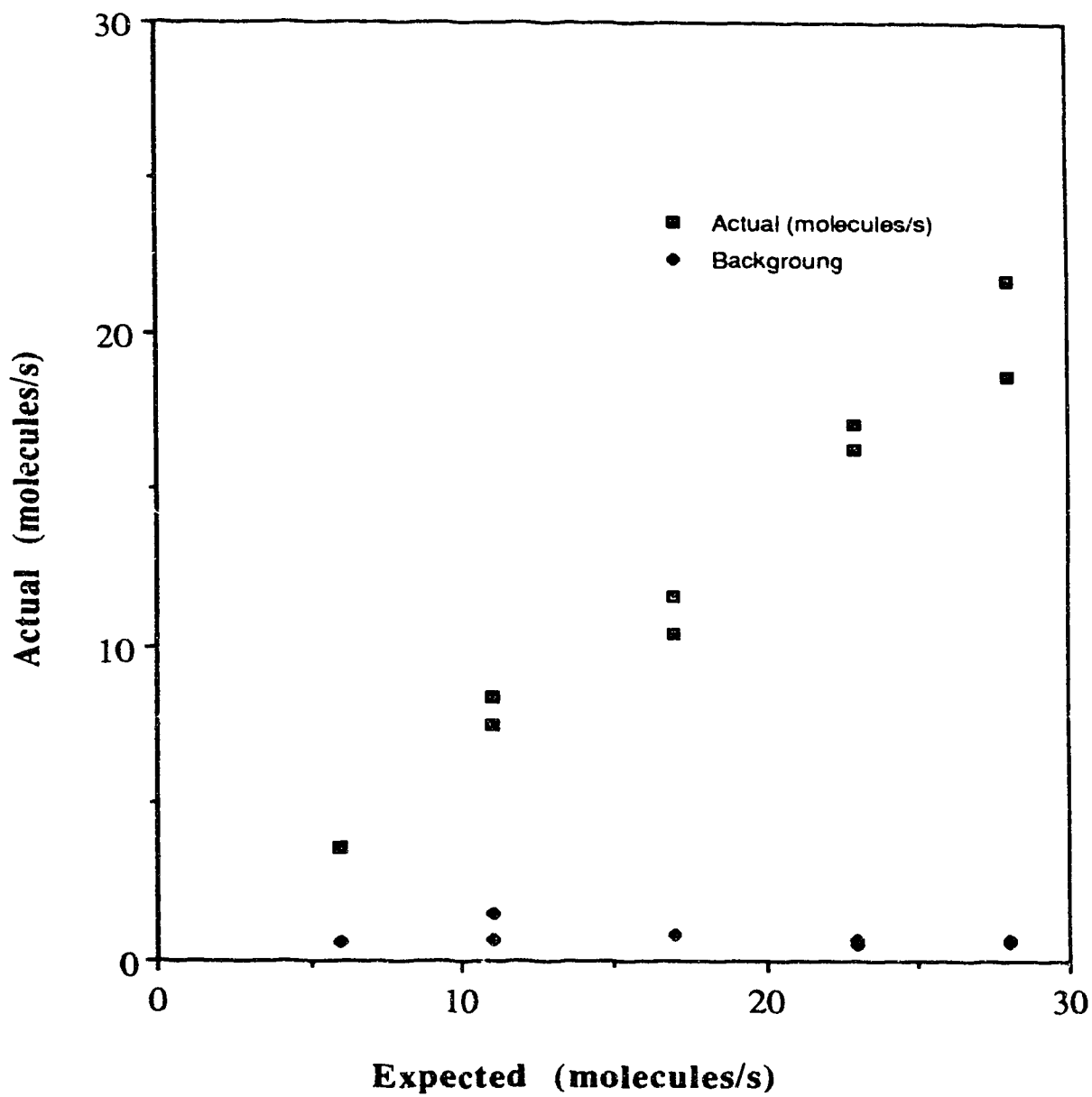


Fig. 2.36 The comparison of expected, actual and background counts of molecules flowing out of the capillary.

References:

1. Smith, R.D., Olivares, J.A., Nguyen, N.T., and Udseth, H.R., *Anal. Chem.*, (1988), **60**(5): p. 436.
2. Udseth, H.R., Loo, J.A., and Smith, R.D., *Anal. Chem.*, (1989), **61**(3): p. 228.
3. Wallingford, R.A. and Ewing, A.G., *Anal. Chem.*, (1987), **59**(4): p. 678.
4. Wallingford, R.A. and Ewing, A.G., *Anal. Chem.*, (1988), **60**: p. 1972.
5. Huang, X., Luckey, J.A., Gordon, M.J., and Zare, R.N., *Anal. Chem.*, (1989), **61**(7): p. 766.
6. Terabe, S., Otsuka, K., Ichikawa, K., Tsuchiya, A., and Ando, T., *Anal. Chem.*, (1984), **56**(1): p. 111.
7. Walbroehl, Y. and Jorgenson, J.W., *J. Chromatogr.*, (1984), **315**, p. 135.
8. Pentoney, S.L.J., Zare, R.N., and Quint, J.F., *Anal. Chem.*, (1989), **61**(15): p. 1642.
9. Bornhop, D.J. and Dovichi, N.J., *Anal. Chem.*, (1987), **59**(13): p. 1632.
10. Yu, M. and Dovichi, N.J., *Mikrochim. Acta*, (1988), **III**: p. 27.
11. Yu, M. and Dovichi, N.J., *Appl. Spectrosc.*, (1989), **43**(2): p. 196.
12. Yu, M. and Dovichi, N.J., *Anal. Chem.*, (1989), **61**(1): p. 37.
13. Cheng, Y.F. and Dovichi, N.J., *Science (Washington, D. C.)*, (1988), **242**(4878): p. 562.
14. Wu, S. and Dovichi, N.J., *J. Chromatogr.*, (1989), **480**, p. 141.
15. Cheng, Y.F., Wu, S., Chen, D.Y., and Dovichi, N.J., *Anal. Chem.*, (1990), **62**(5): p. 496-503.
16. Burton, D.E., Sepaniak, M.J., and Maskarinec, M.P., *J. Chromatogr. Sci.*, (1986), **24**(8): p. 347.
17. Wright, B.W., Ross, G.A., and Smith, R.D., *J. Microcolumn*, Sep, 1989. **1**(2): p. 85.
18. Gassmann, E., Kuo, J.E., and Zare, R.N., *Science (Washington, D. C.)*, (1985),

- 230(4727): p. 813.
19. Nickerson, B. and Jorgenson, J.W., *J. High Resolut. Chromatogr. Chromatogr. Commun.*, (1988), **11**(7): p. 533.
 20. Christensen, P.L. and Yeung, E.S., *Anal. Chem.*, (1989), **61**(13): p. 1344.
 21. Swaile, D.F. and Sepaniak, M.J., *J. Microcolumn , Sep.*, (1989), **1**(3): p. 155.
 22. Green, J.S. and Jorgenson, J.W., *J. Chromatogr.*, (1986), **352**: p. 337.
 23. Pentoney, S.L.J., Huang, X., Burgi, D.S., and Zare, R.N., *Anal. Chem.*, (1988), **60**(23): p. 2625.
 24. Nickerson, B. and Jorgenson, J.W., *J. Chromatogr.*, (1989), **480**: p. 157.
 25. Dovichi, N.J. and Cheng, Y.F., *Am. Biotechnol. Lab.*, (1989), **7**(2): p. 10
 26. Smith, M.L., ~~Cheng, Y.F.~~ and Griffin, C.W., *J. Bacteriol.*, (1962), **83**: p. 1358
 27. Brandtzaeg, P., *Ann. NY Acad. Sci.*, (1975), **254**: p. 35.
 28. Herzenberg, L.A., Sweet, R.G., and Herzenberg, L.A., *Sci. Am.*, (1976), **234**: p. 108-117.
 29. Folestad, S., Johnson, L., and Josefsson, B., *Anal. Chem.*, (1982), **54**: p. 925
 30. Kuhr, W.G. and Yeung, E.S., *Anal. Chem.*, (1988), **60**(17): p. 1832.
 31. Zarrin, F. and Dovichi, N.J., *Anal. Chem.*, (1985), **57**: p. 2690.
 32. Dovichi, N.J., Martin, J.C., Jett, J.H., and Keller, R.A., *Science (Washington, D. C.)*, (1983) **219**: p. 845.
 33. Dovichi, N.J., Martin, J.C., Jett, J.H., Trkula, M., and Keller, R.A., *Anal. Chem.*, (1984), **56**: p. 348.
 34. Nguyen, D.C., Keller, R.A., Jett, J.H., and Martin, J.C., *Anal. Chem.*, 1987. **59**: p. 2158.
 35. Peck, K., Stryer, L., Glazer, A.N., and Mathies, R.A., *Proc. Natl. Acad. Sci.*, 1989. **86**: p. 4087.
 36. Knoll, J.E., *J. Chrom. Sci.*, 1985. **23**: p. 422.

Part II

DNA Sequencing with Capillary

Gel Electrophoresis

Chapter 3 Single-Color Laser-Induced Fluorescence Detection and Capillary Gel Electrophoresis for DNA Sequencing*

3.1 Introduction

In 1977 Sanger's group reported a powerful technique for DNA sequencing[1]. A set of radioactively labeled DNA fragments is generated in four reactions and separated in adjacent lanes of a high resolution polyacrylamide gel. Autoradiography is used for detection of the bands of DNA fragments. The sequence is interpreted from a series of alternating bands in the lanes corresponding to the terminal base.

An advance in sequencing technology occurred in 1986-87 when Smith and co-workers in Hood's laboratory, workers in Ansorge's group, and Prober and co-workers at DuPont reported DNA sequencers that replaced the radioactive labels and autoradiography in Sanger's method with fluorescent labels and laser-based detection[2-4]. In Smith's and Prober's automated sequencers, one of four fluorophores is associated with the terminating dideoxynucleotide either through use of four separate dideoxynucleotide reactions with four labeled primers that are pooled before use (Smith) or through use of fluorescently labeled dideoxynucleotides in a single reaction mixture (Prober). In Ansorge's method, a single fluorescent label is used with each dideoxynucleotide chain terminating reaction and the products are run on separate lanes of a slab gel. These automated fluorescence sequencers have been commercialized by Applied Biosystems, Pharmacia, and DuPont; as an example, the Applied Biosystem instrument runs 16 lanes simultaneously on a slab gel to produce sequencing rates of 75 bases/hour/lane or 1,200 bases/hour/slab. Similar

* Some of the material in this chapter has been published in *Analytical Chemistry* (63, 24, 2835-2842, 1991), *Journal of Chromatography* (559, 1-2, 237-246, 1991), and *SPIE: Optical methods for Ultrasensitive Detection and Analysis: Techniques and Applications* (1435, 161, 1991)

sequencing rates are produced by the other instruments. Sequence may be determined, by use of computer algorithms, to about 450 bases, and is limited by the resolution of the gel.

In 1990, Richardson and Tabor, and independently Ansorge, reported a sequencing technique based on a single fluorophore; by varying the amount of dideoxynucleotide in the reaction mixture, each base is identified with a particular fluorescence peak height during separation in a single lane of an acrylamide gel[5-6]. This technique relies on uniform labeling of the reaction product through use of the manganese-T7 polymerase reaction. In the work that has been published, a fluorescein labeled primer is excited with an argon ion laser at 488 nm; emission is detected in a single spectral band.

Gel filled capillaries have attracted interest for DNA sequencing because their high surface-to-volume ratio provides excellent heat transport properties, allowing use of very high electric field strength. Early work with capillary-dimension electrophoresis media was performed by Edstrom, who described the use of very fine cellulose fibers (5 μm diameter) for electrophoresis of nucleic acids from single cells at an electric field gradient of 125 V/cm.[7-8]. In 1965, Matioli and Niewisch studied hemoglobin from single cells on fine polyacrylamide fibers of 50 μm diameter[9]. Grossbach reported the use of gel filled glass capillaries of 50-micrometer diameter in 1974[10]. Slightly larger scale capillary polyacrylamide gel electrophoresis was reported in 1970 by Neuhoff, et al. who used 5- μl capillaries for the study of ribonucleic acid polymerase[11]. In 1983, Hjerten reported the use of a 150- μm ID capillary polyacrylamide electrophoresis separation of several samples, including monomers through pentamers of bovine serum albumin[12]. Beginning in 1987, Karger and colleagues have reported capillary polyacrylamide gel electrophoresis for the separation of proteins, chiral amino acids, and polyadenosic acid fragments[13-16]. Several patents have been issued that describe the use of a bifunctional reagent to chemically bind polyacrylamide to the capillary surface[17-19]. Swerdlow and Gesteland have described the DNA sequence analysis by use of capillary polyacrylamide gel electrophoresis with on-column fluorescence detection[20]. Drossman and co-workers in

Smith's laboratory reported the separation of a single reaction mixture in gel-filled capillaries[21]. When operating at 400 V/cm, the system produced sequencing rates of 1,000 bases/minute after elution of the primer, a roughly twenty five times higher sequencing rate than produced by conventional slab gel electrophoresis. Resolution of the capillary based system was a factor of 2.4 superior to that produced by a slab gel. Luckey and co-workers in Smith's laboratory used a four-color sequencing system with the reaction products of the ABI sequencing system[22].

Laser-induced fluorescence detection in slab-gel electrophoresis requires low detection limits, typically on the order of 1 to 100 attomoles of each fragment[2-3]. This detection performance is complicated for both Smith's and Prober's techniques because the fluorescence signal must be measured in several spectral channels. However, the detection requirement in capillary gel electrophoresis is more severe. Based on a comparison of the cross-section of a capillary with the cross-section of a loading well in a slab-gel, Drossman has estimated that the sample loading in capillary gel electrophoresis will be on the order of 1 to 10 attomoles[21]. Detection limits in the zeptomole range (1 zeptomole = 10^{-21} mole = 600 molecules) are necessary for DNA sequencing by capillary gel electrophoresis. This task is complicated further by the requirement that the detection volume be less than 10^{-9} L to preserve the separation efficiency of the nano-scale electrophoresis technique. Swerdlow and Gesteland's system used an on-column laser-induced fluorescence detection with detection limits of 200 zmol of fluorescently labeled product[20]. Smith and co-workers described the use of one- and four-channel on-column fluorescence detectors; both the single- and four-channel detector produced detection limits of about 100 zmol of labeled fragment[21-22]. We have reported the use of a post-column fluorescence detector in the gel electrophoresis separation of the products of a single chain terminating reaction; detection limits were 10 zmol[24].

3.2 Experimental Section

A nested set of fluorescently labeled DNA fragments was kindly provided by C. Fuller of the United States Biochemistry Corporation. The method of Tabor and Richardson was adapted for capillary gel sequencing using a single fluorescent dye primer Tamra (tetramethylrhodamine labeled primer), and the template was an M13mp18 plasmid[5]. The sample was prepared to yield a nominal 8:4:2:1 ratio of peak heights for T, G, C, and A, respectively.

An interesting phenomenon was observed when the gel-filled capillary was operated at high electric field strength: the gel migrated about 100- μm from the detection (positive electrode) end of the capillary. This migration is different from the well known migration of the gel from the injection (negative electrode) end of the capillary caused by electro-osmosis. The migration from the detection end, presumably due to electrostriction, is undesirable because the gel can block the laser beam which is positioned a few micrometers beyond the tip of the capillary. To eliminate this migration, the gel was covalently bound to the wall of the detection tip of the capillary; the last five millimeters of the detection end of the capillary was dipped for a few seconds into a 0.5% by volume solution of γ -methacryloxypropyltrimethoxysilane in a 1:1 water:acetic acid solvent. The gel was poured within 15 minutes of treatment of the capillary tip.

The polyacrylamide gel (6%T, 5%C, 6 M urea, 30% formamide) was covalently cross-linked to the walls of the 50- μm inner diameter, 190- μm outer diameter capillary thorough use of a bifunctional silane reagent. The sample was injected at 150 V/cm for 30 seconds; after injection, the sample was replaced with a fresh vial of 1 \times TBE. The separation proceeded at 150 V/cm. The sheath stream was 1 \times TBE at a flow rate of 0.16 ml/hr.

A 0.75 mW helium-neon laser beam ($\lambda = 543.5 \text{ nm}$) was focused with a 4 \times microscope objective about 200- μm below the exit of the capillary with a 200- μm square

flow chamber and 2-mm thick windows (Figure 3.1). Fluorescence was collected at right angles with a 18×, 0.45 numerical aperture objective and imaged onto a 0.8-mm diameter pinhole. A single interference filter (590 nm center, 40 nm band pass) was used to block scattered laser light. Fluorescence was detected with an R1477 photomultiplier tube, cooled to -15° C. The photomultiplier tube output was passed through a 1-s RC low-pass filter and digitized by a computer at 2 Hz and was passed through a 21 point quadratic-cubic polynomial filter before display.

3.3 Results and Discussion

3.3.1 Peak height encoded one color DNA sequencing

Our capillary gel electrophoresis detector is based on a post-column sheath flow cuvette to reduce the background signal. In this detector, similar to that used in flow cytometry, the sample flows as a narrow stream in the center of a 200- μ m square flow chamber, surrounded by a sheath stream consisting of conducting buffer. The high optical quality windows of the cuvette produce much less light scatter than does an on-column detector. Also, by transferring the analyte to the moving sheath stream, the linear velocity, and hence the illumination time of the analyte, is independent of fragment length. The extent of photobleaching, which depends on illumination time, is constant for all analyte. We have reported the use of a single spectral channel fluorescence detector based on the sheath flow cuvette for capillary zone electrophoresis separation of zeptomole quantities of fluorescently labeled amino acids and for capillary gel electrophoresis separation of zeptomole quantities of the products of a single dideoxynucleotide reaction[23-26]; Keller's group has reported high sensitivity detection for neat solutions of highly fluorescent dyes[27,28]. Recently, Keller's group has reported, and Mathies' group has

Fig. 3.1

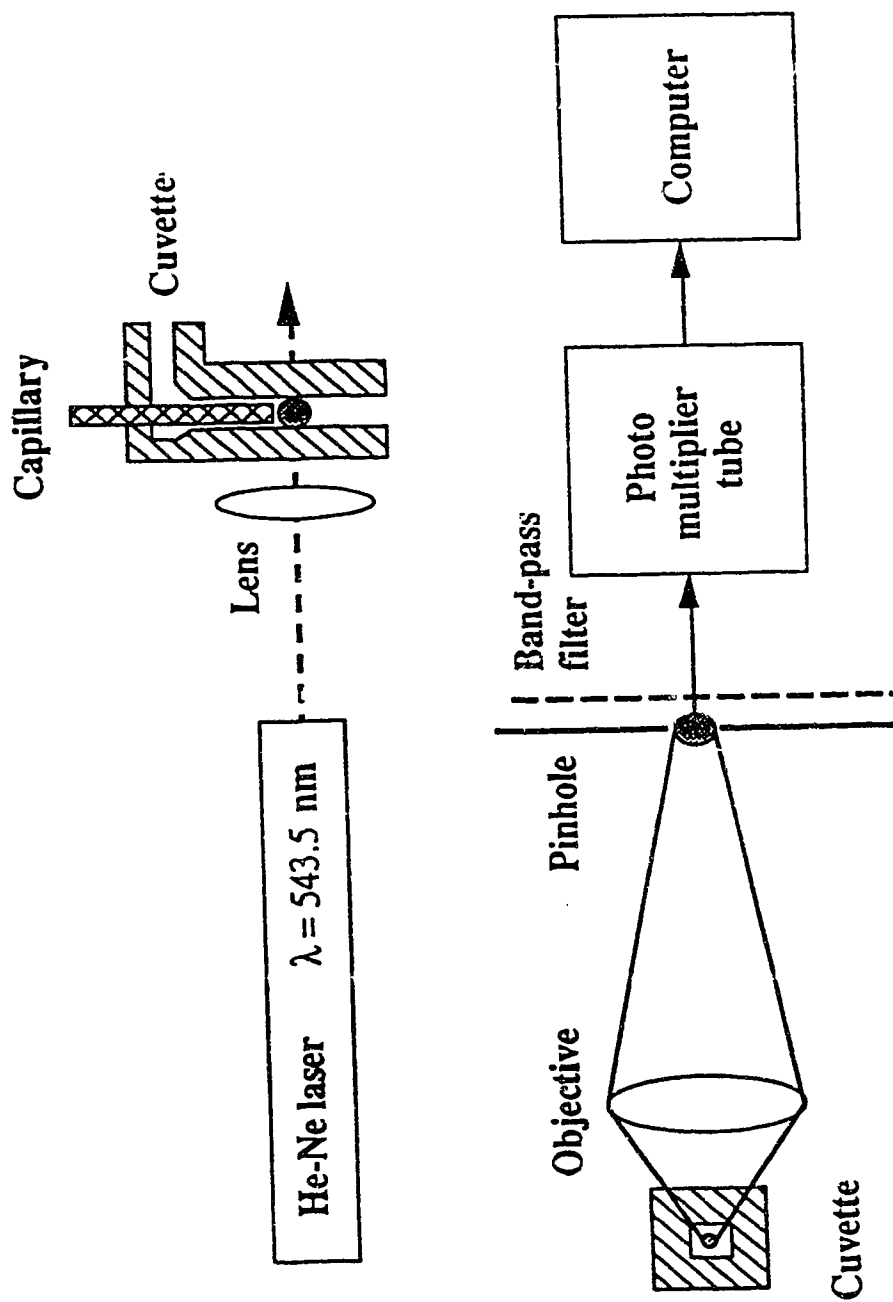


Fig. 3.1 Laser-induced fluorescence detector for one-spectral channel sequencing. A 0.75 mW helium-neon laser beam ($\lambda = 543.5$ nm) was focused with a 4 \times microscope objective about 200- μ m below the exit of the capillary in a sheath flow cuvette. The cuvette had a 200- μ m square flow chamber and 2-mm thick window. Fluorescence was collected at right angles with an 18 \times , 0.45 numerical aperture objective and imaged onto a 0.8-mm diameter pinhole. A single interference filter (590 nm center, 40 nm band pass) was used to block scattered laser light. Fluorescence was detected with an R1477 photomultiplier tube, cooled to -15 $^{\circ}$ C. The photomultiplier tube output was passed through a 1-s RC low-pass filter and digitized by a computer. The signal is digitized at 2 Hz and passed through a quadratic-cubic polynomial filter before display.

confirmed, detection of single phycoerythrin molecules in neat solution with a single spectral channel fluorescence detector[29,30].

Fluorescence is collected with a high efficiency microscope objective and imaged onto a pinhole to restrict the field of view of the photodetector to the illuminated sample stream. A single band-pass filter is used to block scattered laser light, followed by detection with a cooled R1477 photomultiplier tube.

In our one-color sequencer, a tetramethylrhodamine-labeled primer is excited by a green helium-neon laser ($\lambda = 543.5 \text{ nm}$). A sheath flow cuvette is used as a post-column fluorescence detector to minimize background light scatter. Further reduction in the background signal comes from the relatively long excitation wavelength and low power excitation beam ($750 \mu\text{W}$). In fact, the major contribution to background signal is dark current produced by the photomultiplier tube. This contribution to the background signal is minimized by cooling the photomultiplier tube to -15°C .

The standard deviation in the background signal for this system corresponds to 700 ymol (1 yoctomole = 1 ymol = 10^{-24} mol) of labeled primer introduced onto the capillary; detection limits are, by definition, a factor of three higher (1,200 molecules). Detection limits improve for higher molecular weight fragments. A very low sheath flow rate is employed to transport analyte from the capillary to the illumination region. During this transit time, analyte can diffuse an appreciable amount, decreasing the effective concentration of analyte in the detector. However, higher molecular weight fragments undergo less diffusion and are more concentrated in the illumination volume. As a result, the detection limit for the system improves for larger DNA fragments which are typically produced in lower concentration by Sanger's method compared with early eluting fragments. These detection limits, produced by a very low power laser, are associated with the excellent spectral properties of the tetramethylrhodamine fluorophore and reflect the simple detector design required by the single color sequencing technique.

By varying the ratio of dideoxynucleotides used in the chain extension reaction, the identity of the terminal dideoxynucleotide is encoded in peak height (Fig. 3.2). In any local neighborhood, peaks associated with T will be higher than peaks associated with G which, in turn are larger than C and A. However, the reaction is not completely accurate. It is not sufficient to mix the dideoxynucleotides in a 8:4:2:1 ratio to obtain a corresponding peak height ratio. Instead, it is first necessary to determine the incorporation efficiency of each dideoxynucleotide and then to modify the dideoxynucleotide ratio to produce the desired peak height ratio. The data shown in Figure 3.2 also suffers from ghost peaks, associated with pauses in the sequencing reaction, which increases peak amplitude. Ghost peaks are a particular problem for the A terminated fragments because of their low amplitude. Superimposed on the peak height modulation associated with the dideoxynucleotide ratios is a general exponential decrease in peak height with base number, which occurs as the reaction mixture is depleted with time.

This reaction, when applied to M13mp18, frequently produces compressions in standard sequencing gels; at 92 minutes in the separation, there is a TA compression that is not resolved by this gel. To minimize compressions, 30% by volume formamide was incorporated in the 6%T, 5%C gel for separation of the sequencing products from an M13mp18 template. Alternatively, rather than performing the separation at room temperature, the gel could be run at higher temperatures to denature the fragments further. The data, obtained at modest electric field strength, 150 V/cm, suffers from low migration rate, 70 bases/hour, and reflects the low mobility of fragments in the formamide modified gels. Much higher separation rates are produced in conventional acrylamide gels at higher electric fields[31]. The peaks across this region are well resolved; the resolution ranges from 1.2 to 1.8, with an average of about 1.5.

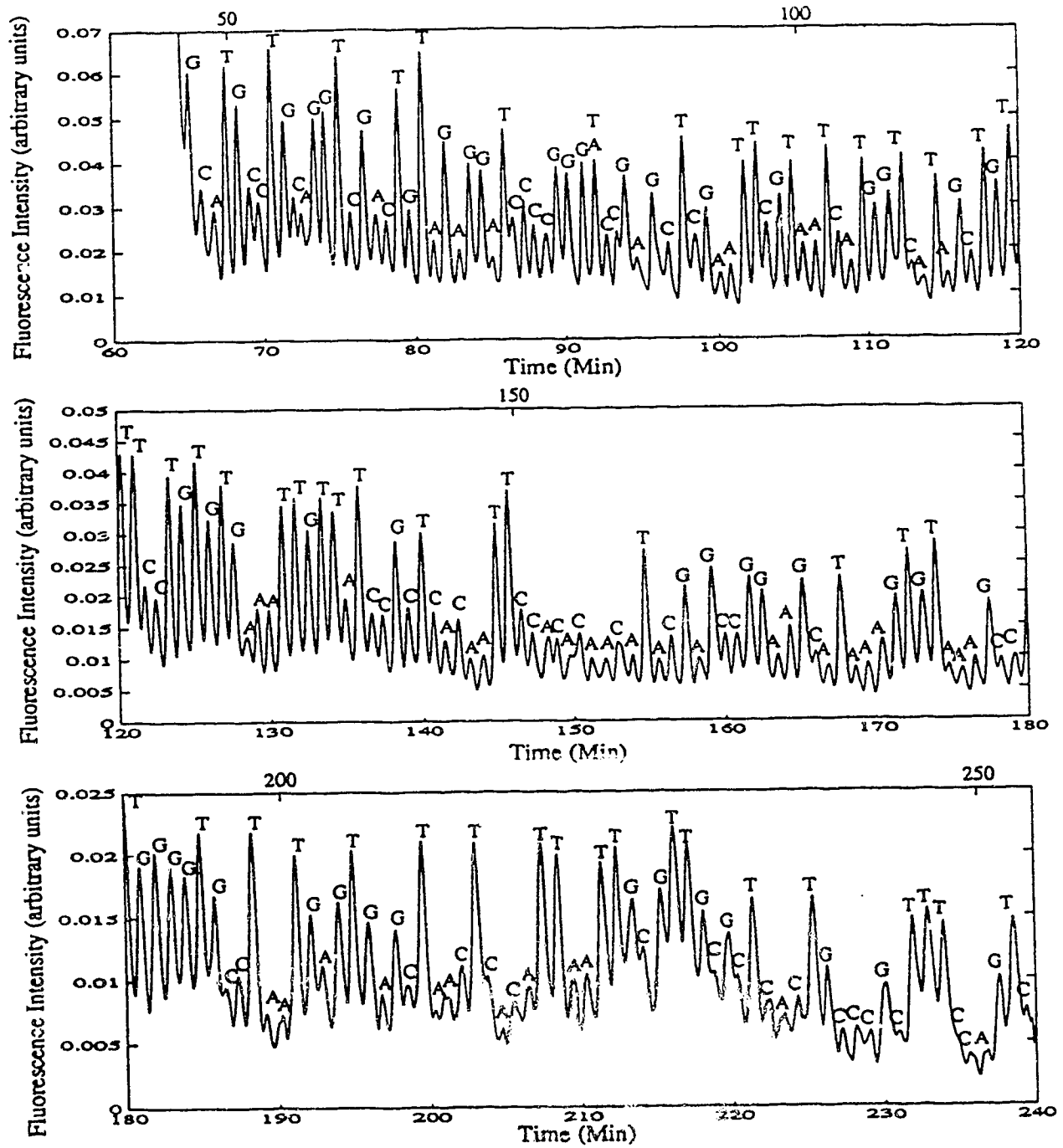


Fig. 3.2 An example of peak height encoded single color DNA sequencing data

3.3.2 The effect of adding formamide into acrylamide gel on separation

Three gels were used in this study. A 6%T, 5%C polyacrylamide, 7 M urea gel was covalently cross-linked to the last 5-mm of the detection end of the capillary of the 31 cm long, 50- μ m inner diameter, 190- μ m outer diameter capillary; this gel was operated at 200 V/cm. Another 6%T, 5%C polyacrylamide, 7 M urea gel with 20% formamide added was covalently cross-linked to the last 5-mm of the 31 cm long, 50- μ m inner diameter, 190- μ m outer diameter capillary; this gel was operated at 150 V/cm. The third gel is 37 cm long, 50- μ m inner diameter, 190- μ m outer diameter capillary was filled with 6%T, 5%C, 30% formamide, 7M urea gel that was covalently bound to the capillary wall through use of γ -methacryloxypropyltrimethoxysilane.

Separation

By varying the ratio of dideoxynucleotides used in the chain extension reaction, the identity of the terminal dideoxynucleotide is encoded in peak height (Fig. 3.3). In any local neighborhood, peaks associated with T will be higher than peaks associated with G which, in turn are larger than C and A. Unfortunately, in our standard sequencing gel, significant compressions are produced with this fluorescently labeled primer. A sequence of GGGTACCG, corresponding to fragments 59 to 66 nucleotides in length, is severely compressed because of the formation of secondary structure. This compression appears to be associated with the low temperature at which the separation proceeds; data generated on a commercial slab gel sequencer showed no compression.

A sequencing gel was modified by addition of 20% by volume of formamide; the data generated on this gel shows only a slight sequencing error for fragments of 63-65 nucleotides in length (figure 3.4). However, this modified gel produces very low sequencing rate, 70 bases/hour at an electric field strength of 150 V/cm. We assume that

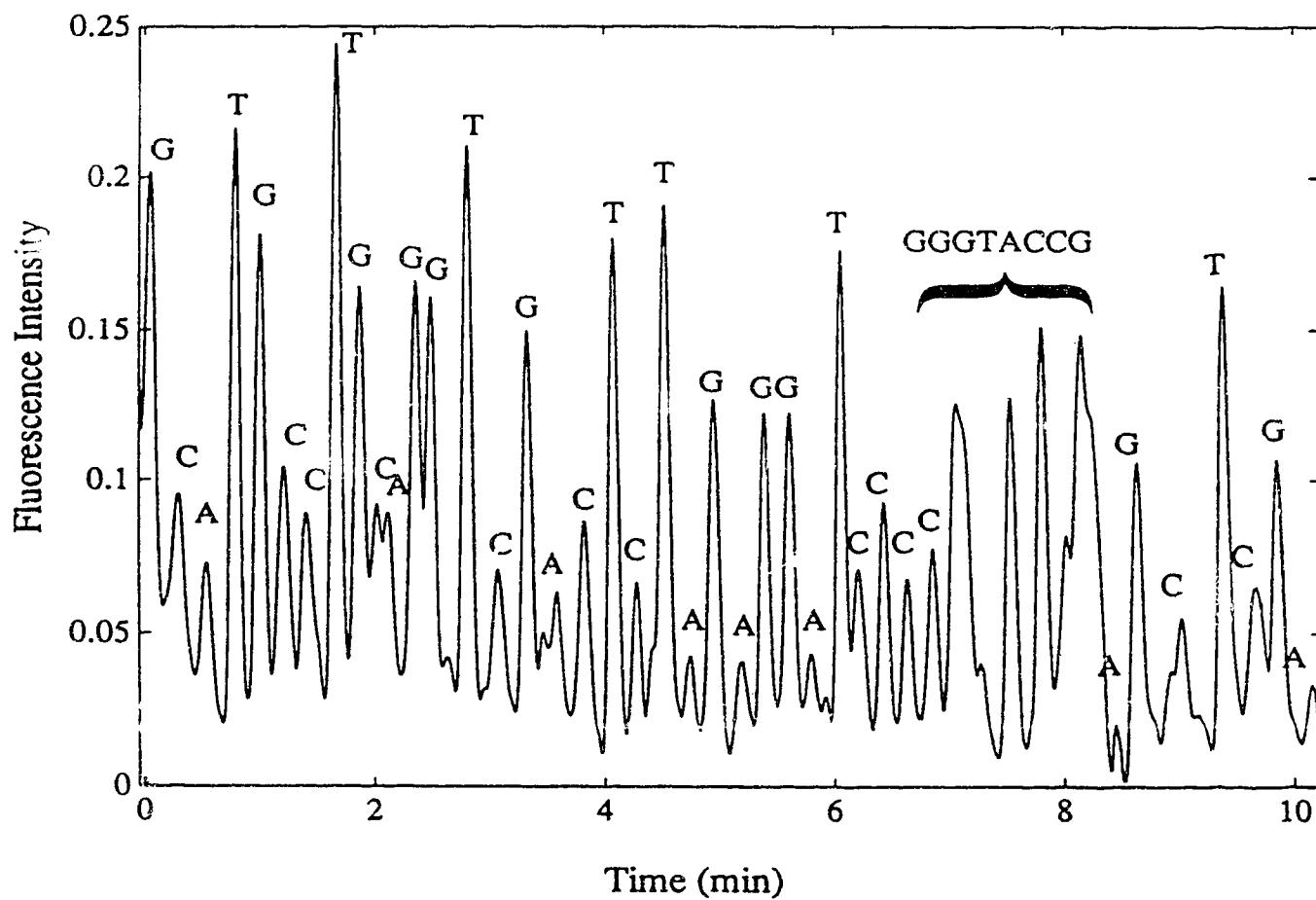


Fig. 3.3 Capillary gel electropherogram of M13mp18 reaction fragments: 6%T, 5%*c*-7M urea acrylamide gel; fragments 28-73 nucleotides in length are shown. Time is arbitrarily set to zero for the fragment 27 nucleotides in length.

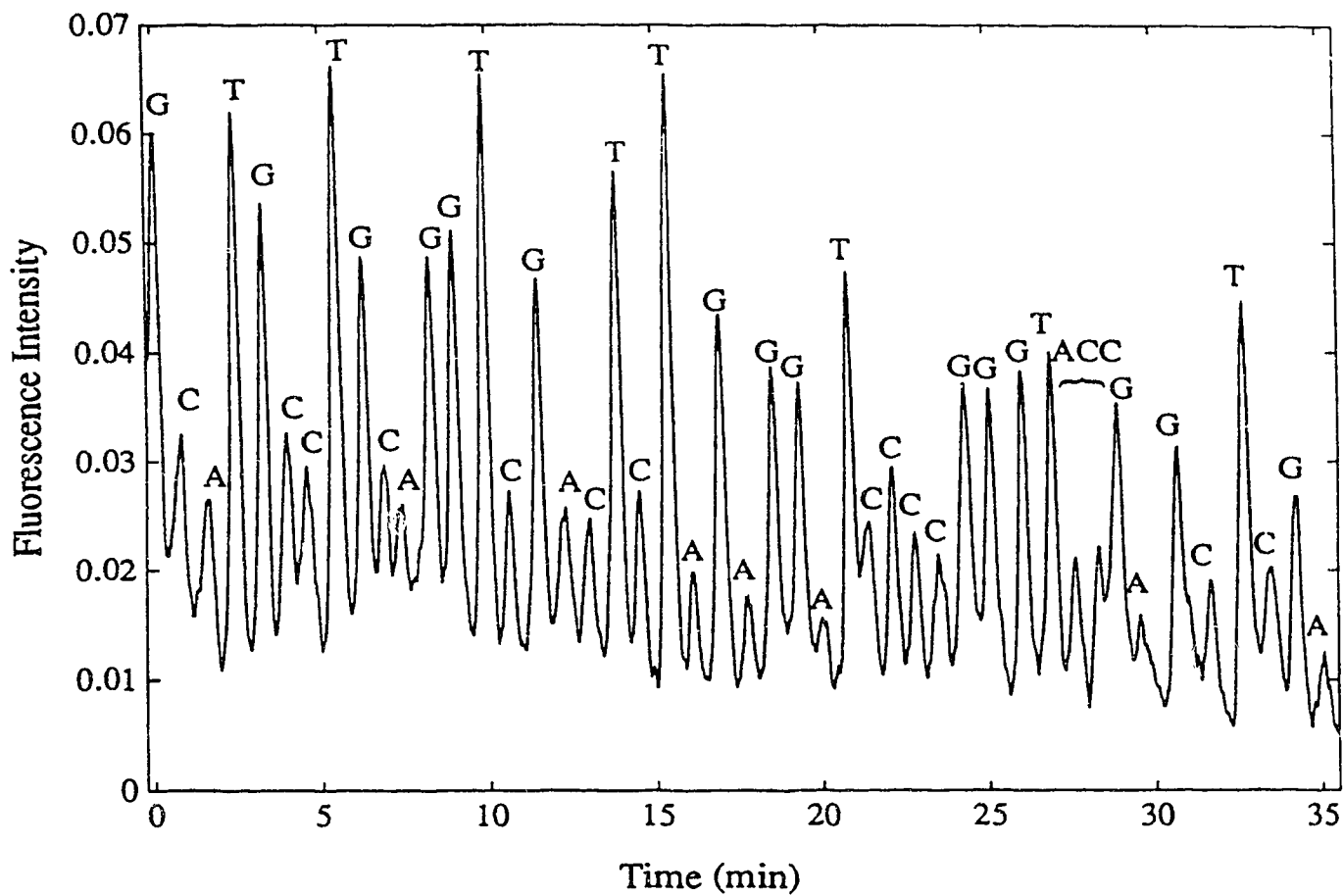


Fig. 3.4 Capillary gel electropherogram of M13mp18 reaction fragments: 6% T, 5% C, 6 M urea, 30% formamide acrylamide gel; fragments 28 to 73 nucleotides in length are shown. Time is arbitrarily set to zero for the fragment 27 nucleotides in length.

operation of conventional gels at a temperature above ambient will eliminate the compressions, providing higher sequencing rates.

In the third experiment, the ratios of nucleotides were adjusted to yield a nominal peak height ratio of 8:4:2:1 for A,C,G,T. 30% by volume formamide was incorporated in the 6%T, 5%C, 7M urea gel for separation of the sequencing products (Fig. 3.5a). Fig. 3.5b presents an expanded region corresponding to the elution of fragments ranging from 60 to 100 nucleotides in length. The data, obtained at modest electric field strength, 200 V/cm, suffers from low migration rate, 80 bases/hour, and reflects the low mobility of DNA in the formamide-urea gels. The peaks across this region are nearly base line resolved; the resolution ranges from 1.2 to 1.8, with an average of about 1.5. This recipe reduced greatly the compressions but yielded a relatively slow separation rate. The sequencing accuracy of this gel appears to be poor, particularly with respect to C and G discrimination, reflecting difficulties in the reaction chemistry. Improved performance should be possible with elimination of ghost peaks and optimization of the dideoxynucleotide ratios.

Conclusion

To obtain accurate base determination with this sequencing method, it is necessary to employ very careful enzymology; minor variations in peak amplitude can lead to poor discrimination in base determination. Pauses in the sequencing reaction can produce ghost peaks that contaminate the peak amplitude. Ghost peaks add the greatest proportional error to the lowest amplitude peaks. It seems that a carefully designed sequencing kit, optimized for a particular sequencing template, must be used to obtain accurate sequencing data from this amplitude modulated sequencing protocol.

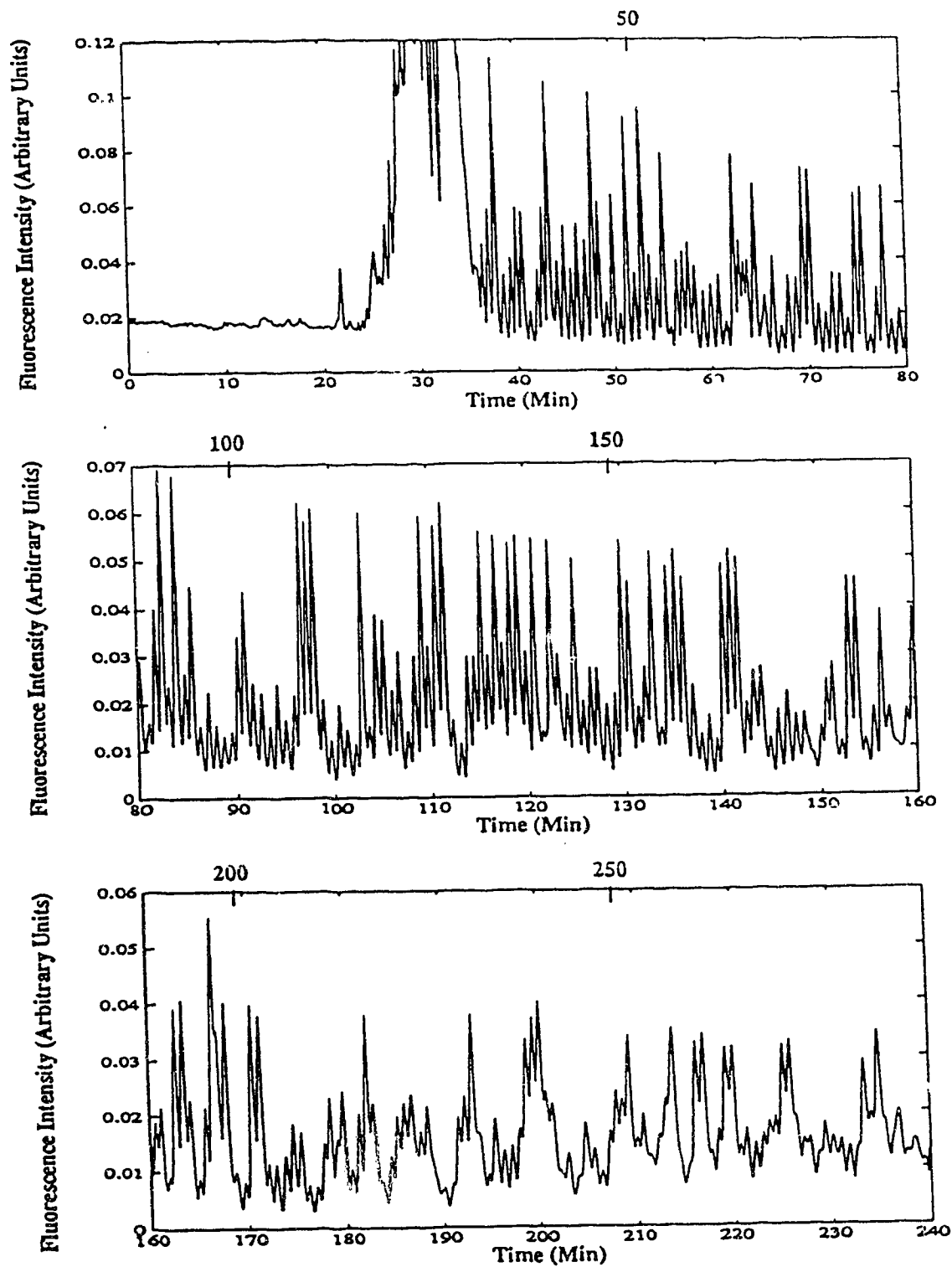


Fig. 3.5a A sequencing run of M13mp18 with 30% by volume formamide was incorporated in the 6%T, 5%C, 7M urea acrylamide gel for separation

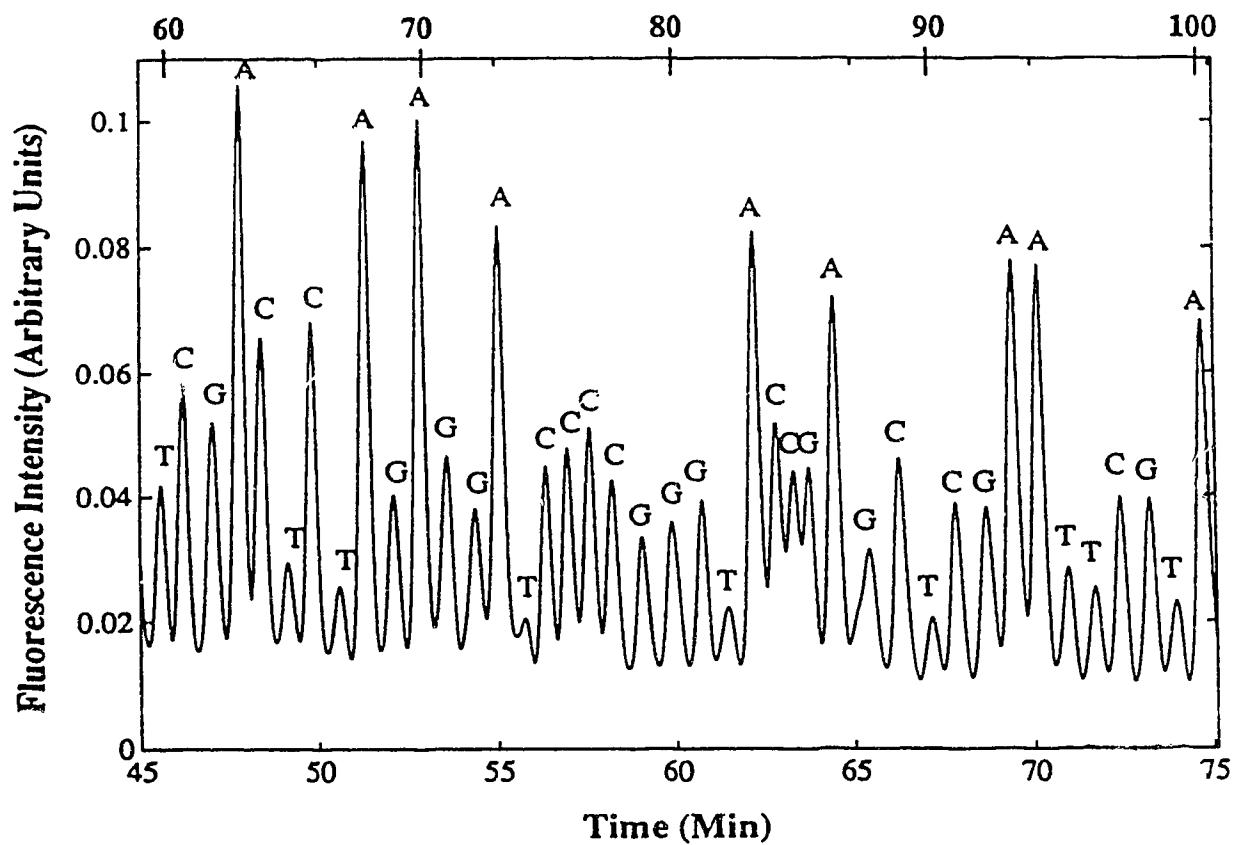


Fig. 3.5b An expanded region corresponding to nucleotides 60-100. Note that the compression around GGGTACCG disappeared.

References:

1. F. Sanger, S. Nicklen, A.R. Coulson, *Proc. Nat. Acad. Sci.* **74**, 5463 (1977).
2. L.M. Smith, J.Z. Sanders, R.J. Kaiser, P. Hughes, C. Dodd, C.R. Connell, C. Heiner, S.B.H. Kent, and L.E. Hood, *Nature* **321**, 674 (1986).
3. W. Ansorge, B.S. Sproat, J. Stegemann, C. Schwager, *J. Biochem. Biophys. Meth.* **13**, 315 (1986).
4. J.M. Prober, G.L. Trainor, R.J. Dam, F.W. Hobbs, C.W. Robertson, R.J. Zagursky, A.J. Cocuzza, M.A. Jensen, and K. Baumeister, *Science* **238**, 336 (1987).
5. S. Tabor and C.C. Richardson, *J. Biological Chemistry* **265**, 8322 (1990).
6. W. Ansorge, J. Zimmermann, C. Schwager, J. Stegemann, H. Erfle, and H. Voss, *Nucleic Acids Res.* **18**, 3419 (1990).
7. J.E. Edström, *Nature* **172**, 809 (1953).
8. J.E. Edström, *Biochimica Biophysica Acta*, **22**, 378 (1956).
9. G.T. Matiolli and H.B. Niewisch, *Science*, **150**, 1824 (1965).
10. U. Grossbach, in "Electrophoresis and isoelectric focusing in polyacrylamide gel", Ed. R.C. Allen and H.R. Maurer, Walter de Gruyter, Berlin, 1974. p. 207.
11. V. Neuhoff, W.B. Schill, and H. Sternbach, *Biochem. J.* **117**, 623 (1970).
12. S. Hjerten, *J. Chromatogr.* **270**, 1 (1983).
13. A.S. Cohen and B.L. Karger, *J. Chromatogr.* **397**, 409 (1987).
14. A. Guttman, A. Paulus, A.S. Cohen, N. Grinberg, and B.L. Karger *J. Chromatogr.* **488**, 41 (1988).
15. A.S. Cohen, D.R. Najarian, A. Paulus, A. Guttman, J.A. Smith, and B.L. Karger *Proc. Nat. Acad. Sci.* **85**, 9660 (1988).
16. A.S. Cohen, D.R. Najarian, and B.L. Karger *J. Chromatogr.* **516**, 49 (1990).
17. B.L. Karger and A.S. Cohen, US Patent 4,865,706 (1989).

18. B.L. Karger and A.S. Cohen, US Patent 4,865,707 (1989).
19. P.F. Bente and J. Myerson, *U.S. Pat.* 4,810,456 (1989);
20. H. Swerdlow and R. Gesteland, *Nucleic Acids Res.* **18**, 1415 (1990).
21. H. Drossman, J.A. Luckey, A.J. Kostichka, J. D’Cunha, and L.M. Smith, *Anal. Chem.* **62**, 900 (1990).
22. J.A. Luckey, H. Drossman, A.J. Kostichka, D.A. Mead, J. D’Cunha, T.B. Norris, and L.M. Smith, *Nucleic Acids Res.* **18**, 4417 (1990).
23. H. Swerdlow, S. Wu, H. Harke, and N.J. Dovichi, *J. Chromatogr.* **516**, 61 (1990).
24. Y.F. Cheng and N.J. Dovichi, *Science* **242**, 562 (1988).
25. S. Wu and N.J. Dovichi, *J. Chromatogr.* **480**, 141 (1989).
26. Y.F. Cheng, S. Wu, D.Y. Chen, and N.J. Dovichi, *Anal. Chem.* **62**, 496 (1990).
27. N.J. Dovichi, J.C. Martin, J.C. Jett, and R.A. Keller, *Science* **219**, 845 (1983).
28. N.J. Dovichi, J.C. Martin, J.C. Jett, M. Trkula, and R.A. Keller, *Anal. Chem.* **56**, 348 (1984).
29. D.C. Nguyen, R.A. Keller, J.H. Jett, J.C. Martin, *Anal. Chem.* **59**, 2158 (1987).
30. K. Peck, L. Stryer, A.N. Glazer, and R.A. Mathies, *Proc. Natl. Acad. Sci.* **86**, 4087 (1989).
31. Swerdlow, H., Zhang, J.Z., Chen, D.Y., Harke, H.R., Grey, R., Wu, S., Dovichi, M.J., and Fulier, C., *Anal. Chem.*, **63**(24), 2835-41, (1991)

Chapter 4 Two-Label Peak-Height Encoded DNA Sequencing By Capillary Gel Electrophoresis*

4.1 Introduction

In 1989, Tabor and Richardson reported the effect of manganese ions on the incorporation of dideoxynucleoside triphosphate (ddNTP) by T7 polymerase [1]. The manganese not only increased the incorporation rate of the ddNTP but also produced uniform termination of DNA sequencing reactions. In 1990, Ansorge and coworkers and Tabor and Richardson independently reported a DNA sequencing protocol based on the manganese-T7 polymerase reaction [2-3]. Both groups reported use of a single sequencing reaction with one fluorescently labeled primer; adjustment of the concentration of ddNTP produces peak heights in an 8:4:2:1 ratio to encode the DNA sequence. Ansorge also reported the use of two sequencing reactions; ddCTP and ddTTP were present in the first while ddATP and ddGTP were present in the second. The products of the two sequencing reactions were separated in adjacent lanes of a polyacrylamide gel.

The single reaction technique offers advantages for primer walking applications: each sample requires only one primer and one reaction. Also, electrophoretic separation of the reaction products occurs in a single lane, increasing the sample throughput. Because the sample is separated in a single lane, the technique is useful in capillary gel electrophoresis, a technique that provides rapid separation of DNA sequencing fragments [4-12].

An 8:4:2:1 peak height ratio leads to poor accuracy in our hands [11]; inevitably, fragments terminated in two of the ddNTP's will generate overlapping distributions of peak height. In this laboratory, the accuracy of the DNA sequence is typically 90% for

* This chapter has been published in *Nucleic Acids Research*, 20 (18),4873-4880,1992.

fragments shorter than 250 bases. There are three sources of errors in sequence determination by this technique. First, the relative variation in peak heights associated with each ddNTP can be about 25% [2]. This distribution in peak amplitude leads to errors in identification of the terminal nucleotide, particularly if the peak height ratio is not carefully adjusted. Second, the smallest peaks are frequently lost when sandwiched between two larger amplitude peaks. This problem becomes most severe for longer fragments where the electrophoretic resolution has degraded; it is difficult to sequence accurately fragments that are longer than 250 bases with the four level sequencing technique. Third, systematic errors occur due to the presence of ghost peaks associated with false priming, the finite processivity of the polymerase, and contaminant oligonucleotides present in the sample. These systematic errors are particularly important for the ddNTP present in lowest concentration; a small contribution from a ghost peak leads to the largest proportional error in peak amplitude. False priming and artifacts from contaminant oligonucleotides require that highly purified DNA be used for sequence determination.

While it is difficult to control a peak height ratio of 8:4:2:1, a peak height ratio of 2:1 is simple to maintain for any two of the ddNTPs. This paper describes a modification to the peak height encoded technique that is similar to that contained in Anson's original paper; we perform two sequencing reactions, each reaction containing a different fluorescently labeled primer and two ddNTP's. The pooled reaction products are separated on a single capillary gel. This procedure provides the accuracy inherent in a two-level discrimination and the convenience of single column separation with the accuracy of multiple labels, albeit at the expense of performing two sequencing reactions.

4.2 Experimental procedure

Instrumental design--Electrophoresis

The DNA sequencing capillary electrophoresis systems are similar to previous reports from this laboratory [7, 9, 11-13]. The polyimide coated, fused silica capillary is 50- μm inner diameter, 190- μm outer diameter, and typically 35-cm long. Gels are prepared in 5-mL aliquots from carefully degassed mixtures of acrylamide and bisacrylamide (4%T, 5%C), 1X TBE, and 7M urea. Polymerization is initiated by addition of 2- μl of TEMED and 20- μl of 10% ammonium persulfate. The gel solution is injected into the capillary by use of a syringe. To prevent deformation of the gel into the detection cuvette, γ -methacryloxypropyltrimethoxysilane is used to bind covalently the gel to the last ~2-cm of the capillary wall. Although polymerization appears complete in 30 minutes, the capillaries are typically stored overnight before use.

A Plexiglas box equipped with a safety interlock holds the injection end of the capillary. The other end of the capillary is inserted into the flow chamber of a locally constructed sheath flow cuvette. The cuvette has a 200- μm square flow chamber with either 1 or 2-mm thick quartz windows.

Detectors

Two different fluorescence detectors are described for the two-color peak-height encoded sequencing technique. In the first fluorescence detector, Figure 4.1, a 6-mW argon ion laser beam ($\lambda = 488 \text{ nm}$) is aligned to be parallel with a 1-mW helium-neon laser beam ($\lambda = 543.5 \text{ nm}$) through use of a dichroic filter. The parallel beams are focused with a $5\times$ microscope objective into the sheath flow cuvette. The helium-neon laser beam is brought to a focus about 100- μm below the tip of the capillary; the argon ion laser beam

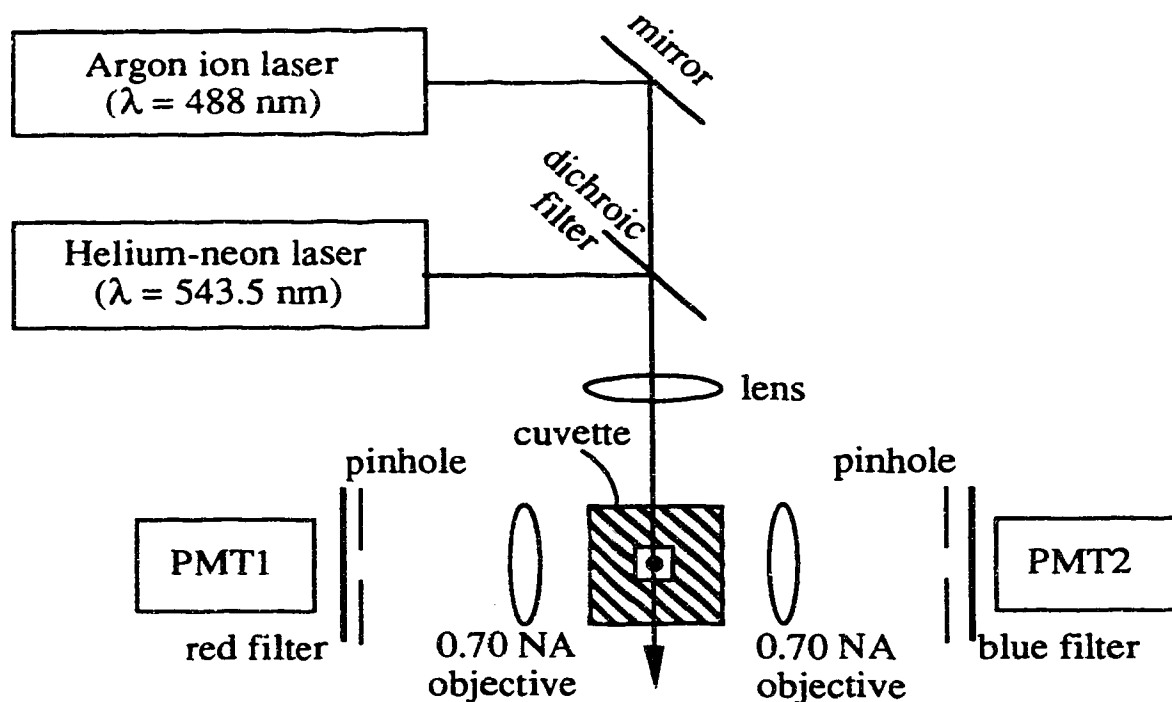


Fig. 4.1. Two laser-two collection optic fluorescence detector. Beams from an argon ion laser and a helium-neon laser are aligned to be parallel after reflection from a dichroic filter. The two beams are focused with a 5× microscope objective into the sheath flow cuvette. The argon-ion laser beam is focused about 200- μm downstream from the helium-neon laser beam. Fluorescence is collected with two 60×, 0.70 NA microscope objectives. Fluorescence excited by each laser beam is imaged by one of the objectives onto a pinhole to block scattered laser light. An appropriate spectral filter is used to isolate fluorescence from each dye. Photomultiplier tubes (PMT) detect the transmitted fluorescence.

is focused about 200- μm downstream from the first laser beam. Two 0.70 NA, 60 \times microscope objectives collect fluorescence at right angles to the beams and cuvette. The fluorescence excited by the helium neon laser is collected with the first objective, imaged onto a 1.5 mm diameter pinhole, passed through a bandpass interference filter with 600 nm center wavelength and 50 nm bandwidth, and detected with a R1477 photomultiplier tube (PMT) operated at -15 $^{\circ}\text{C}$. Fluorescence excited by the argon ion laser is collected with a second objective, imaged onto a 1.5 mm diameter pinhole, passed through a bandpass interference filter with 518 nm center wavelength and 25-nm bandwidth, and detected with a R1477 PMT operated at room temperature. The output from each PMT is conditioned with a simple low-pass electronic filter with 0.01-s time constant and digitized by a National Instruments A/D board in a Macintosh IIsi computer. The data are treated with a Gaussian-shaped digital filter before presentation. The sheath flow is provided by a simple siphon based on 7-cm difference in height between the sheath flow reservoir and the waste collection vial.

The second detector, figure 5.2, is identical to the first, except that fluorescence from both dyes is excited by a 20-mW argon ion laser beam ($\lambda = 488 \text{ nm}$) and both collection optics are focused on the illuminated sample.

SAMPLE PREPARATION

Two samples are used. In each case, the sequencing reaction is carried out in 40 mM MOPS buffer, pH 7.5, 50 mM NaCl, 10 mM MgCl_2 , and 15 mM sodium isocitrate. For the first sample, 8 pmole of fluorescein labeled primer (Applied Biosystem -21M13 FAM) is annealed to 10 μg of M13mp18 single stranded DNA at 65 $^{\circ}\text{C}$ for 2 min. followed by slow cooling. A mixture of deoxy- and dideoxynucleoside triphosphates is added to give an average nucleotide ratio (dNTP/ddNTP) of 1500:1 with 7-deaza-2'-deoxyguanosine-5'-triphosphate used in place of dGTP. The ratios of dideoxynucleotides

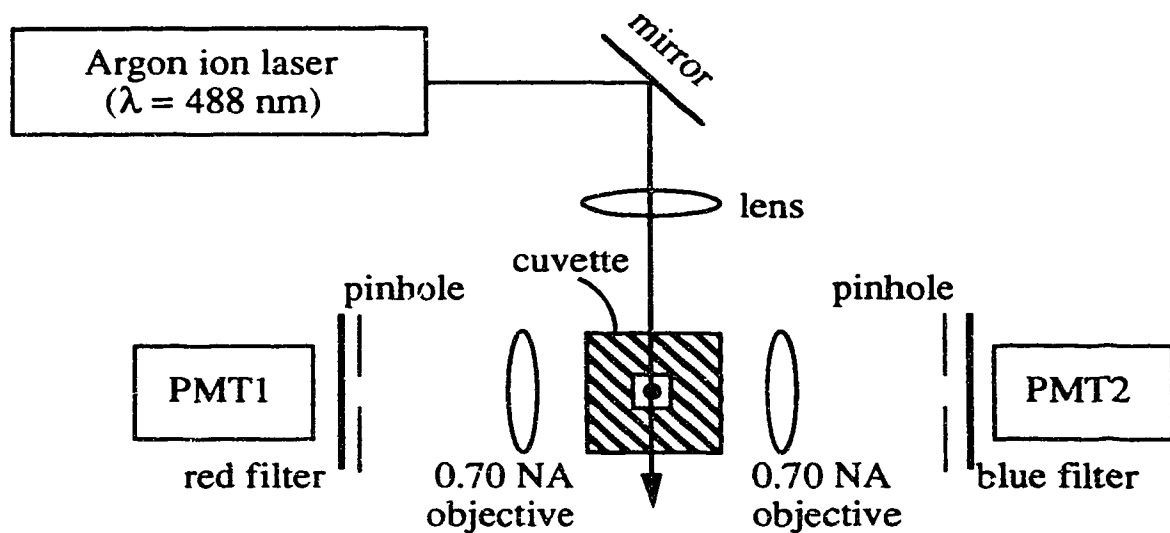


Fig. 4.2. One laser-two collection optic fluorescence detector. This system is identical to that of figure 1 with two exceptions. First, only the argon ion laser excited fluorescence. Second, both collection optics are focused onto the single laser beam.

are adjusted to yield a nominal peak height ratio of 2:1 for T and G. After the mixture is warmed to 37 °C, 6 units of Sequenase Version 2.0 and 0.006 units of pyrophosphatase are added. Incubation continues at 37 °C for 30 min., after which the DNA is precipitated with ethanol [2]. Identical experimental conditions are used with a tetramethyl rhodamine-labeled primer (Applied Biosystems -21M13 TAMRA) to yield a nominal peak height ratio of 2:1 for A and C. The samples are resuspended in a 49:1 mixture of formamide-EDTA. Three microliter aliquots are taken from the resuspended samples, heated to 95 °C for two minutes, and injected onto the capillary by applying a 150 V/cm electric field for 60 seconds.

The second sample was prepared in a similar manner, except that the peak height ratios were adjusted to 3:1 for both ddATP/ddCTP and ddTTP/ddGTP.

SEQUENCE DETERMINATION

In each case, sequence is interpreted by eye from the smoothed electrophoresis data. The data are plotted in 20 minute intervals with approximately 60 peaks per plot. Two lines are drawn across the plot corresponding to the discrimination level for each fluorescent dye. For fragments between 350 and 400 bases in length, small amplitude fragments occasionally suffer from overlap with neighboring peaks. Interpretation of these small amplitude peaks is usually simple, particularly for samples prepared with a 3:1 peak height ratio.

4.3 Results and Discussion

Two laser-Two collection optic system

The first optical system minimizes cross-talk between fragments labeled with the two dyes. A helium-neon laser, operating at 543.5 nm, efficiently excites TAMRA labeled fragments; FAM labeled fragments are transparent at this wavelength. An argon ion laser, operating at 488 nm, efficiently excites FAM labeled fragments; the molar absorptivity of TAMRA is an order of magnitude less than FAM at this wavelength. In this detection system, the helium-neon laser beam was focused about 50- μm upstream from the argon ion laser beam to minimize photobleaching effects [13]. Fluorescence of the TAMRA-labeled fragments is collected by an optical system tuned to the emission maximum of that dye. Fluorescence of the FAM-labeled fragments is collected by an optical system that transmits fluorescence of FAM but blocks the low level fluorescence of TAMRA.

Figure 4.3a presents data from the two-laser system. Here, A and C terminated fragments are present in a 2:1 ratio in the solid trace while T and G are present in a 2:1 ratio in the dashed trace. The two traces are offset for presentation. The region from 200 to 250 bases, top panel of Figure 4.3b, demonstrates the high quality data produced by this instrument. Tall peaks in the dashed channel are A, short peaks in the dashed channel are C, tall peaks in the solid channel are T, and short peaks in the solid channel are G. For fragments of this length, the resolution between adjacent peaks ranges from 1.0 to 1.5 and the theoretical plate count is 4.6 million for a fragment with 200 nucleotides. The bottom panel in figure 4b shows the portion of the electropherogram corresponding to fragments ranging from 300 to 350 bases in length. Here, resolution ranges from 0.5 to 0.75; degradation in resolution for longer fragments is associated with increased band-broadening. Molecular diffusion dominates band-broadening under these experimental conditions [12]. The theoretical plate count was 2.1 million plates for fragments 334 bases

Fig. 4.3a

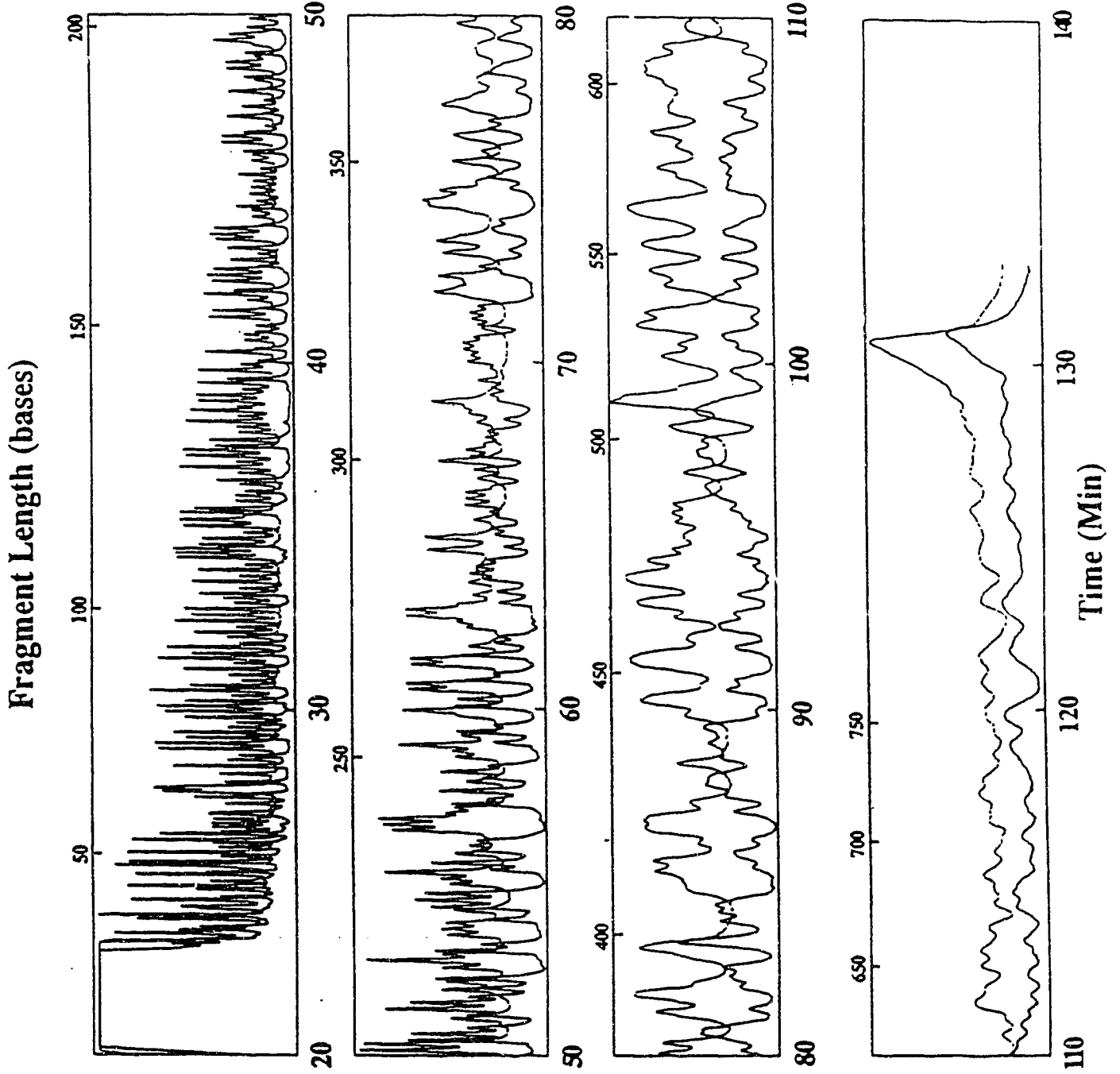


Fig. 4.3. Sequencing data for M13mp18 generated with the two-laser two-collection optic peak height encoded sequencing method. Fluorescein labeled primer is used to generate fragments terminated in A and C in a 2:1 peak height ratio. Tetramethyl rhodamine labeled primer is used to generate fragments terminated in T and G in a 2:1 peak height ratio. Fluorescence collected in the red spectral channel is presented in the solid trace and fluorescence collected in the blue spectral channel is presented as the dashed trace. Figure 4.3a. Entire separation. The sample was injected at $T = 0$. Figure 4.3b presents data for fragments from 200 to 250 bases in length (top panel) and from 300 to 350 bases in length (bottom panel).

in length. For fragments much longer than 400 bases, peak overlap often swamps C and G peaks. However, the pattern produced by the larger peaks may be compared with the known sequence; sequence may be identified for fragments up to 750 bases in length.

The sequence for fragments ranging from 70 to 350 bases in length contained five errors, producing an overall sequencing accuracy of 97.5%. In our system, three errors were associated with a missing C (bases 196, 198, and 326); in each case a minor compression caused the C to be lost as a shoulder on an adjacent A peak. Operation of the capillaries above room temperature or addition of formamide to the sequencing gel minimizes compressions. Regression analysis should prove useful in detection of these poorly resolved bases. In the other two cases (bases 281, 282), a T was called for a G. These errors arise from inaccurate setting of a discrimination level for the G-T peaks. Although careful interpretation of the peak heights might lead to improved discrimination, the latter errors can be minimized by use of a 3:1 peak height ratio rather than a 2:1 peak height ratio.

Regression analysis appears necessary for accurate determination of sequence for fragments longer than 400 bases. A particular advantage of this two-laser system comes in designing an algorithm for peak identification. One of the more critical tasks in interpreting the electrophoretic data is determination of the signal baseline. Because the signals from the two dyes do not interfere, the signal drops to the baseline whenever more than a few consecutive bases appear in the other spectral channel.

One laser-Two collection optic system

The two-laser system is experimentally complicated. To simplify the system, a single argon ion laser can excite fluorescence from both FAM and TAMRA. Two microscope objectives image the single fluorescent spot into two spectral channels equipped with appropriate spectral filter and photomultiplier tube. Because the absorbance cross-

section for TAMRA is much less than the absorbance of FAM at 488 nm, a relatively high laser power should be used. The higher laser power is sufficient to photobleach FAM but not TAMRA. The signal amplitude from the two dyes is similar because of this photobleaching.

To improve sequencing accuracy, a 3:1 peak height ratio was used to generate the sequencing sample shown in Figure 4.4. Figure 4.4a presents data for the entire separation. Figure 4.4b presents a more detailed view of the data. The top panel presents data taken for fragments ranging from 200 to 250 bases in length. Fragments that produce a large signal in both spectral channels are A, fragments with small signals in both spectral channels are C, peaks with large signals in the solid channel are T, and peaks with small signals in the solid channel are G. Resolution ranges from 1.0 to 1.5 for these fragments. Two minor compressions are observed in this data (peaks 223-224 and 225-226). These compressions are not observed in the data of figure 4 and may represent incomplete denaturing of the sample before injection. The bottom panel of Figure 4.4b presents sequence for fragments ranging from 300 to 350 bases in length. Resolution ranges from 0.5 to 0.75. As the resolution between adjacent peaks degrades, sequence determination becomes more problematic, particularly for the case where a low amplitude peak (C or G) is sandwiched between two high amplitude peaks.

Fig. 4.4a

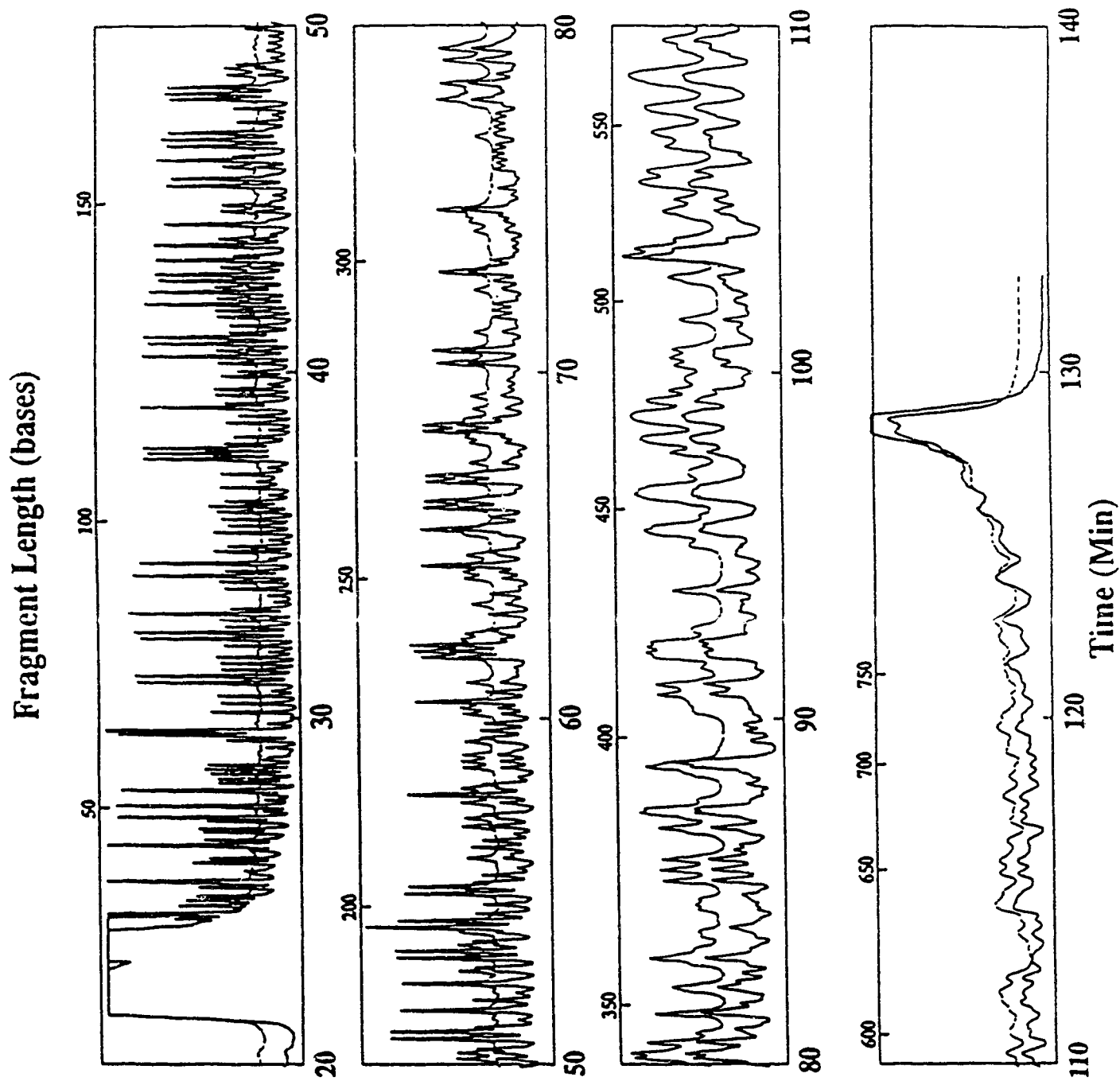


Fig. 4.4b

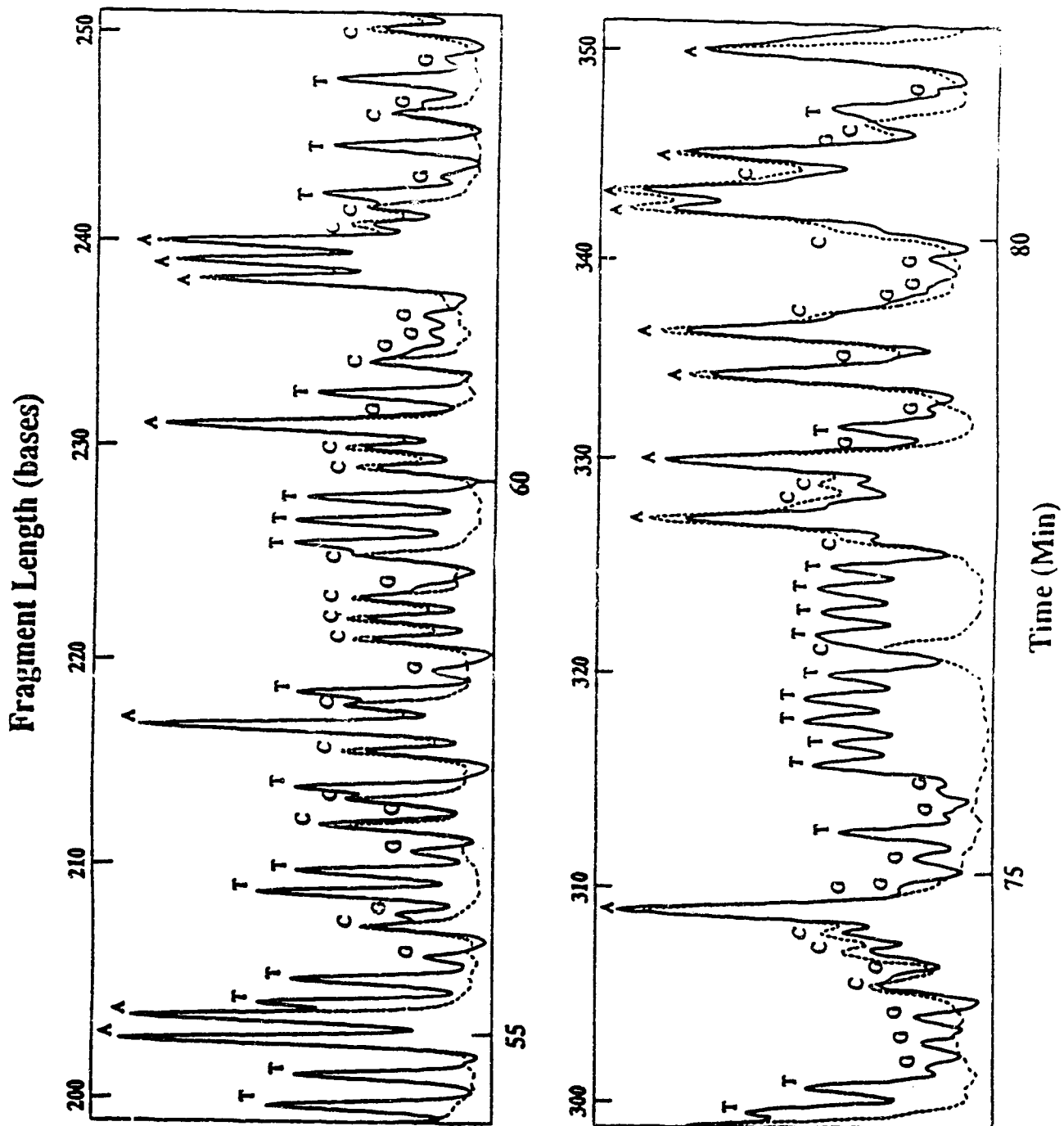


Fig. 4.4c

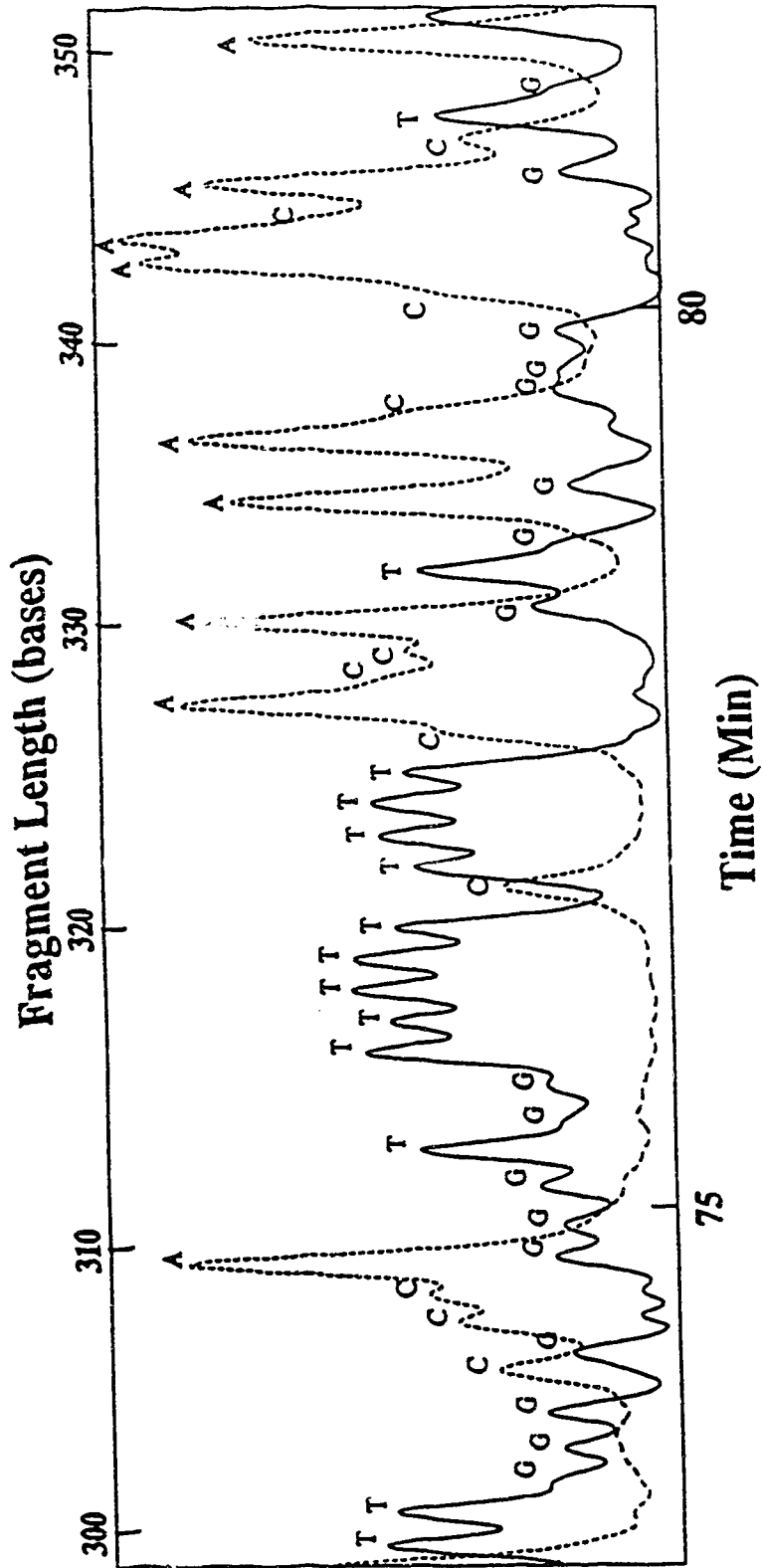


Fig. 4.4 Sequencing data for M13mp18 generated with the one-laser two-collection optic peak height encoded sequencing method. Fluorescein labeled primer is used to generate fragments terminated in A and C in a 3:1 peak height ratio. Tetramethyl rhodamine labeled primer is used to generate fragments terminated in T and G in a 3:1 peak height ratio. Fluorescence collected in the red spectral channel is presented in the solid trace and fluorescence collected in the blue spectral channel is presented as the dashed trace. Figure 4.4a. Entire separation. The sample was injected at $T = 0$. Figure 4.4b presents data for fragments from 200 to 250 bases in length (top panel) and from 300 to 350 bases in length (bottom panel). Figure 4.4c plots the blue spectral data as the dashed trace and the difference between the red and blue data as the solid trace for fragments ranging from 300 to 350 bases in length.

Subtraction of the second channel from the first channel improves data interpretation. Figure 4.4c presents the subtracted data along with the raw data for channel 2 for fragments ranging from 300 to 350 bases in length. Several poorly resolved peaks in Figure 4.4b are clearly resolved in the subtracted data; in particular, peaks 310, 331, 335, 338, and 346 are difficult to distinguish by eye in the raw data of Figure 5.4b but are clearly resolved as G's in the processed data of Figure 4.4c. This processed data produces excellent sequencing accuracy. In the range of 70 to 350 bases, there are two errors: a C is missing at base 198 due to a minor compression where a C is sandwiched between two A's, a G is missing at base 291 due to overlap with a T. For fragments in this size range, sequencing accuracy exceeds 99%.

Accuracy degrades for longer fragments: for bases 354-356 an A is called for CCC, a C is missing at base 361, a G is missing at base 368, a C is missing at base 386, a C is missing at base 395, and a C is missing at base 399; for fragments ranging from 70 to 400 bases, the accuracy exceeds 97%. In this data set, most errors are associated with missing bases: there are five missing C's and one missing G. Bases ending in C and G produce low amplitude peaks that are easily swamped by higher amplitude neighboring peaks.

4.4 Conclusions

There is an optimum ratio of peak heights for this sequencing technique. If the ratio is near 1, then errors arise because of insufficient discrimination between peak heights. If the ratio is larger than 3, then errors are made late in the run for low amplitude peaks. It appears that a ratio of 2.5 to 3 is ideal in obtaining high sequencing accuracy for at least 400 bases. Improved signal-to-noise ratio and computer algorithms will inevitably produce superior results for longer fragments.

The sequencing accuracy of the 3:1 peak height ratio technique ranges from 97 to 99.5% for fragments up to 400 bases in length. This sequencing accuracy should be compared with that reported by Karger, Harris, and Gesteland, who sequenced M13mp18 with both an ABI 373A slab-gel sequencer and a capillary gel electrophoresis system based on four dye-labeled primers [10]. They reported an accuracy of 97% for both the ABI sequencer and the capillary gel electrophoresis system for fragments up to 350 bases in length.

The two-color peak height encoded system produces accuracy equal to or greater than conventional fluorescence based sequencing. However, only two fluorescently labeled primers are required for the sequencing reaction, compared with four labels for the ABI sequencer. As a result, the two-color peak height encoded system could be cost effective for primer walking experiments, particularly when the rapid throughput of capillary electrophoresis outweighs disadvantages of preparing two labeled primers. The two-color sequencing protocol suffers from one significant disadvantage: the technique requires use of T7 polymerase. Until a thermally stable polymerase is discovered that produces uniform incorporation of dideoxynucleosides, cycle sequencing and PCR-based sequencing will remain impractical with the peak-height encoded sequencing techniques.

We have presented systems designed for use with the following pairs of Applied Biosystems primers: FAM - TAMRA and JOE - FAM. The former optical system also works well with JOE - ROX, JOE - TAMRA, and FAM - ROX. Any of these reaction pairs could be separated with an ABI sequencer. The JOE-FAM system can be separated with the DuPont Genesis sequencer. The peak-height encoded technique may be employed on commercial sequencers with appropriate software modification.

One last system can be considered based on TAMRA - ROX. These dyes are excited efficiently by the low cost green helium neon laser; the use of a single collection optic and a dichroic filter to split the emission spectrum to two photodetectors would result in a low cost and compact detector.

References:

1. Tabor, S. and Richardson, C.C. (1989) *Proc. Natl. Acad. Sci. USA* **86**, 4076
2. Tabor, S. and Richardson, C.C. (1990) *J. Biol. Chem.* **265**, 8322.
3. Ansorge, W., Zimmermann, J., Schwager, C., Stegemann, J., Erfle, H. and Voss, H. (1990) *Nucleic Acids Res.* **18**, 3419.
4. Swerdlow, H. and Gesteland, R. (1990) *Nucleic Acids Res.* **18**, 1415.
5. Drossman, H., Luckey, J.A., Kostichka, A.J., D'Cunha, J. and Smith, L.M. (1990) *Anal. Chem.* **62**, 900.
6. Cohen, A.S., Najarian, D.R. and Karger, B.L. (1990) *J. Chromatogr.* **516**, 49
7. Swerdlow, H.P., Wu, S., Harke, H.R. and Dovichi, N.J. (1990) *J. Chromatogr.* **516**, 61.
8. Luckey, J.A., Drossman, H., Kostichka, A.J., Mead, D.A., D'Cunha, J., Norris, T.B. and Smith, L.M. (1990) *Nucleic Acid Res.* **18**, 4417.
9. Chen, D.Y., Swerdlow, H.P., Harke, H.R., Zhang, J.Z. and Dovichi, N.J. (1991) *J. Chromatogr.* **559**, 237.
10. Karger, A.E., Harris, J.M. and Gesteland, R.F. (1991) *Nucleic Acids Res.* **19**, 4955.
11. Swerdlow, H.P., Zhang, J.Z., Chen, D.Y., Harke, H.R., Grey, R., Wu, S., Fuller, C. and Dovichi, N.J. (1991) *Anal. Chem.* **63**, 2835.
12. Harke, H.R., Bay, S., Zhang, J.Z., Rocheleau, M.J. and Dovichi, N.J. *J. Chromatogr.* in press.
13. Wu, S. and Dovichi, N.J. (1989) *J. Chromatogr.* **480**, 141.

Part III

Hydrodynamic Sample Introduction in Capillary Electrophoresis System with a Sheath Flow Cuvette

Chapter 5. Hydrodynamic Sample Introduction Using a Three Way Valve in Capillary Electrophoresis.

5.1 Sample introduction in capillary electrophoresis

In most separation methods, the amount of sample analyzed is usually on the order of microliter, milliliter or even more. The sample volumes may be measured with a syringe or a injection valve. The amount of sample introduced into the capillary is an important factor for separation and detection efficiencies in capillary electrophoresis. None of the injection methods developed for other separation techniques fit capillary electrophoresis. Even the smallest amount of sample introduced by other injection methods will cause sample overload. It was reported that, for a 10 minutes separation, the optimum sample length should be less than 0.4 mm[1]. Assuming an inner diameter of the capillary of 50 μm , the optimum volume of the sample will be less than 0.8 nL. Several methods have been developed specifically for the purpose of capillary electrophoresis. These methods will be discussed in this section.

5.1.1 Electrokinetic injection

Electrokinetic injection, also called electromigration injection, is the first injection method developed for capillary electrophoresis, and the easiest way of introducing samples into capillaries. All the earlier work and most recent work in this area are done with this injection method.

The electrokinetic injection procedure

Electrokinetic injection is usually done as follows: first, the capillary is filled with

eluting buffer with a syringe, then both the platinum electrode and the injection end of the capillary are inserted into the sample reservoir. The high voltage power supply is turned on with the voltage set at 1 to 2 KV in the injection mode for a short period of time to drive the sample into the capillary. After the sample has been injected into the capillary, both the electrode and the injection end of the capillary are lifted from the sample and inserted into the eluting buffer to wash off the sample outside of the capillary and put into a fresh buffer vial. Then the high voltage power supply is turned on at a much higher voltage to start the separation. All these procedures have to be done consistently in a reasonably short period of time to limit sample diffusion, which may cause extra band broadening.

The injection volume

The volume of injected sample can be expressed as:

$$V = \pi r^2 L \quad (5.1)$$

where V is the volume of sample, r is the radius of the capillary, and L is the length of the injected sample inside the capillary.

The length of sample in the capillary can be determined by:

$$L = t_i (v_{ep} + v_{eo}) \quad (5.2)$$

where t_i is the injection time, v_{ep} is the electrophoretic velocity of the sample molecule, and v_{eo} is the electroosmotic flow velocity of the sample solution. These velocities can be calculated by:

$$v_{ep} = \mu_{ep} E_i = \frac{\mu_{ep} V_i}{L_c} \quad (5.3)$$

and

$$v_{eo} = \mu_{eo} E_i = \frac{\mu_{eo} V_i}{L_c} \quad (5.4)$$

where μ_{ep} is the electrophoretic mobility of the sample molecule, μ_{eo} is the electroosmotic mobility of the sample solution, E_i is the injection field strength, V_i is the injection voltage,

and L_c is the length of the capillary. Substitution of equations (5.2), (5.3) and (5.4) into equation (5.1) gives the injection volume:

$$V = \pi r^2 L = \frac{\pi r^2 t_i V_i (\mu_{ep} + \mu_{eo})}{L_c} \quad (5.5)$$

The amount of solute injected can be calculated by:

$$Q = \pi r^2 L C = \frac{\pi r^2 t_i V_i (\mu_{ep} + \mu_{eo}) C}{L_c} \quad (5.6)$$

where Q is the moles of solute of a certain species, and C is the concentration of that species in sample solution.

The corrected injection volume

It is obvious that the electrophoretic mobility is different for different solute species. If there were more than one sample in the solution, a corrected volume relative to each sample should be calculated.

The corrected volume can be estimated by[2]:

$$V_{cor} = V_c \left(\frac{t_i}{t_r} \right) \left(\frac{V_i}{V_{ep}} \right) \quad (5.7)$$

where V_{cor} is the corrected injection volume for a certain component in the sample solution, V_c is the volume of the capillary, t_r is the retention time, V_i is injection voltage and V_{ep} is the high voltage of electrophoresis.

Automation of the electrokinetic sampler

The first automated electrokinetic sampler was described in 1989 by Rose and Jorgenson[3]. Two stepper motors were used in the sampler, one motor to control a specially designed sample tray, the other to control a lifter with a specially designed blade

on it. The sample tray had holes in it and a open slit at the bottom of each hole. Sample vials were placed in the holes. At the time of injection, one stepper motor turned the sample tray to send the sample vial into the right position, then the second stepper motor controlled the lifter so that the blade on the lifter lifts up the sample vial to a cone shaped guide so that the water levels and the two ends of the capillary were the same. Finally the capillary and electrode were inserted into the sample vial through the cone shaped guide. The injection voltage power supply was then turned on, and the injection initiated.

When the injection was finished, the sample vial was lowered by the stepper motor. The sample tray was then turned to the next position. This time, a vial containing eluting buffer solution was sent to the position where the sample used to be, and electrophoresis was started. The whole system was controlled by a IBM PC/XT together with a multifunction input/output interface board. A reproducibility of about 4.1% RSD was reported for this injection system.

Discussion

There are some advantages for the electrokinetic injection method because it is well studied and is easy to understand, the amount of sample injected into the capillary can be easily controlled by controlling the injection voltage, capillary length, etc., and sufficiently small amount of sample can be injected for separation and detection.

Some problems do exist in this injection method. From Equation (5.5), we can see that the injection volume depends on quite a few factors. The injection time, voltage used for injection, the electrophoretic mobility and the electroosmotic mobility will all affect the volume of injection. Although the precision of injection time and high voltage values are not a problem in automated electrokinetic sampling, the electrophoretic mobility and electroosmotic mobility will differ if the conductivity of the sample is different[2] from the buffer solution inside the capillary, so the detected peak area is directly proportional to the

resistance of the each sample in the solution. As a result, equation (5.5) can be applied only when the conductivity of the sample solution is approximately the same as the conductivity of the eluting buffer solution.

In addition, the use of electrokinetic injection may introduce bias in terms of concentration of each component of a injected sample compared with the original sample solution. Slow moving molecules under the electric field will be injected less and fast moving molecules will be injected more. Although from Equation (5.7) we can account for this effect, the bias still exists in a practical sense. It is not unusual to see in an electrophogram that peaks coming out first are much higher than the peaks coming out later.

Also, because there are capacitances in the high voltage power supply system, the voltage may not quickly rise to the set value, which may also introduce bias to the injection volume, especially when the injection time is short.

5.1.2 Hydrodynamic Injection

Hydrodynamic injection, or siphoning injection, is a relatively new technique for sample introduction in capillary electrophoresis. It can be implemented manually by lifting the sample vial, with the injection end of the capillary, above the waste reservoir. Manual siphoning sample introduction, however, can only be used for qualitative analysis, because of its poor reproducibility. An automated siphoning injector was first described by Honda *et al.* in 1987[4]. The precision of their auto sampler was within 3%.

The volume of hydrodynamic injection

The volume of sample solution introduced by a siphoning sampler can also be expressed by Equation (5.1). The length of the injected sample inside the capillary, L ,

can be calculated from Poiseuille's equation in hydrodynamics. Poiseuille's equation is:

$$u^* = \frac{\Delta P r^2}{8 \eta L_c} \quad (5.8)$$

where u^* is the linear velocity of sample during the injection, η is the viscosity of the sample solution, and ΔP is the pressure difference between the two ends of the open tube, in this case, the capillary. L_c and r are the length and radius of the capillary respectively as mentioned before.

The length of injected sample is:

$$L = u^* \times t \quad (5.9)$$

where t is the time of injection.

The pressure difference between the two ends of the capillary can be calculated by:

$$\Delta P = \rho g \Delta h \quad (5.10)$$

where ρ is the density of the liquid inside the capillary, g is the gravitational constant, and Δh is the height different between the two ends.

Substituting equations (5.8) and (5.10) into equation (5.9), we get an expression for the length of sample injected:

$$L = \mu^* t = \frac{\rho g \Delta h r^2 t_i}{8 \eta L_c} \quad (5.11)$$

The volume of injected sample can be calculated by substituting equation (3.11) to equation (5.1):

$$V = \pi r^2 L = \frac{\pi r^4 \rho g \Delta h t_i}{8 \eta L_c} \quad (5.12)$$

The volume of sample injected is the same for all component in the bulk sample solution. There is no discrimination against solutes with different electrophoretic mobility.

Automation of hydrodynamic sampling

Honda *et al.* introduced an automatic siphoning sampler for capillary zone electrophoresis in 1987[4]. The electrode at the detection end of electrophoresis system and one end of the capillary were fixed at one position throughout the analysis.

The heart of this sampling system is the design at the injection end of the capillary. The electrode at the injection end of the capillary was fixed at the same height as the electrode at the detection end. The injection end of the capillary was held by a "T" shaped rubber stopper so that the two ends of the capillary were at the same level. The injection end of the capillary can be lifted up easily if needed. The sample solution and the eluting buffer solution were supported by a turntable. The height of the turntable was adjusted by a microcomputer controlled motor.

Before injecting the sample, the capillary was filled with buffer solution. At the time of injection, the turntable was lowered and rotated to put the sample vial under the capillary. Then the turntable and the injection end of the capillary were raised to create a level difference between the solutions of the two ends for a certain period of time. When the injection was finished, the turntable was lowered again and rotated to put the eluting buffer under the anode and capillary end, then the turntable was raised to make the two buffer levels the same again, and the separation is started. With capillaries of 100 μm or 250 μm inner diameter, the coefficient of variation of the peak heights or peak areas is usually less than 3% from the electrophorograms generated by this instrument.

Another example was demonstrated by Rose and Jorgenson in 1988[3]. The set up was basically the same as described in the last section, except that when the blade lifts the sample vial to the cone shaped guide, instead of stopping and turning on the injection power supply, it lifts the vial further to create a level difference. The sample solution is then injected by the effect of siphoning. The reproducibility of their sampler was 2.9%.

Discussion

The siphoning injection technique is an effective injection method for zone capillary electrophoresis. This technique offers a way to introduce a very small amount of sample into the capillary, with remarkably good reproducibility. The 3% RSD is usually

insignificant compared with the other errors introduced by other processes in capillary zone electrophoresis, such as sample preparation, sample stability, and signal detection.

Many disadvantages of electrokinetic injection are minimized or eliminated by siphoning injection. First, there is no discrimination of solutes with respect to electrophoretic mobility. The amount of the sample injected into the capillary is the same for every component because no electric field is involved during the injection step. Thus, the peak heights (or areas) on the electrophorogram will reflect the real concentration of the components. Second, there is no uncertainty induced by the delay of voltage caused by the capacitance in the power supply system because there no need to use the high voltage.

However, there are two major problems with siphoning injection. The sample reservoir has to be raised to the desired level during the process of injection, which will cause disturbance to the flow of the sample solution. In addition, as we have noted, the Poiseuille's equation requires the pressure difference between the two ends of the capillary to be constant to get a constant liquid flow rate u^* . Raising the sample vial changes the pressure difference, which leads to errors in the calculated injection volume. Although not affecting precision of the injection, this changing pressure difference can affect accuracy.

5.1.3 Other injection methods

Because sample introduction in capillary electrophoresis is such an important issue, quite a few other injection methods have been studied[5-8]. These methods will be described in this section. However, the descriptions will be brief because these methods are not widely used.

Rotary type injector

Rotary type injectors are widely used in HPLC and other separation techniques. There is a problem in using the commercially available rotary type injectors in capillary electrophoresis. Bubbles can be generated due to an electrochemical reaction at the metal surface inside the injector[5], and this will shut off the current flow from the anode to the cathode.

A rotary type injector was described by Tsuda *et al.* in 1987[5]. They designed the injector using one rotor, two stators and one central pin made from fine ceramic. The rotor and stators have two flow passages, after one passage is filled with a sample solution, the rotor is rotated 90° by hand to come in line with the head of the column. The flow passage in the rotor had a 0.3 mm i.d. and a length of 5 mm, that is 0.35 μL in volume. The average coefficient of variation was about 1.9%. Although the reproducibility of this injector was good, the volume of injection was too big for most capillary electrophoresis systems.

Microinjectors

Ultrasmall volume sampling from a microenvironment is not an easy task in capillary electrophoresis. A series of microinjectors specially designed for this purpose were introduced in 1987 by Wallingford and Ewing[6, 7].

This series of injectors can be dual-barreled or single-barreled. The barrels are made from glass capillary which was heated and pulled to very small tip diameters. For a dual-barreled system, one barrel is filled with eluting buffer. The capillary column is inserted into the other end of the barrel, this part is the sample intake. The other barrel, which is arranged back to back to the first, can be either filled in with mercury with a carbon fiber electrode as anode, and a platinum electrode inserted into the mercury as a

connector to the high voltage power supply, or filled with eluting buffer with a platinum electrode inserted directly into the buffer solution. For a single barreled injector, the platinum electrode is simply placed somewhere around the barrel inserted with the capillary column. The injection is accomplished by inserting the barrel(s) into the sample, turning on the voltage for a short period of time, taking off the barrel(s), inserting the capillary column to the eluting buffer, then starting the separation.

These microinjectors work in the same way as the electrokinetic injection, but with a much smaller tip diameter. Although sample injection can be done in a smaller environment, it has all the advantages and disadvantages the electrokinetic injector has. In addition, the turbulence caused by sample flow from a very small tip to a relatively much larger capillary will be another source of band broadening.

Electric sample splitter

An electric sample splitter has also been used as an injector in capillary electrophoresis. This work was done by Derril *et al.* in 1985[8].

The injection system consists of two capillaries, one called the dosing capillary, the other the separation capillary. First, a 1 μL sample, which is at the end of the dosing capillary at a distance of 10 cm from the splitting point, migrates electrophoretically along the dosing capillary; at the splitting point, because another electric field is applied along the separation capillary, a part of the sample enters the capillary and is separated while the major part of the sample continuously moves along the dosing capillary and goes to the waste. Precision of the sample splitter was found to be better than 3% RSD when the splitting current ratio is compared with the actual splitting amounts. The main problem for this system is that it is difficult to apply to a separation column with a inner diameter less than 100 μm , while the capillaries typically used are less than 100 μm in diameter.

Conclusion

Among the injection techniques discussed in this section, electro kinetic injection and hydrodynamic injection are the most successful and widely accepted methods. This is mainly because of their simplicity and reproducibility. However, each of them, in their present forms, have disadvantages. It is difficult to solve the biased injection problem in electrokinetic injection, and it is also difficult to inject repeatedly an accurate amount of sample due to the continuous level changing before the capillary being raised to a certain level in hydrodynamic injection.

An ideal sample injector should be simple, accurate, and precise. The amount of injected sample should be easily controlled and should be described by a relatively simple mathematical equation, involving easily controlled parameters, and resulting in no significant bandbroadening.

5.2 Hydrodynamic sample introduction using a three way valve

A number of injection methods have been discussed in Section 5.1; among these methods, electrokinetic and hydrodynamic injections are the most widely used techniques. There are some fundamental disadvantages in electrokinetic injections such as the discrimination against solutes with low electrophoretic mobility, the delay of injection due to the capacitances inside the power supply, etc.

In this chapter, a newly designed hydrodynamic injector with a three way electronically actuated valve is introduced. Using this injector, an injection volume precision of about 2.5% is obtained. The accuracy of this injector is reflected by the excellent agreement of the injection volume calculated using Poiseuille's equation, with the injection volume obtained from electrokinetic injection. There is no extra bandbroadening introduced during injection.

5.2.1 Theory

For a pressure induced flow of liquid in an open tube, when the flow rate is low, with a laminar flow profile, the average flow rate is described by the Poiseuille's equation:

$$u^* = \frac{\Delta P r^2}{8 \eta L_c} \quad (5.8)$$

where u^* is the average linear velocity of the fluid through the tube obtained by integrating the linear velocity in the cross section of the tube and dividing by the tube cross sectional area. All the parameters in equation (5.8) are the same as described before. The injection volume then can be calculated by:

$$V = \pi r^2 L = \frac{\pi r^4 \rho g \Delta h t_i}{8 \eta L_c} \quad (5.12)$$

The parameters used in this equation are also defined in the last section.

5.2.2 Experimental Section

Separation and detection

The capillary zone electrophoresis system and laser induced fluorescence detector have been described in Section 2.1.1. A 50 μm inner diameter fused silica capillary (Polymicro Technology) was used for separation. A 30 KV power supply (Spellman) was used to drive the electrophoresis. A platinum electrode provided electrical contact with the eluting buffer at the injection end of the capillary. This end of the capillary was enclosed within a safety-interlock equipped plexiglass box. The detector end of the capillary was inserted into a sheath flow cuvette (home made) that was held at ground potential. The sheath fluid was pumped by a high-pressure syringe pump (Isco) at flow rate of 0.5 ml/h. Fluorescence was excited by a 0.75 mW green He-Ne laser (Melles Griot) with wavelength of 543.5 nm. The beam was focused with a 25 mm focal length (5 \times) microscope objective

(Melles Griot) into the cuvette. Fluorescence was imaged with an 18×, 0.45 numerical aperture (NA) microscope objective (Melles Griot) onto a 400 μm radius pinhole. The collected light was filtered with a 570 to 610 nm band pass filter (Omega Optical) and was detected with a R1477 photomultiplier tube (Hamamatsu). The output of the photomultiplier tube was conditioned with a 0.1 sec. RC filter and sent to the strip chart recorder.

Chemicals

Rhodamine B (Aldrich), and a solution of 6 amino acids (Fluka) derivatized with Tetramethyl-Rhodamine-Isothiocyanate (TRITC) (Molecular Probes) were used to characterize the system. Rhodamine B solution, $7.9 \times 10^{-4} \text{M}$, was prepared in acetone, and diluted with 5 mM borate buffer which is added with 10 mM sodium dodecyl sulfate, SDS (Aldrich), pH = 8.8, to a concentration of $7.9 \times 10^{-8} \text{M}$ before injection into the capillary. The eluting buffer is also 5 mM borate buffer with 10 mM SDS., pH = 8.8, and this will be called the eluting buffer for simplicity through this chapter. TRITC derivatized amino acid solution was prepared as follow: a $2.3 \times 10^{-5} \text{M}$ TRITC solution was prepared in acetone, and 1 mM solutions of alanine, arginine, cysteine, glutamate, lysine and 2 mM glycine were prepared in 0.2 M aqueous borate buffer, pH = 9.0. A mixture of 6 amino acids, 200 μl each, were added with 1200 μl TRITC solution and allowed to react overnight.

The injector

The injector (Fig. 5.1) introduced in this chapter is constructed by connecting the inlet and one outlet of a three way electrically actuated valve (LFAA1200118H, The Lee Co.) between the end of the sheath flow cuvette and the waste reservoir of the system

introduced in Chapter 2. The third port of the valve is connected to an injector reservoir. The valve was controlled by a 555 timer and the controlling circuit is shown in Figure 5.2.

Before injection, the capillary and all tubing in the system were filled with eluting buffer solution. The height of the liquid surfaces of the sample cell and waste reservoir were carefully set to the same level. This level matching is achieved by directing a red He-Ne laser to the sample cell, with the He-Ne laser parallel to the working table, and adjusting the height of the laser until the diffraction pattern caused by the liquid-air interface in the sample cell is seen (the sample cell is transparent); then the laser beam is rotated to the waste reservoir, and the height of the waste reservoir adjusted at this time until the same diffraction pattern is seen. This set the liquid levels of the two containers at the same height. The liquid level in the injector reservoir is set to be lower than the other two to form a level difference, Δh . The initial state of the electric valve is that the gate to the waste reservoir is open and the gate to injector reservoir is closed (Figure 5.1a). When the circuit is triggered, a pulse, which is set to be 10 seconds, will be sent to the valve, the gate to injector reservoir will be opened and the gate to the waste reservoir will be closed (Figure 5.1b). Due to siphoning effect induced by the Δh of water levels of sample and injector reservoir, the sample solution will be injected into the capillary. After 10 seconds, the three way valve will be automatically turned to the initial position, and the injection is finished. If a injection time longer than 10 seconds is required, it can be done by either adjusting the potentiometer at pin 7 of the 555 timer, or holding the trigger at the ground position so that the valve remains open to the injector reservoir as long as required; the injection is finished when the trigger is released.

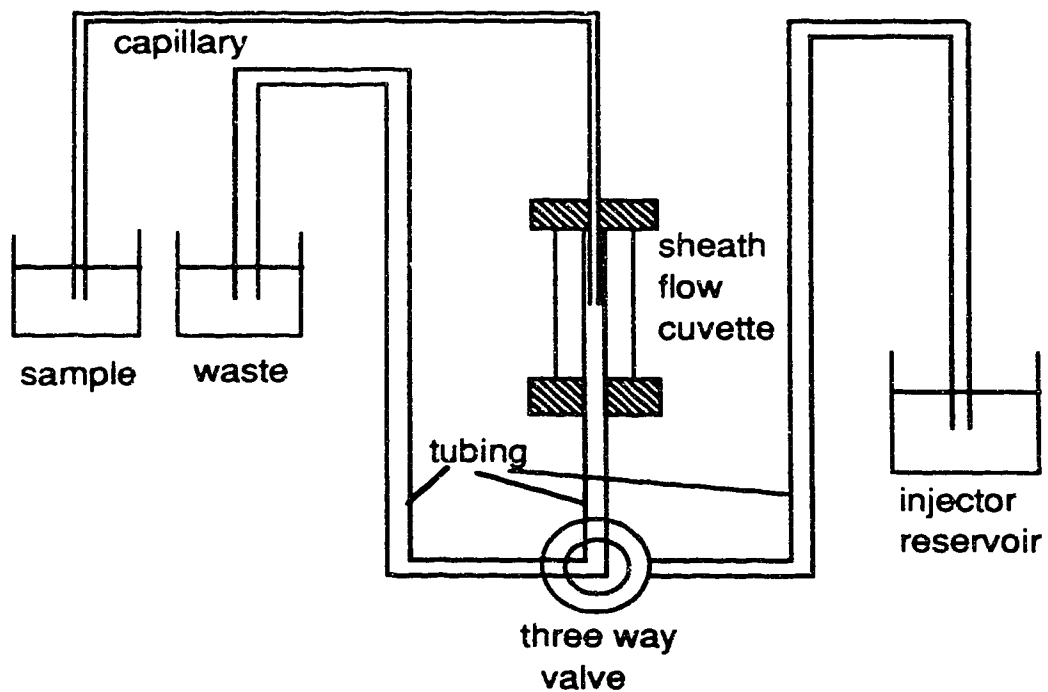


Fig. 5.1a The siphoning injector with a three way valve before and after injection, in a electrophoresis system and a sheath flow cuvette detector.

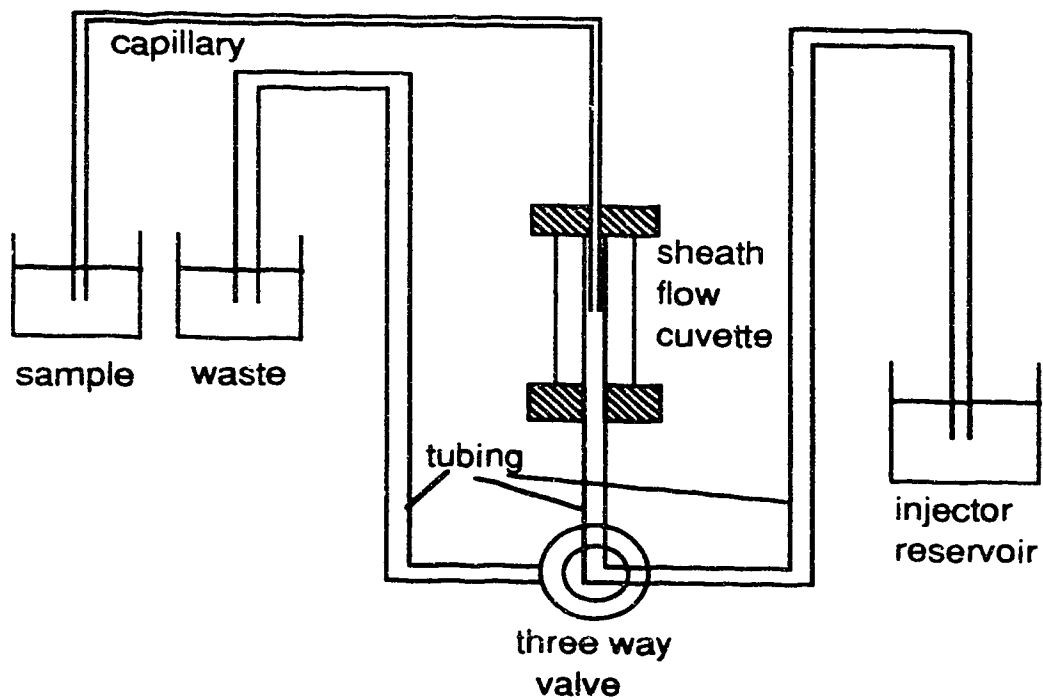


Fig. 5.1b The siphoning injector with a three way valve at the time of injection, in a electrophoresis system and a sheath flow cuvette detector.

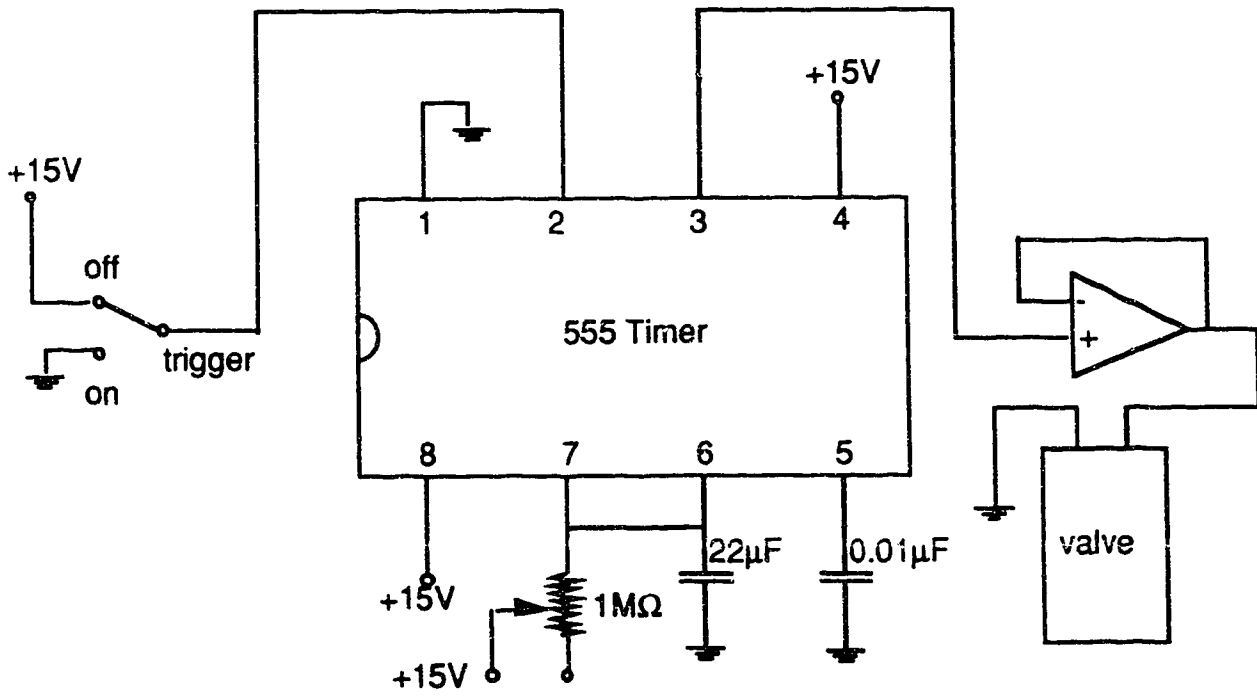


Fig. 5.2 Controlling circuit for the three way valve

5.2.3 Results and discussion

Injection volume

An experiment was done to obtain the injection volume for a certain period of time at a certain liquid level difference Δh , so that the average sample flow velocity can be obtained. 7.9×10^{-8} M Rhodamine B was injected to a 92 cm long capillary at Δh of 108 mm for 10 minutes. The electrophorogram shows a 36 s wide band for a elution time of 644 s. The length of sample injected to the capillary can be calculated by:

$$L = \frac{t_w}{t_e} \times L_c \quad (5.13)$$

where L is the length of sample injected into capillary, t_w is width of the band in s, t_e is the elution time, and L_c is the length of the capillary. The linear flow rate of the sample, is then equal to L/t , where t is the time of injection. Thus, the volumetric flow rate of the sample injected can be calculated as:

$$v = \pi r^2 \times \frac{t_w \times L_c}{t_e \times t} \quad (5.14)$$

where v is the volumetric flow rate of the injected sample, and r is the radius of the capillary. For a 10 second injection, the volume of the sample was calculated to be 1.68 nanoliter (nL). This experiment is repeated three times, and the volume of injection for 10 s is 1.69 ± 0.01 nL.

The linear average velocity for liquid in an open tube is discussed in many books in fluid dynamics. It is given by the form of Poiseuille's Law which is given by equation (5.8).

$$u^* = \frac{\Delta P r^2}{8 \eta L_c} \quad (5.8)$$

where u^* is the linear velocity of sample during the injection, η is the viscosity of the sample solution, in this case, the viscosity of water at 22°C, 0.9548 cP, was used. ΔP is the pressure difference between the two ends of the open tube, the capillary (the resistance

from other part of the system is much smaller than the resistance inside the capillary because the diameter is much larger, the pressure is mainly located at the capillary). Because of using of the sheath flow cuvette as a part of the detector in this system, the back pressure induced by the flow of the sheath solution has also to be considered, so that the ΔP should be:

$$\Delta P = r g \Delta h - P_B \quad (5.15)$$

where r is the density of the sample solution, which is about the same as that of water, i.e. 1 g/cm^3 , g is the gravity, 9.8 m/s^2 , and P_B is the back pressure induced by the sheath flow[9], which is about 3 mm water at the sheath flow rate of about 0.5 mL/h in this case. Equation (5.2) is then:

$$V = \frac{\pi r^4 g \Delta h t_i}{8 \eta L_c} (\Delta h - P_B) \quad (5.16)$$

Applying this equation to the conditions used in the experiment, where $\Delta h = 108$ mm, $P_B = 3$ mm, $L_c = 92$ cm, and $r = 25 \text{ } \mu\text{m}$, for a 10 s injection, the volume injected should be 1.79 nL, which is very close to the experimental results, 1.69 ± 0.01 nL.

Precision test

To determine the precision of the injection volume using this injector, a 76 cm long capillary was used, Δh was set to be 108 mm, and t was set to be 10 s. 7.9×10^{-8} M Rhodamine B dissolved in eluting buffer was used as sample. The peak height obtained within each set of data has a relative standard deviation of about 2.5%, which is comparable to other injection methods, if not better. A set of electrophorograms is shown in figure 5.3.

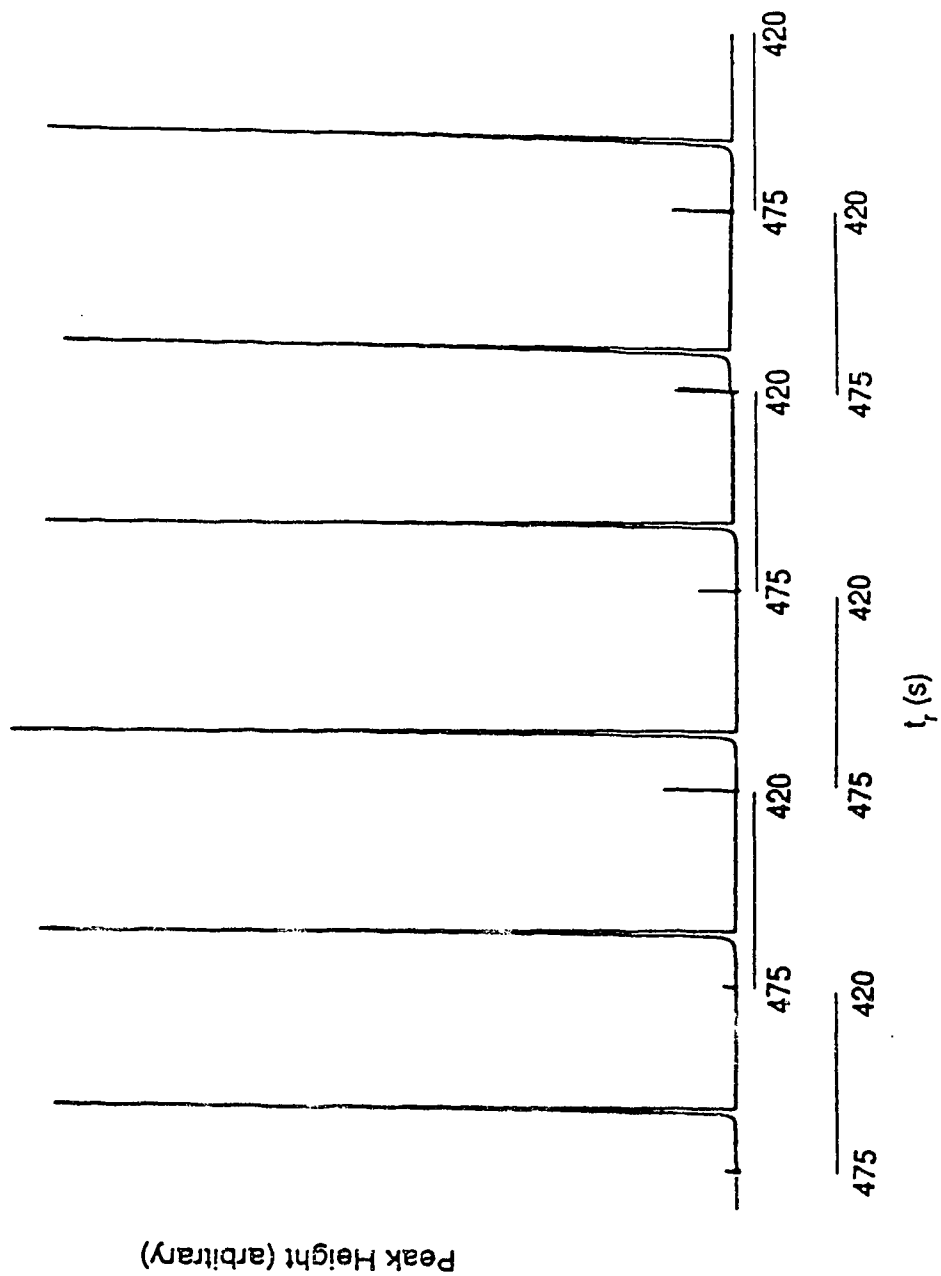


Fig. 5.3 Electropherograms for precision test of the hydrodynamic injector

Volume of Injection as a Function of Δh

The same condition was used as the precision test, except Δh was a variable in this experiment. The change of peak height vs. Δh is plotted and shown in figure 5.4.

The results shows the linear relationship between Δh and peak height, and we know peak height is directly proportional to the injection volume. Thus Δh vs V_i is linear, in agreement with Poiseuille's Law, with a slope of about 2 in this curve. If we use the linear velocity calculated from equation (5.1), the injection volume V will be:

$$V = \pi r^2 t u^* = \frac{\pi r^4 t \rho g}{8 \eta L_c} \Delta h \quad (5.17)$$

For $r = 25\mu\text{m}$, $t = 10\text{s}$, $\rho = 1\text{g/cm}^3$, $g = 9.8\text{m/s}^2$, $\eta = 0.9548\text{cP}$, and $L_c = 76\text{ cm}$, the slope is $2.01 \times 10^{-11} \text{ m}^2$, the unit of volume is nL if the unit of Δh is mm. For a $\Delta h = 100\text{ mm}$, the injection volume is 2.2 nL.

The graph shows that when $\Delta h = 0$, the peak height is not zero. The reason for this may be the result of insertion of the capillary into the sample solution, which may displace a small volume of the sample into the capillary; diffusion of the solute into the capillary may also occur.

Peak shape comparison

To confirm there is no additional band broadening introduced by siphoning injection, the same conditions were used as the previous two experiments. For siphoning injection, Δh was set at 106 mm, $t = 10\text{ s}$; and for electrokinetic injection, the injection potential was set at 1 KV for 10 second. The result is shown on figure 5.5. From the two electropherograms, we can not see any significant differences between the shape of peaks obtained by siphoning injection or electroosmosis injection. The volume of injection for the electrokinetic injection is 2.12 nL, and the volume of injection with the siphoning

injector is calculated to be 2.13 nL. From the two peaks in figure 5.5, we can see the accuracy of the siphoning injector.

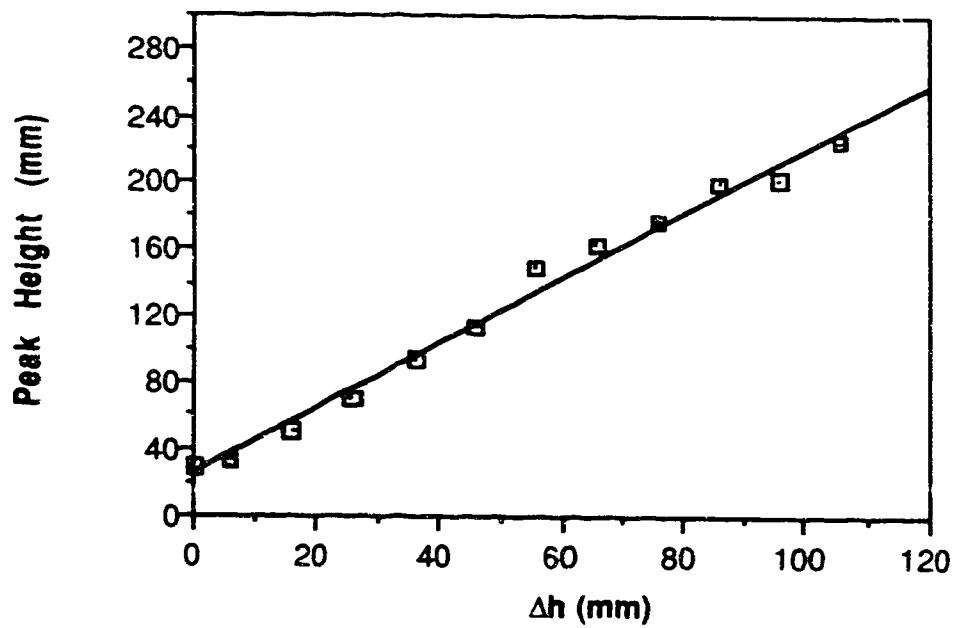


Fig. 5.4 Peak height vs. water level difference Δh .

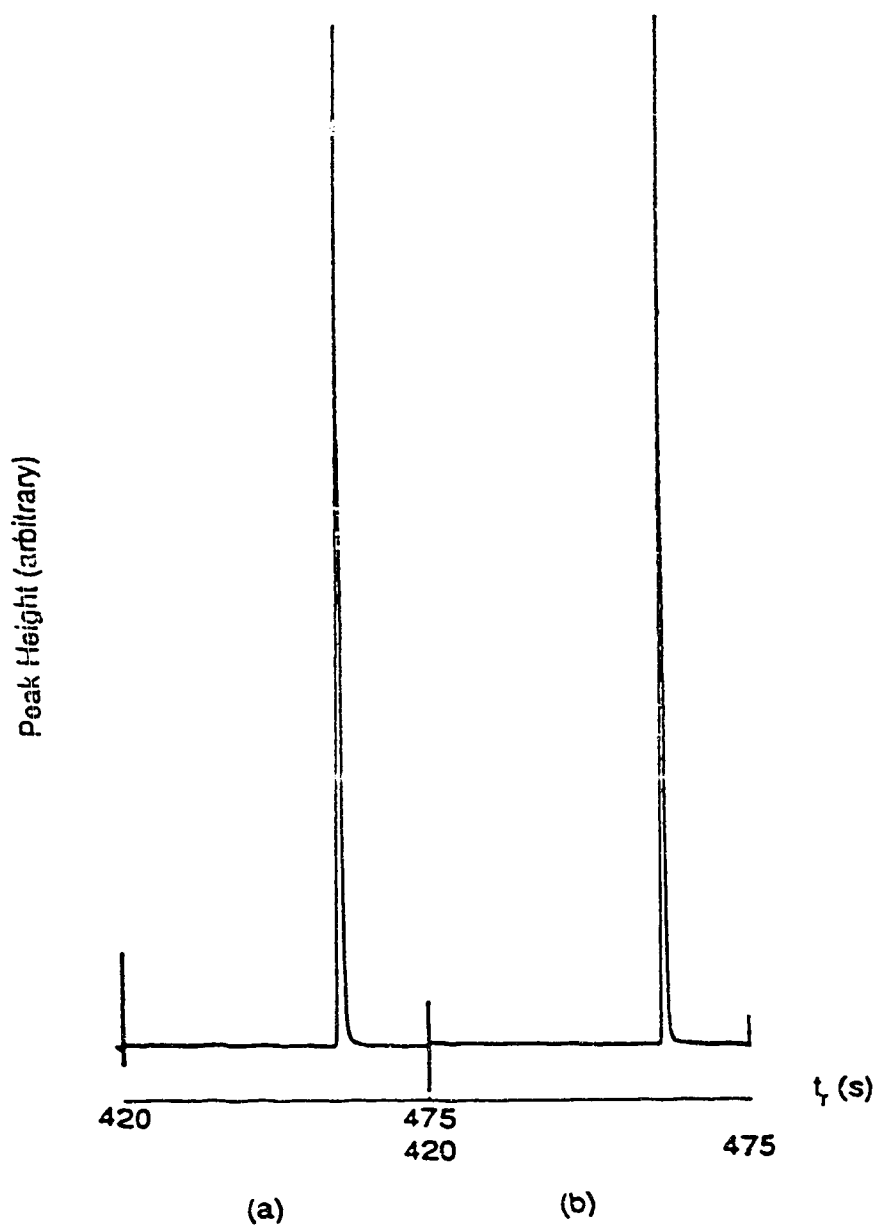


Fig. 5.5 Electropherograms for peak shape comparison: (a) electrokinetic injection; (b) siphoning injection.

Comparison of two methods of injection

One weakness of electroosmosis injection is that it introduces bias in the analysis; analytes with high electrophoretic mobility travel at a greater speed and thus are introduced to a great extent than slower moving analytes.

With siphoning injection, there should be no discrimination against the electrophoretic mobility of different molecules. This is demonstrated by separating a mixture of TRITC derivatized amino acids with different injection techniques. Using a 55 cm long capillary, 20 KV potential for electrophoresis, the results are shown on figure 5.6. Fig. 5.6 (a) is the electrophorogram of sample introduced by electroosmosis injection; Fig.5.6 (b) is the electrophorogram of sample introduced by siphoning injection. The bias of sample introduction by electroosmosis is seen.

Discussion

Hydrodynamic injection has distinct advantages over other injection methods in the areas like precision, small injection volume, and reflect the real amount of each component in the sample solution without bias. However, previous designs for this kind of injection suffer from the change of liquid levels and the movement of the injection end of capillary during the injection. These movements will affect the accuracy of the injection volume and may cause disturbance to the injected sample and introduce extra band broadening. The injector introduced in this chapter makes it possible to inject sample without any significant movement of instrument. All levels of liquid, include the height difference for the injection are previously set, which has preserved the advantages of all siphoning injections, and overcome the problem of inaccuracy in other designs of siphoning injection.

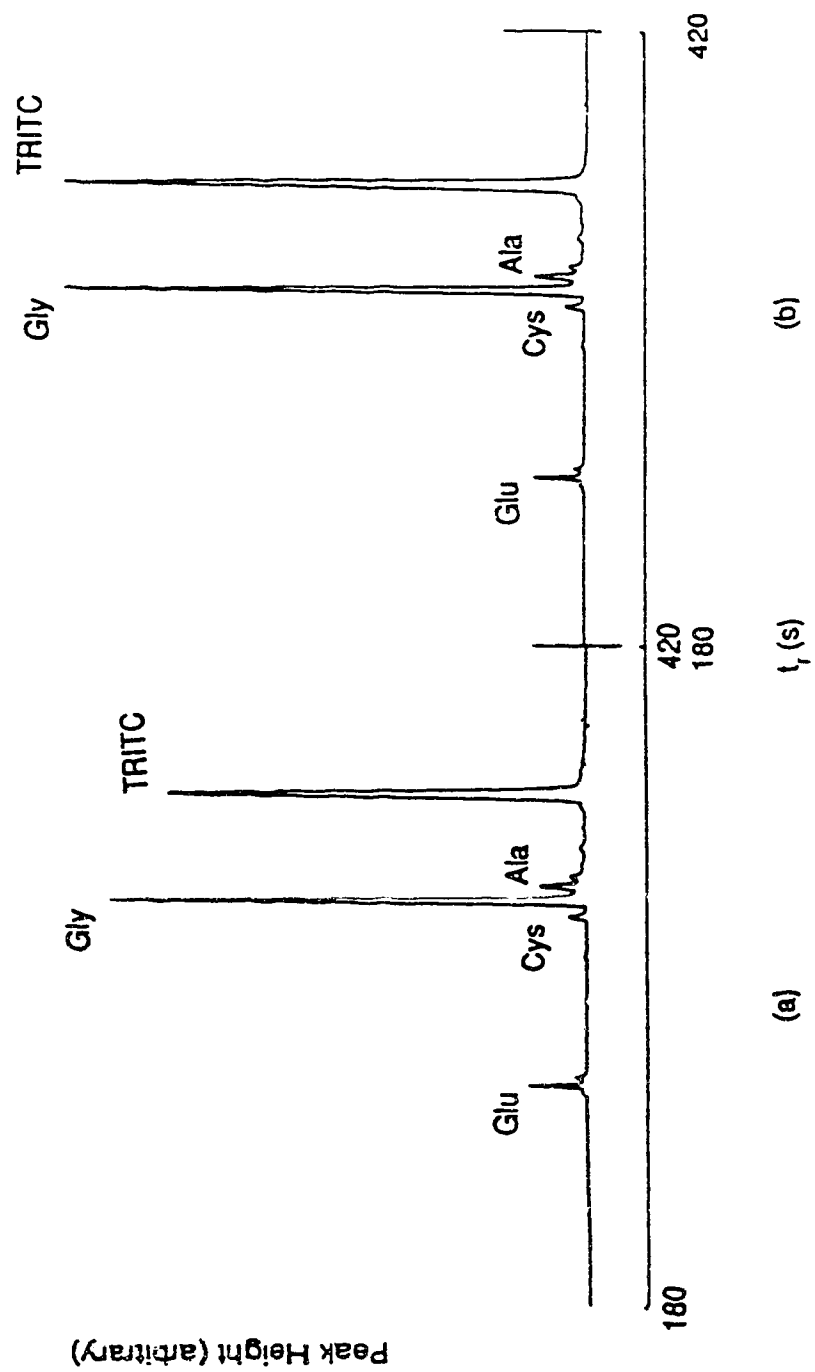


Fig. 5.6 Comparison of two methods of injection: (a) electrokinetic injection; (b) siphoning injection.

References:

1. Grushka, E. and McCormick, R.M., *J. Chromatogr.*, (1989), **471**: p. 421.
2. Huang, X., Gordon, M.J., and Zare, R.N., *Anal. Chem.*, (1988), **60**(4): p. 375
3. Rose, D.J.J. and Jorgenson, J.W., *Anal. Chem.*, (1988), **60**(7): p. 642.
4. Honda, S., Iwase, S., and Fujiwara, S., *J. Chromatogr.*, (1987), **404**(2): p. 313
5. Tsuda, T., Mizuno, T., and Akiyama, J., *Anal. Chem.*, (1987), **59**(5): p. 799.
6. Wallingford, R.A. and Ewing, A.G., *Anal. Chem.*, (1987), **59**(4): p. 678.
7. Wallingford, R.A. and Ewing, A.G., *Anal. Chem.*, (1988), **60**: p. 1972.
8. Deml, M., Foret, F., and Bocek, P., *J. Chromatogr.*, (1985), **320**(1): p. 159.
9. Cheng, Y.F., Wu, S., Chen, D.Y., and Dovichi, N.J., *Anal. Chem.*, (1990), **62**(5): p. 496-503.

The undersigned grant the permission that the material published in

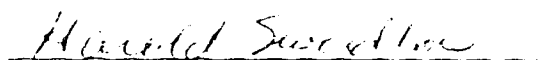
Analytical Chemistry, 1991, 63, 2835-2841

entitled: Three DNA sequencing methods using capillary gel electrophoresis and laser-induced fluorescence

be used in the PhD thesis of David Da Yong.



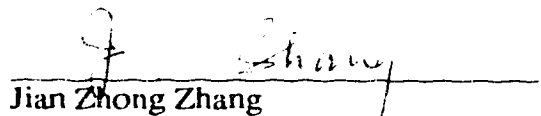
Norman J. Dovichi



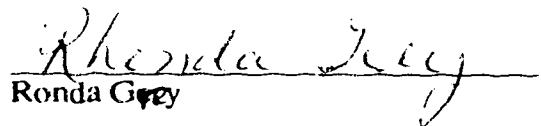
Harold P. Swerdlow



Heather R. Harke




Jian Zhong Zhang



Ronda Grey

Shaole Wu



Carl Fuller

The undersigned grant the permission that the material published in

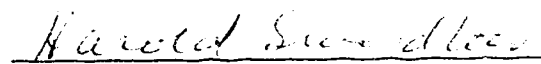
SPIE Vol.1435 Optical Methods for Ultrasensitive Detection and Analysis: Techniques and Applications (1991), p161-167

entitled: Single-color laser-induced fluorescence detection and capillary gel electrophoresis for DNA sequencing

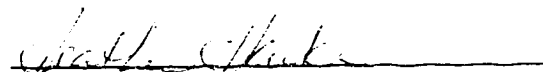
be used in the PhD thesis of David Da Yong.



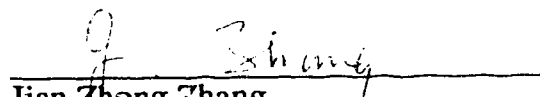
Norman J. Dovichi



Harold P. Swerdlow



Heather R. Harke



Jian Zhong Zhang

The undersigned grant the permission that the material published in


Journal of Chromotography, 559 (1991) 237-246

entitled: Low cost, high-sensitivity laser-induced fluorescence detection for DNA sequencing by capillary gel electrophoresis

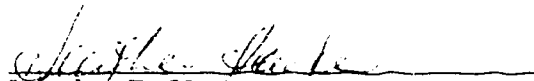
be used in the PhD thesis of David Da Yong.



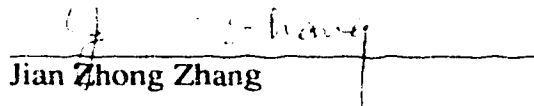
Norman J. Dovichi



Harold P. Swerdlow



Heather R. Harke



Jian Zhong Zhang